INL/EXT-13-28118
Revision 1

Drop Hammer Test of Concrete Cylinders Considering Fiber Reinforcement and Elevated Temperature

A.M. Weidner
C.P. Pantelides
W. D. Richins
T. K. Larson
J. E. Blakeley

October 2012

The INL is a U.S. Department of Energy National Laboratory operated by Battelle Energy Alliance

INL/EXT-13-28118
Revision 1

Drop Hammer Test on Concrete Cylinders Considering Fiber Reinforcement and Elevated Temperature

A.M. Weidner
C.P. Pantelides
W. D. Richins
T. K. Larson
J. E. Blakeley

October 2012

Idaho National Laboratory
Idaho Falls, Idaho 83415

http://www.inl.gov

Prepared for the
U.S. Department of Energy
Through the INL LDRD Program
Under DOE Idaho Operations Office
Contract DE-AC07-05ID14517

Abstract

Idaho National Laboratory engineers collaborated with students and staff from the University of Utah to perform a series of drop hammer impact tests of concrete cylinders. A facility, which allows for a hammer composed of steel weights to be dropped from a height of 16 ft, was built at the University of Utah Structures Laboratory to deliver the dynamic force. In July 2011 the drop hammer was used to perform tests on cylinders with and without fiber reinforcement from drop heights of 16 ft and 8 ft. In April 2012, additional tests were conducted using the same procedure on concrete cylinders at elevated temperatures. A data acquisition system was used to collect strain gauge and load cell data. The tests were also recorded using two high speed cameras. The tests were designed to determine the dynamic properties at high strain rates of normal weight concrete and fiber reinforced concrete in tension and compression at room and elevated temperatures.

Summary

Concrete, when loaded dynamically, has been reported to have a higher strength than when loaded statically. A variety of tests have been performed on different specimen types to determine dynamic impact factors (DIF) for concrete. The DIF is a ratio of the dynamic to static strength and is often reported as a function of the strain rate. Here, the DIF is taken as the ratio of the maximum dynamic to average static load. Several methods were developed to calculate the dynamic strain rate, the results of which were analyzed to determine which method was most accurate.

The DIF is of importance for defensive design purposes. The first phase of this project involved analyzing the performance of 4 ft x 4 ft concrete panels under blast loading[1]. The results of these tests provided information about how different reinforcement types influence the performance of a structural member. To determine how the concrete material was influenced by dynamic loading at high strain rates, concrete cylinders were cast at the same time as the panels. The cylinders were 4 in. diameter by 8 in. high, or 6 in. diameter by 12 in. high. These cylinders were tested dynamically by dropping steel plates from elevated heights, using what is referred to as the drop hammer facility.

One form of reinforcement considered in the blast tests was fiber reinforced concrete (FRC), which is composed of macro-synthetic polypropylene fibers. One percent by volume of the FRC specimens consisted of 2 in. long Propex Concrete Systems Enduro 600 fibers. In July 2011, both FRC and normal weight concrete (NWC) cylinders were tested under different rates of dynamic impact by releasing a drop hammer weight from heights of 8 ft and 16 ft.

When concrete is loaded dynamically in defense related facilities or nuclear power plants it is likely that it is also at an elevated temperature. In April 2012 additional tests were performed to determine how temperature, up to 400°F, affects the response of different concrete types under dynamic loading. These tests were of special interest in the case of fiber reinforced concrete. It is also possible that heated concrete can be loaded dynamically after it has had time to cool. A small number of tests were performed on cylinders that were allowed to cool down for approximately 18 hours after being heated to 400°F.

Tests were performed to determine both dynamic tension and compression properties at high strain rates for all specimen types. The dynamic test was designed and analyzed to follow standard static test procedures as close as possible so that a comparison between the two could be made. For this purpose, all types of dynamic tests were also preformed statically.

At room temperature: the dynamic strength of NWC in compression was between 1.1 and 3.2 times the static strength; the dynamic strength of NWC in tension was between 1.0 and 4.1 times greater the static strength; the dynamic strength of FRC in compression was between 1.5 and 2.3 times the static strength; the dynamic strength of FRC in tension was between 1.6 and 2.7 times the static strength.

At elevated temperature: the dynamic strength of NWC in compression was between 1.3 and 2.8 times the static strength; the dynamic strength of NWC in tension was between 1.0 and 3.2 times the static strength; the dynamic strength of FRC in compression was between 1.3 and 2.2 times the static strength; the dynamic strength of FRC in tension was between 1.5 and 2.1 times the static strength.

For compression tests at room temperature, FRC specimens did not perform as well as NWC. For tension tests, fibers add strength when tested statically. However, when tested dynamically, FRC specimens did not perform as well as NWC specimens.

For both compression and tension tests on NWC, heated specimens had higher DIFs when tested with an 8 ft drop heights. However, when tested at a 16 ft drop height, the DIFs decreased for heated specimens. All FRC specimens tested at elevated temperatures saw a decrease in DIF when compared to room temperature.

Acknowledgement

The authors acknowledge the assistance of Timothy Garfield, former University of Utah graduate student, for his work on the drop hammer facility and his involvement in the project and initial tests. The authors would also like to acknowledge Mark Bryant, University of Utah Structures Laboratory Technician, for his assistance in building and operating the drop hammer facility. The authors acknowledge the participation of the INL staff.

CONTENTS

FIGURES

TABLES

Acronyms

DIF	Dynamic Increase Factor
ASTM	American Society for Testing and Materials
NWC	Normal Weight Concrete
FRC	Fiber Reinforce Concrete
TF	Tension, Fiber Reinforced Concrete, Static
CF	Compression, Fiber Reinforced Concrete, Static
TN	Tension, Normal Weight Concrete, Static
CN	Compression, Normal Weight Concrete, Static
TF8	Tension, Fiber Reinforced Concrete, 8 ft Drop Height
CF8	Compression, Fiber Reinforced Concrete, 8 ft Drop Height
TN8	Tension, Normal Weight Concrete, 8 ft Drop Height
CN8	Compression, Normal Weight Concrete, 8 ft Drop Height
TF16	Tension, Fiber Reinforced Concrete, 16 ft Drop Height
CF16	Compression, Fiber Reinforced Concrete, 16 ft Drop Height
TN16	Tension, Normal Weight Concrete, 16 ft Drop Height
CN16	Compression, Normal Weight Concrete, 16 ft Drop Height
TF0-400-4	Tension, Fiber Reinforced Concrete, Static, 400°F, 4 in. diameter cylinder
TF0-R-6	Tension, Fiber Reinforced Concrete, Static, Room Temperature, 6 in. diameter cylinder
CF0-400-4	Compression, Fiber Reinforced Concrete, Static, 400°F, 4 in. diameter cylinder
CF0-400-6	Compression, Fiber Reinforced Concrete, Static, 400°F, 6 in. diameter cylinder
CF0-R-6	Compression, Fiber Reinforced Concrete, Static, Room Temperature, 6 in. diameter cylinder
TN0-400-4	Tension, Normal Weight Concrete, Static, 400°F, 4 in. diameter cylinder
TN0-R-4	Tension, Normal Weight Concrete, Static, Room Temperature, 4 in. diameter cylinder
CN0-400-4	Compression, Normal Weight Concrete, Static, 400°F, 4 in. diameter cylinder
CN0-R-4	Compression, Normal Weight Concrete, Static, Room Temperature, 4 in. diameter cylinder

TF8-400-4 Tension, Fiber Reinforced Concrete, 8 ft Drop Height, 400°F, 4 in. diameter cylinder

CF8-400-4 Compression, Fiber Reinforced Concrete, 8 ft Drop Height, 400°F, 4 in. diameter cylinder

TN8-400-4 Tension, Normal Weight Concrete, 8 ft Drop Height, 400°F, 4 in. diameter cylinder

TN8-0-4 Tension, Normal Weight Concrete, 8 ft Drop Height, Room Temperature, 4 in. diameter cylinder

CN8-400-4 Compression, Normal Weight Concrete, 8 ft Drop Height, 400°F, 4 in. diameter cylinder

CN8-0-4 Compression, Normal Weight Concrete, 8 ft Drop Height, Room Temperature, 4 in. diameter cylinder

TF16-400-4 Tension, Fiber Reinforced Concrete, 16 ft Drop Height, 400°F, 4 in. diameter cylinder

CF16-400-4 Compression, Fiber Reinforced Concrete, 16 ft Drop Height, 400°F, 4 in. diameter cylinder

TN16-400-4 Tension, Normal Weight Concrete, 16 ft Drop Height, 400°F, 4 in. diameter cylinder

TN16-0-4 Tension, Normal Weight Concrete, 16 ft Drop Height, Room Temperature, 4 in. diameter cylinder

CN16-400-4 Compression, Normal Weight Concrete, 16 ft Drop Height, 400°F, 4 in. diameter cylinder

CN16-0-4 Compression, Normal Weight Concrete, 16 ft Drop Height, Room Temperature, 4 in. diameter cylinder

CN16-cooled-4 Compression, Normal Weight Concrete, 16 ft Drop Height, Cooled for roughly 18 hours, 4 in. diameter cylinder

Equipment and Data Collection

A drop hammer facility at the University of Utah was built as part of this project and used to perform dynamic tests on concrete cylinders at high strain rates. High speed cameras, strain gauges and a load cell system were used to collect data during dynamic tests. Static tests were also performed using a Satec™ series Instron® machine. During one series of tests, cylinders were heated using a Despatch oven.

Drop Hammer Facility

To begin constructing the drop hammer facility a new foundation was cast to ensure that the dynamic force from the drop weight would have minimal effects on the surrounding facilities. The existing floor slab was replaced with a 7 ft x 9 ft by 4 ft deep concrete foundation. Gravel, 3 in. deep, was used as a base, and large pieces of steel were added as reinforcement. Twelve cubic feet of concrete was then cast and allowed to cure for 28 days to complete the foundation.

The base of the drop hammer structure is a 3 ft x 5 ft, 2 in. thick steel plate, as shown in Figure 1. Welded to the base plate are three, 23 ft tall legs made from 6 in. x 6 in. by 0.25 in. thick hollow steel square tubes. The main section of the drop hammer is a 0.25 in. thick, 16 in. diameter pipe, through which the drop weight falls.

The legs and tube are connected by welded and bolted plates along the length of the drop hammer. The pipe is slotted in the front to help prevent the drop weight from binding in the tube. One foot increment markings, measured from the impact target where the cylinder is placed are shown on the side of the slotted pipe. To complete the facility, a protective cage was built around the base of the drop hammer to reduce the spread of concrete as the specimens break. An image of the finished drop hammer is shown in Figure 2.

The drop weight used to deliver the dynamic load is composed of 14 in. diameter steel plates with a thickness of either 0.5 or 1 in. These plates, have a central whole diameter of 1.25 in. and were added to a 1 in. thick base plate with a 1 in. diameter rod welded through its center.

Once the desired drop weight was reached, a square tub was placed on the base plate rod. The square tube had a checkerboard pattern placed on it to calculate the velocity of the drop hammer as it fell using high speed camera recordings. An additional thin plate was then placed on top of the square tube. To finalize the drop hammer construction, the plates and square tuber were tightened together using a fastening gig which was bolted onto the base plate rod. This configuration, shown in
Figure **3**, was designed to distribute the weight along the length of the drop hammer, thus preventing it from oscillating as it fell. The drop hammer was connected to an electric cable hoist using a quick release hook as shown in Figure 4.

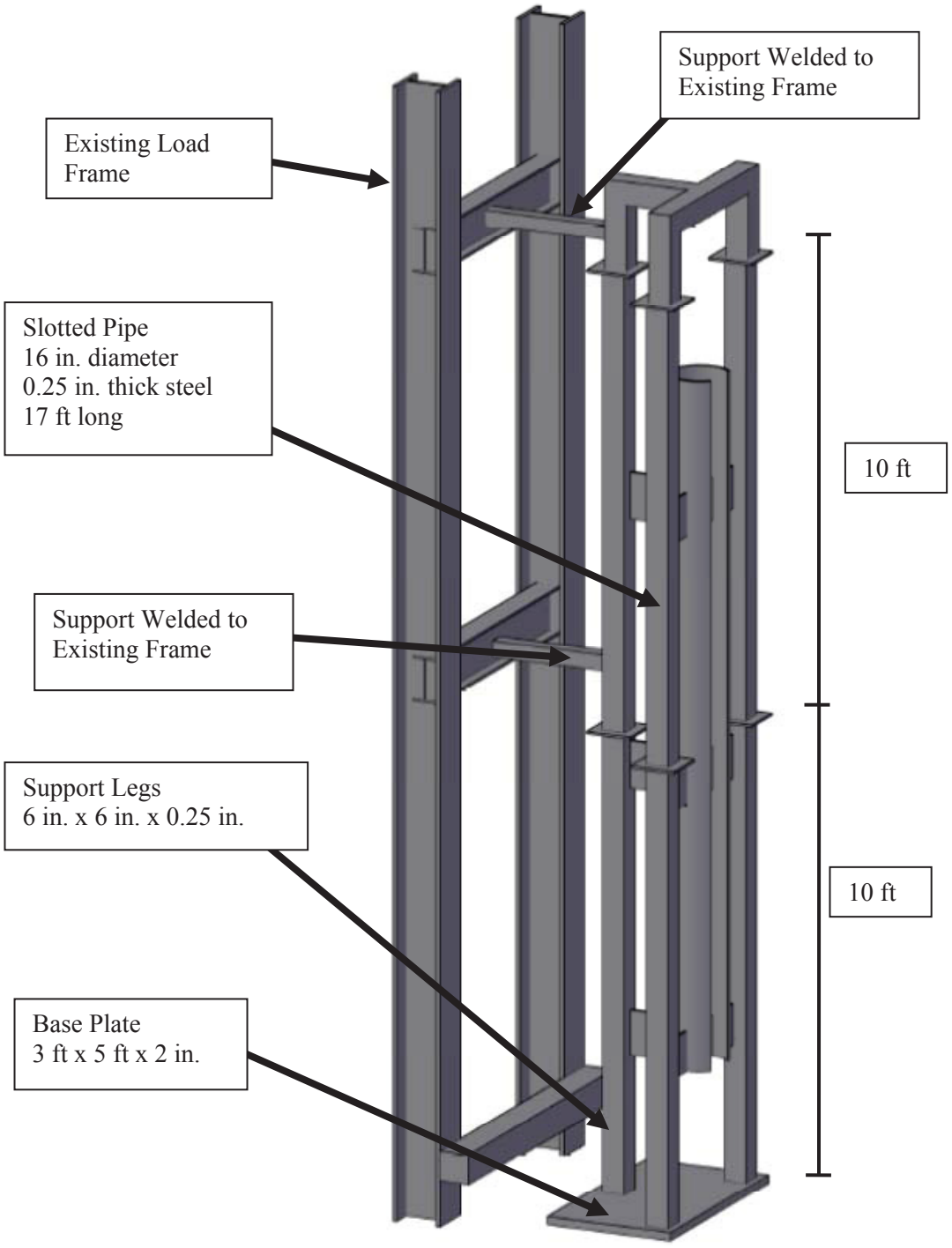

Figure 1 - Drop Hammer Facility Model (Courtesy of Timothy Garfield[1])

Figure 2 - Drop Hammer Facility

Figure 4 - Electrical Cable Hoist

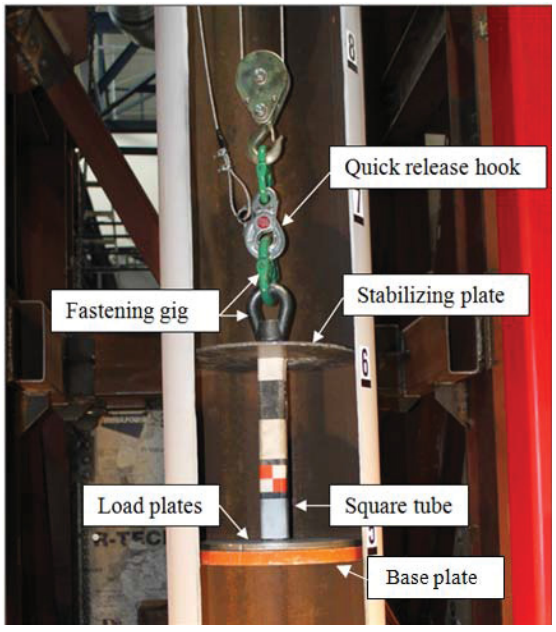

Figure 3 - Drop Hammer

High Speed Cameras

During the July 2011 tests, two high speed cameras were used to record failure of the specimens. A Phantom v12 camera with a signal to noise ratio of 7968, an exposure of 99 microseconds and a resolution of 400x504 pixels was placed directly in front of the specimen and recorded the tests at a rate of 8000 frames per second (FPS). A second camera, a Phantom v7.3 with a signal to noise ratio of 7966, an exposure of 123 microseconds and a resolution of 640x480 pixels, was placed toward the side of the specimen, recording at a rate of 7005 FPS.

To achieve high quality videos, shop lights were required during the tests. A touch pad was used to signal the cameras to begin recording. The touch pad was triggered as the hammer was being released. To demonstrate the data recorded, consecutive image shots of the video are shown in Figure 5 for tension and Figure 6 for compression.

Strain Gauges

For the July 2011 tests, 120 ohm strain gauges were placed on each specimen. Vishay Precision Group strain gauges were used. Most specimens had two strain gauges: the first was a model 10CBE, 1 in. gauge (referred to as Strain Gauge 0) and the second a model 20CBW, 2 in. gauge (referred to as Strain Gauge 1). For the splitting tension tests, two strain gauges were placed on

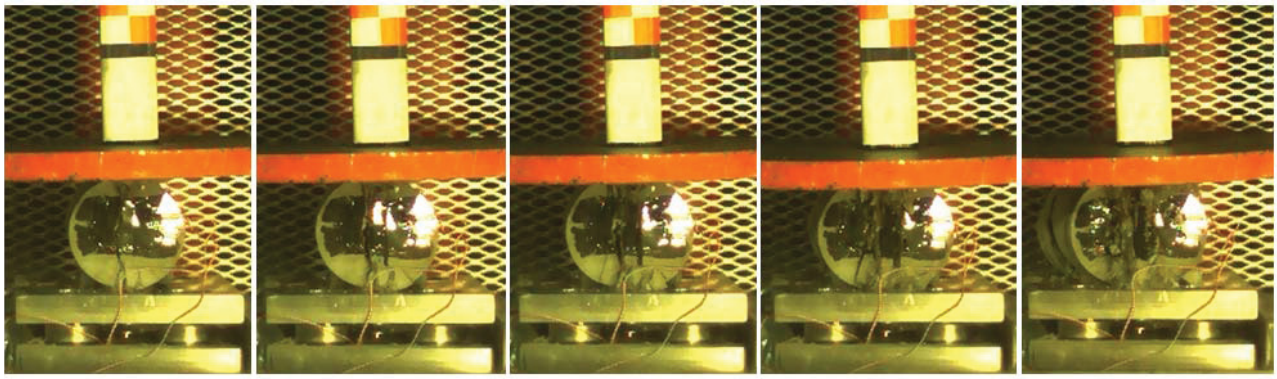

Figure 5 - Time Lapse of Tension Tests

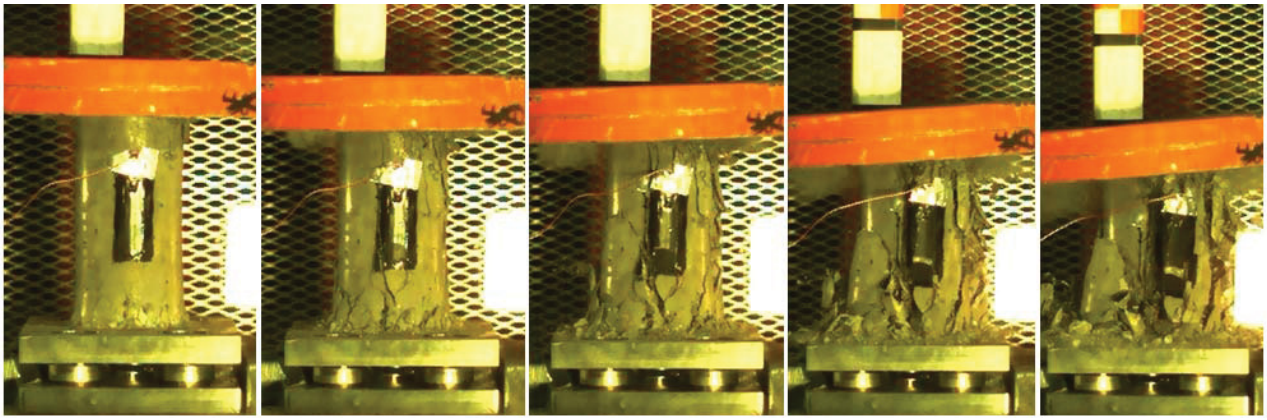

Figure 6 - Time Lapse of Compression Test

the top face of the cylinder and the drop weight was released onto the side of the cylinder, as shown in Figure 7. This configuration was typical for most tests; however, some splitting tension specimens had gauges on their sides instead of the top face (Figure 8) due to a limitation of appropriate strain gauge configuration. For the compression tests, two strain gauges were placed on opposite vertical sides and the drop weight was released onto the top face of the cylinder as shown in Figure 9. There were a number of instances where one of the strain gauges failed and no output was recorded.

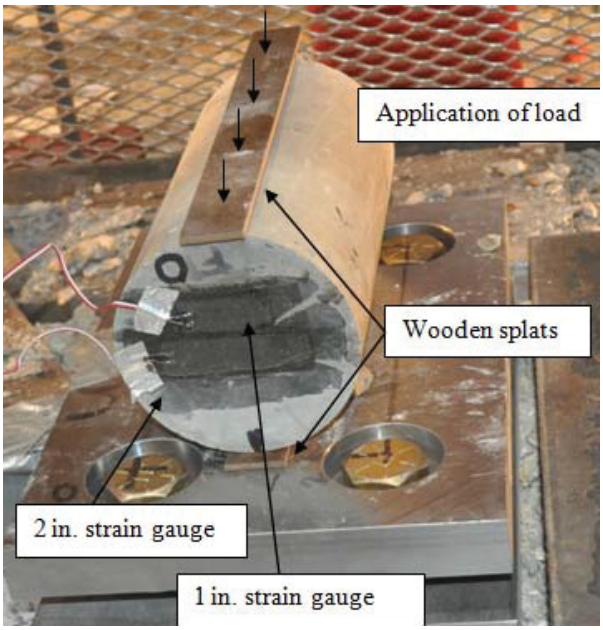

Figure 7 – Typical Strain Gauge Location and Cylinder Placement for Split Tension Tests

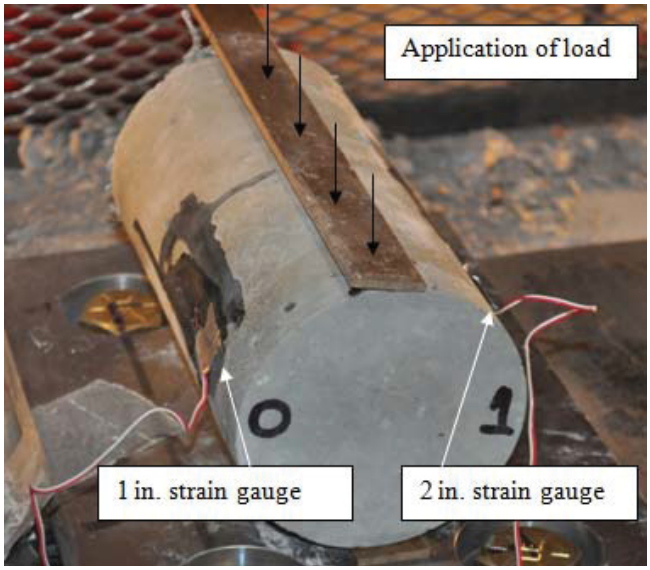

Figure 8 - Side Strain Gauge Location for Split Tension Tests

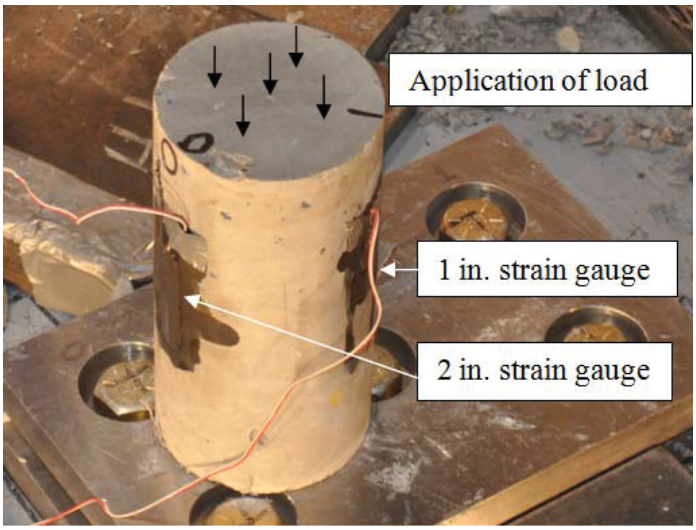

Figure 9 - Strain Gauge Location and Cylinder Placement for Compression Tests

Load Cells

To measure the dynamic load on the cylinders, a load cell system composed of load sensors, steel plates, and mounting hardware, was built. For the load cell sensors to record accurate data, they need to be loaded concentrically to reduce the possibility of induced bending moments. This is best achieved by using multiple sensors placed between two flat plates that prevent the sensor from bending.

Five force sensors were placed between two, 12 in. x 8 in. by 1 in. thick steel plates. The load sensors and plates were held together using HEX HD 7/8-14 UNF-2Bx1-3/4 LG beryllium copper mounting studs. These studs are elastic, which allows for the applied force to transfer to the force sensor. A pilot bushing is used between the mounting stud and sensor to ensure that they are centered together. Two anti-friction washers, placed above and below each sensor, are also used to protect the surface of the sensor when the mounting stud is being tightened. A schematic of the load cell system assembly is shown in Figure 10. The final load cell system is shown in Figure 11.

Model 206C ICP® Dynamic Force Sensors (Figure 12), which can record up to 80,000 pounds of force, were used in the load cell system. A constant current between 2 and 20 mA was supplied to the sensor from the data acquisition system. When a load was applied, the sensor measured the high impedance of the supplied current and converted it to a low impedance voltage signal that was recorded. The sensors had a target pre-load of 16,000 pounds, which is required to ensure that the sensor will perform as calibrated[2].

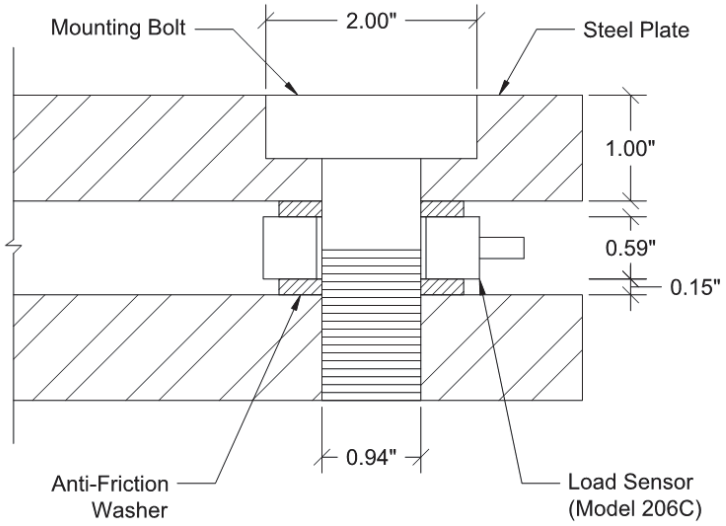

Figure 10 - Load Cell System Assembly

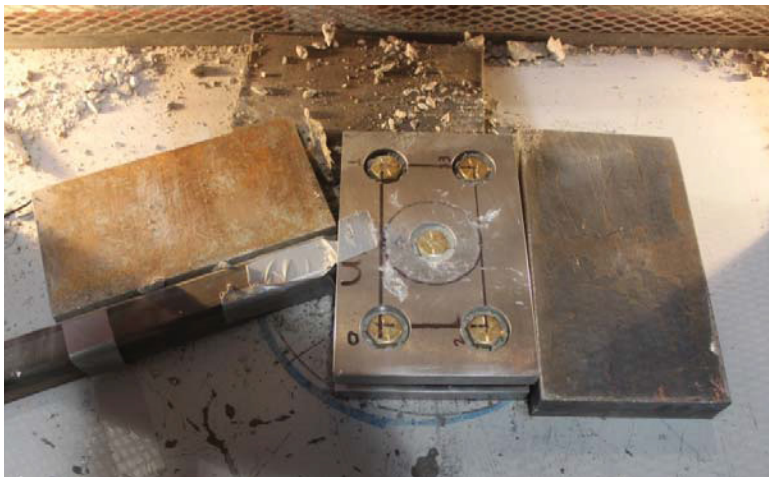

Figure 11 - Load Cell System Configuration, July 2011

Figure 12 - Model 206C ICP Dynamic Force Sensor

To achieve this pre-load amount the initial pre-load and voltage was measured using the data acquisition system and a digital voltmeter respectively. A ratio of the current pre-load to the target pre-load was added to the measured voltage. This calculated value was the desired voltage. A torque was applied to the mounting studs until the desired voltage was achieved, as measured from the digital voltmeter. If necessary, as determined from analyzing the output of the sensors after tests, the load cells were readjusted back to the proper pre-load value.

For the July 2011 tests the load cell system was held in place on the drop hammer facility's base plate by placing steel plates around it. In April 2012, small steel angles were welded to the drop hammer facility's base plate to hold the load cell system in place. In addition, a hemispherical steel plate was placed on top of the load cell system during tests.

As shown in Figure 13, the hemispherical plate is composed of two joining convex and concave hemispherical plates. Reviewing the individual load cell data from the July 2011 tests showed that some force sensors were recording significantly larger loads than others. It was believed that the plate containing the load cells was deflecting unevenly during tests due to concentrated forces. The hemispherical plate was added to the testing configuration to distribute the load more evenly among the load cells, and to prevent the load cell system plates from deflecting unevenly.

Satec™ Series Instron® Machine

A Satec™ Series Instron® machine was used to test the concrete cylinders statically. The Instron machine applied a constantly increasing load to the cylinders. The American Society for Testing and Materials (ASTM) standard C496/C496M-04e1 Standard Test Method for Splitting Strength of Cylindrical Concrete Specimens[3] and C39/C39M-09a Standard Test Method for Compressive Strength of Cylindrical Concrete[4] were used to determine the appropriate loading rate. The loading rate is a function of the size of cylinder used. Equations (1) and (2) were used to determine the loading rate for split tension and compression respectively.

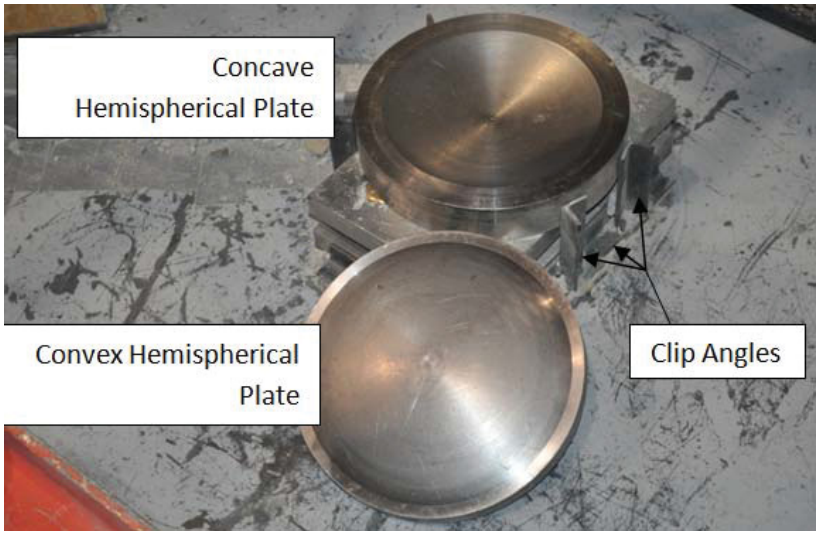

Figure 13 - Hemispherical Steel Plate and Load Cell Configuration, April 2012

$$Tension\ Applied\ Loading\ Rate = 2.5\ psi/sec * \frac{\pi * L * D}{2} \quad (1)$$

$$Compression\ Applied\ Loading\ Rate = 40\ psi/sec * \frac{\pi * D^2}{4} \quad (2)$$

For the 4 in. diameter by 8 in. long cylinders, the loading rates were 500 pound force per sec (lbf/sec) and 130 lbf/sec for compression and tension respectively. For 6 in. diameter by 12 in. long cylinders, the loading rate was 1130 lbf/sec and 285 lbf/sec for compression and tension respectively.

Despatch Oven

An LBB2-18-1 Despatch oven, with a maximum temperature of 400°F was used to heat the cylinders for the April 2012 tests. To determine the time required for the cylinder to be placed in the oven, a thermocouple was placed on a NWC 4 in. diameter by 8 in. high cylinder and a NWC 6 in. diameter by 12 in. high cylinder. The resulting rate of temperature increase is shown in Figure 14. The maximum interior temperature reached for the 4 in. diameter by 8 in. high cylinders was 386°F. For the 6 in. diameter by 12 in. high cylinders, the maximum temperature was 381°F. The 4 in. diameter by 8 in. high cylinder reached its maximum temperature after approximately 5 hours. The 6 in. diameter by 12 in. high cylinder took significantly longer to reach its maximum temperature. From these results, it was decided to allow all cylinders 24 hours of heating before being tested.

Specimen types CN0-400, CN8-400, CN16-400 and TN16-400-1, comprising 15 cylinders, were placed in the oven when it was not preheated. Twenty one additional cylinders, specimen types TN16-400, TN8-400 and CN16-cooled, were added 31 hours later. At 52 hours of heating, specimen types TF16-400, CF16-400 and CF8-400 were added to the oven. At this point in time several of the heated cylinders had been removed and tested but many cylinders still remained in the oven. Two hours later, TF8-400, CF0-400, TN0-400 and TF0-400 were also added to the oven. At this point in time many of the fully heated cylinders had been removed.

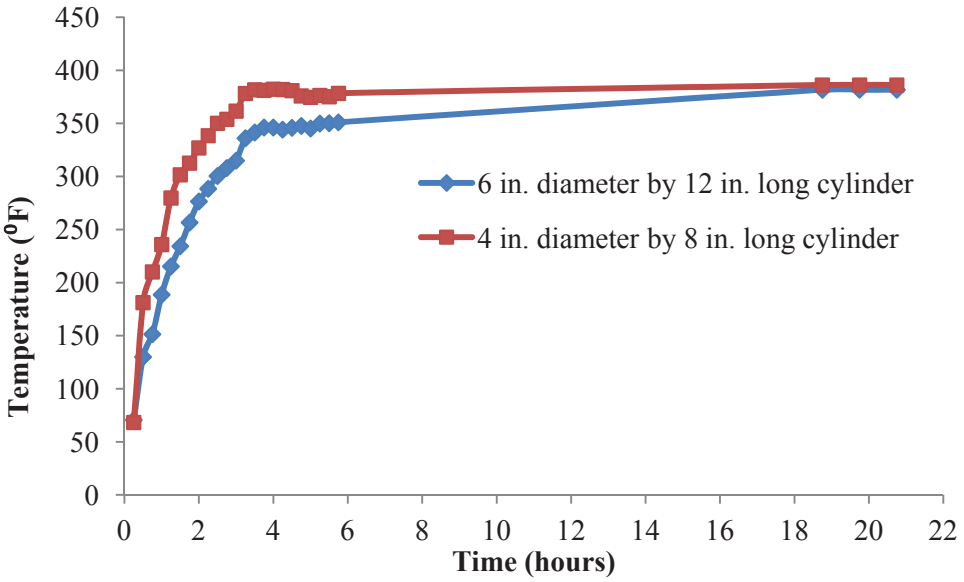

Figure 14 – Heating of Cylinders

The addition of so many room temperature specimens caused the surface temperature of the remaining fully heated cylinders to decrease. The interior temperature of the cylinder was most likely maintained during the addition of the room temperature cylinders. However, since the recorded temperature value was that of the surface temperature, testing was delayed until the surface temperature of all cylinders once again reached the typical maximum readings. This would result in recorded temperatures that were more reflective of the interior temperature of the cylinder. The approximate amount of time each specimen was placed in the oven is shown in Table 1.

The surface temperature of the cylinders was measured using a Fluke® 65 infrared thermometer. Temperatures were recorded as the cylinders came out of the oven and just prior to testing. The temperatures of the cylinders as they were coming out of the oven ranged from 352°F to 407°F, with an average temperature of 391°F. Readings between 323°F and 365°F, with an average of 353°F, were recorded just prior to testing. By comparison, the room temperature cylinders had an average surface temperature of 63°F.

Data Acquisition System

A data acquisition system, provided and operated by INL specialists, was used to collected strain gauge and load cell data.

Test Setup and Procedure

The test setup and procedure is described for the July 2011 and April 2012 dynamic tests. Details are also provided for the static tests that were performed in both July 2011 and April 2012.

July 2011 Dynamic Tests

In July 2011 dynamic tests were performed on concrete cylinders considering three parameters: test type, concrete composition and drop height. The test types included compression and tension, the composition was either normal weight concrete (NWC) or fiber reinforced concrete (FRC), and the drop weight was released from either 8 ft or 16 ft. All combinations of parameters were considered and tested as shown in Table 2.

Table 1 - Heating of Specimens

Specimen Type	Approximate Heating Time (hrs)	Specimen Type	Approximate Heating Time (hrs)	Specimen Type	Approximate Heating Time (hrs)
TF8-400	25.0	TF16-400	23.0	TF0-400	45.5
CF8-400	26.0	CF16-400	24.5	CF0-400	45.0
TN8-400	43.0	TN16-400**	44.0	TN0-400	45.0
CN8-400	53.0	CN16-400***	72.5	CN0-400	51.0
		CN16-cooled	49.0		

** TN16-400-4-1 was heated for 74 hours
*** CN16-400-4-1 was only heated for 54 hours

The cylinders were placed directly on top of the load cell system. For the tension test the cylinders were placed on their side directly in the middle of the five load cells as shown previously in Figure 7 and Figure 8. A wooden slat, similar to those used in static tests, was placed above and below the cylinders. Clay, or a small piece of aggregate, was used to stabilize the cylinders during tests and avoid rolling. For the compression tests the cylinders were placed in an upright position directly in the middle of three load cells to best distribute the load. The typical placement for compression tests was shown previously in Figure 9.

Prior to testing, trial tests were performed to determine what drop weight would be appropriate from a certain height. The drop weights listed in Table 2 were believed to achieve results that would best represent proper failure of the cylinders. At the time of testing, tension tests were of more interest than compression tests. For this reason, more tension tests were performed with this test type.

April 2012 Dynamic Tests

Additional tests at elevated temperatures, with parameters similar to those used in July 2011 tests, were performed in April 2012. The elevated temperature tests were not initially planned when the specimens were cast; therefore the quantity of fiber reinforced concrete cylinders was limited. Both normal weight and fiber reinforced concrete was tested at 400°F for each test type and drop height. The test matrix for the April 2012 dynamic tests is shown in Table 3. With the use of the hemispherical plate for the April 2012 tests, the cylinders were simply placed centrally on top of the hemispherical plate as shown in Figure 15 and Figure 16.

Table 2 - July 2011 Dynamic Test Matrix

Specimen Notation	Number of Tests	Test Type	Composition	Drop Weight (lbf)	Drop Height (ft)
CN8	3	Compression	Normal Weight	92	8
CF8	3	Compression	Fiber Reinforced	158	8
CN16	3	Compression	Normal Weight	70.5	16
CF16	3	Compression	Normal Weight	92	16
TN8	8	Tension	Fiber Reinforced	70.5	8
TF8	9	Tension	Normal Weight	92	8
TN16	9	Tension	Normal Weight	49.5	16
TF16	7	Tension	Fiber Reinforced	49.5	16

Figure 15 – Specimen Placement for Dynamic Split Tension Tests

Figure 16 - Specimen Placement for Dynamic Compression Tests

Only NWC cylinders were tested for room temperature tests since FRC specimens were not available. Tests on the same specimen types were performed in July 2011; however, different drop weights were used. The drop weight was modified from the July 2011 test in an effort to be more representative of the static test procedure.

The change in drop weight was the reason for repeating the same room temperature tests in April 2012 that were performed in July 2011. Even though heated cylinders were not tested in July 2011 it was desirable to know what overall effects the change in drop weight would have on the results. Knowing the effects of the drop weight, it could be determined if it would be appropriate to make comparisons between the room temperature, FRC tests done in July 2011 with elevated temperature, FRC tests done in April 2012 at different drop weights. An additional purpose for repeating tests at room temperature is the fact that concrete strength changes over time. For this reason room temperature static tests were also performed.

Table 3 - April 2012 Dynamic Test Matrix

Specimen Notation	Number of Tests	Test Type	Temperature	Composition	Drop Weight (lbf)	Drop Height (ft)
CN8-400	5	Compression	400°F	Normal Weight	223	8
CF8-400	3	Compression	400°F	Fiber Reinforced	223	8
CN8-R	3	Compression	Room	Normal Weight	223	8
CN16-400	5	Compression	400°F	Normal Weight	136	16
CF16-400	3	Compression	400°F	Fiber Reinforced	136	16
CN16-R	3	Compression	Room	Normal Weight	136	16
TN8-400	5	Tension	400°F	Normal Weight	92	8
TF8-400	3	Tension	400°F	Fiber Reinforced	92	8
TN8-R	3	Tension	Room	Normal Weight	92	8
TN16-400	5	Tension	400°F	Normal Weight	53.5	16
TF16-400	3	Tension	400°F	Fiber Reinforced	53.5	16
TN16-R	3	Tension	Room	Normal Weight	53.5	16

Table 4 - Change in Drop Weights

	Drop Weight (lbf)	
Specimen Type	**July 2011**	**April 2012**
CN8	92	223
CF8	158	
CN16	70.5	136
CF16	92	
TN8	70.5	92
TF8	92	
TN16	49.5	53.5
TF16	49.5	

The results from the July 2011 tests were such that the concrete did not break completely (see Appendix A for pictorial results). This was the case more so for the compression tests than for the tension tests. Therefore, the drop weights were increased significantly for the compression tests and slightly for the tensions tests. It was desirable for each specimen type, and for every height, to have the same drop weight for comparison purposes. For example, every compression test with a drop height of 8 ft had a drop weight of 223 pounds. Table 4 shows each test type and its corresponding drop weight for both July 2011 and April 2012 tests.

To better understand and compare the dynamic impact of the different drop hammer weight and drop height combinations, the potential and kinetic energy were determined. The potential energy (U) was computed by taking into account the weight (W) and height (h) of drop as shown in Equation (3). The delivered kinetic energy (E_K) was calculated using the mass (m = W/g, where g=32.2 ft/sec) of the drop weight and the measured velocity (v) determined from the high

speed cameras (as explained in subsequent sections). The velocity for the 8 ft and 16 ft drop heights were 21.2 ft/sec and 30.9 ft/sec respectively. To determine the kinetic energy Equation (4) was used.

$$U = W * h \tag{3}$$

$$E_K = \frac{1}{2} * m * v^2 \tag{4}$$

The values for potential and kinetic energy are given for the July 2011 and April 2012 tests in Table 5 and Table 6 respectively. The average 10% difference between the potential and kinetic energy is from the frictional resistance that occurs when releasing the drop hammer, and from air resistance. The kinetic energy is considered as the impact energy delivered to the test specimen.

Table 5 - Energy of Drop Hammer for July 2011

Specimen Type	Drop Weight (lbf)	Potential Energy (ft-lbf)	Kinetic Energy (ft-lbf)
CN8	92	736	643
CF8	158	1264	1104
CN16	70.5	1128	1046
CF16	92	1472	1365
TN8	70.5	564	492
TF8	92	736	643
TN16	49.5	792	734
TF16	49.5	792	734

Table 6 - Energy of Drop Hammer for April 2012

Specimen Type	Drop Weight (lbf)	Potential Energy (ft-lbf)	Kinetic Energy (ft-lbf)
CN8 CF8	223	1784	1558
CN16 CF16	136	2176	2018
TN8 TF8	92	736	643
TN16 TF16	53.5	856	794

Static Testing

Static tests were performed to establish a basis for comparison with the dynamic drop hammer results. These tests were performed on the same day as the drop hammer tests to reduce variability in specimens. Static tests were performed for both compression and split tension on

both normal weight and fiber reinforced concrete. Due to the limited number of FRC specimens available in April 2012, some static tests utilized 6 in. diameter by 12 in. high cylinders specimens so that all dynamic tests could be performed using 4 in. diameter by 8 in. high cylinders. The static test matrices are shown in Table 7 for the July 2011 and Table 8 for the April 2012 tests.

The configuration for the static compression test is shown in Figure 17. Two steel caps were placed on both ends of the cylinder to distribute the load evenly. The split tension tests were performed using a loading jig that held the cylinder on its side between two wood strips as shown in Figure 18. The loading jig held a steel rod directly over the center of the cylinder. A steel plate was then placed on top of the rod to distribute the load and achieve the desired split tension break.

Figure 17 - Static Compression Test

Figure 18 – Static Split Tension Test

Table 7 - July 2011 Static Test Matrix

Specimen Notation	Number of Tests	Test Type	Composition
CN	3	Compression	Normal Weight
CF	3	Compression	Fiber Reinforced
TN	3	Tension	Normal Weight
TF	3	Tension	Fiber Reinforced

Table 8 - April 2012 Static Test Matrix

Specimen Notation	Number of Tests	Test Type	Temperature	Composition
CN0-R	4	Compression	Room	Normal Weight
CF0-R*	3	Compression	Room	Fiber Reinforced
CN0-400	4	Compression	400°F	Normal Weight
CF0-400**	3	Compression	400°F	Fiber Reinforced
TN0-R	4	Tension	Room	Normal Weight
TF0-R*	3	Tension	Room	Fiber Reinforced
TN0-400	4	Tension	400°F	Normal Weight
TF0-400**	2	Tension	400°F	Fiber Reinforced

* All specimens were 6"x 12" Cylinder

** One of the specimens was a 6" x 12" Cylinder

July 2011 Dynamic Test Procedure

The procedure for the dynamic tests performed in July 2011 was as follows:

1. Test load cells and strain gauge connections periodically. Torque load cells or adjust strain gauge connections if necessary.
2. Prepare data acquisition and camera software.
3. Prepare drop hammer with appropriate weight and connect to electric cable hoist.
4. Connect strain gauges to the data acquisition system. Test wiring periodically with a volt meter to ensure correct readings are being recorded.
5. Raise the drop weight high enough to place the specimen centrally below the weight.
6. Place the cylinder with the correct orientation and in the correct location with respect to the load cell system.
7. Release the safety on the quick release hook and close the protective cage around the base of the drop hammer.
8. Raise drop weight to desired height.
9. Simultaneously begin data acquisition system, trigger camera and pull on quick release hook to drop weight.
10. Visually inspect and record break before removing specimen and debris.
11. Filter and save data collected from data acquisition system and high speed cameras.

April 2012 Dynamic Test Procedure

The procedure for the dynamic tests performed in April 2012 is listed below. Figure 19 through Figure 25 show visual implementation of the test procedure.

1. Test load cells and torque if necessary.
2. Prepare drop hammer with appropriate weight and connect to electric cable hoist.
3. Release the safety on the quick release hook and raise drop weight above safety bar location.
4. Insert safety bar into slotted pipe and raise weight to desired height.
5. Prepare data acquisition software.
6. Remove specimen from the oven and record temperature.
7. Place on cart and cover with Styrofoam box. Transport to drop hammer facility.
8. Place the cylinder in the correct orientation on the hemispherical plate and close the protective cage around the base of the drop hammer
9. Measure and record temperature.
10. Remove safety bar.
11. Simultaneously begin data acquisition system, trigger camera and pull on quick release hook to drop weight.

12. Visually inspect and record break before removing specimen and debris
13. Filter and save data collected from data acquisition system.

Static Test Procedure

The procedure for static tests performed in July 2011 and April 2012 is listed below. Handling of heated specimens for static tests followed the same procedure as outlined in the April 2012 dynamic test procedure.

1. Set the Satec™ series Instron® machine to the appropriate loading rate
2. Place cylinder on Instron platform.
    a. For compression tests, place steel caps on the top and bottom of the cylinder.
    b. For tension test, place the cylinder in the loading jig.
3. Close the protective cage.
4. Raise the Instron platform until a minimal load is applied.
5. Arm the Instron machine and begin test.
6. Visually inspect and record break before removing specimen and debris
7. Filter and save data collected from data acquisition system.

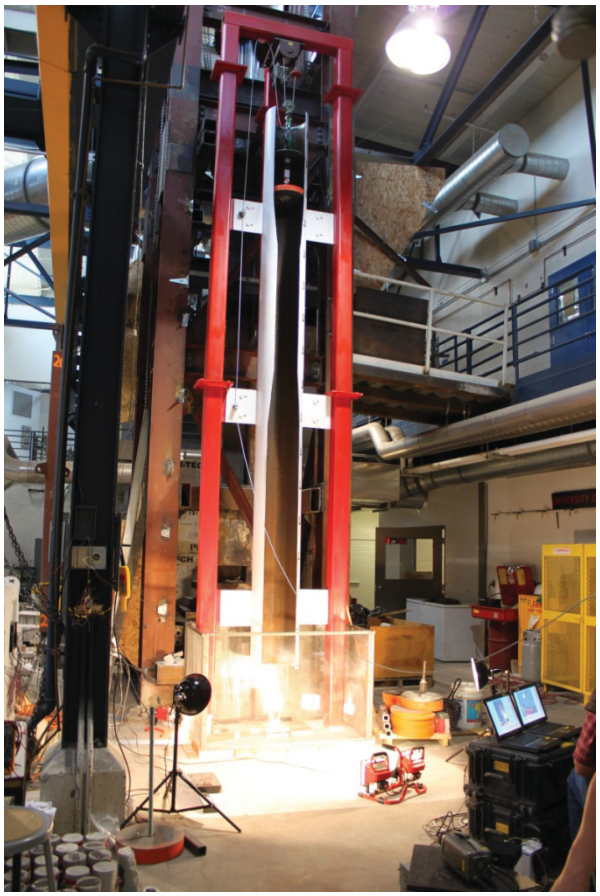

Figure 19 - Drop Hammer Facility Set Up

Figure 21 - Heated Cylinder

Figure 22 - Cylinder Transport

Figure 20 – Despatch Oven

Figure 23 - Cylinder Placement

Figure 24 - Temperature Reading

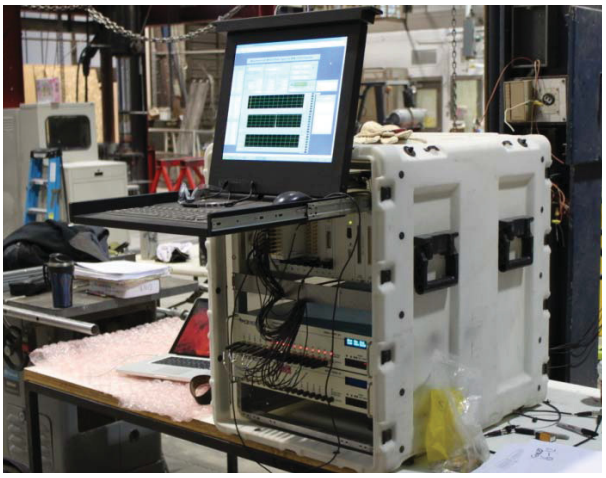

Figure 25 - Data Acquisition System

Additional Static Tests for Compression Tests

Upon review of the initial test results, it was found that the DIF for the compression tests were much lower than expected. The DIF is inversely proportional to the static strength of the concrete. It is also a ratio of the dynamic to static strength. For best results, the dynamic and static tests need to be performed in as similar a manner as possible to reduce variability. The static tests were performed using a steel cap, which is the standard method to determine compressive strength of concrete. However, it was not practical to utilize the caps in the dynamic tests.

The steel caps are used to evenly distribute load to the cylinder, which results in a higher static strength and a lower DIF. Considering this fact, it was decided to perform additional static tests without using the steel caps. This would result in better uniformity between the dynamic and static test methods. In place of the steel caps, the hemispherical plate used in the dynamic tests was also used in the additional static tests, thus producing the most similar test setup possible.

The additional static tests were done in December 2012 for the non-heated specimens and in February 2013 for heated specimens. The only cylinders available from the same batch used in the dynamic tests were 6 in. by 12 in. The compressive strength of a 6 in. by 12 in. cylinder is comparable with a 4 in. by 8 in. cylinder when appropriate loading rates are used. However, the DIF is a ratio of maximum loads, which are not comparable between the two cylinder sizes. For this reason, an equivalent maximum load of a 4 in. by 8 in. cylinder ($P_{4x8\ equi.}$) was calculated using the maximum load of the 6 in. by 12 in. cylinders (P_{6x12}). The equivalent load is given in Equation (5) for compression. In addition, a small number of 6 in. by 12 in. FRC cylinders were used for tension tests in April 2012. An equivalent maximum load for tension tests is given in Equation (6).

$$P_{4x8\ equi.} = \frac{P_{6x12}}{\pi * 6^2/4} * \frac{\pi * 4^2}{4} \tag{5}$$

$$P_{4x8\ equi.} = \frac{P_{6x12}}{(\pi * 6 * 12)/2} * \frac{(\pi * 4 * 8)}{2} \tag{6}$$

The equivalent load is the only property of these additional static tests that was considered. The original compression static tests performed with capped cylinders in July 2011 and April 2012 were considered for finding concrete compressive strength. This compressive strength, as discussed later, is used to determine strain rates using elastic theory. This theory considers the compressive strength of the concrete, which is best represented by the capped tests.

Data Reduction

Three software programs were used to reduce the information collected from the test equipment. Diadem, a Labview software, was used to reduce data collected from the data acquisition system, which recorded data from the load cells and strain gauges. A video review program was used to review high speed camera recordings and take measurements at given time increments. Partner Material Testing software was used to record data for the static tests performed on the Satec series Instron.

DIAdem

DIAdem version 11.1, a National Instruments software program[5], was used to filter data collected from the data acquisition system. For each strain gauge, data was recorded for strain at a given point in time. For the load cells system, a load was recorded for each load sensor. A script was written in DIAdem that combined and filtered the five load sensors giving data for one load at a given point in time for each test.

Video Program

Phantom Cine Viewer v2.0 software[6], which allows high speed videos to be played per frame, was used to measure how the cylinder dimensions changed over time. Frames could be viewed approximately every 10^{-4} seconds.

The Cine Viewer has tools that can be used to make measurement on a given frame. Initially, a calibration is made. For the tension test the diameter of the cylinder, and for the compression test the cylinder height were used to calibrate the measuring tool. The Cine Viewer also provides time information with accuracy of 10^{-6} second. Details about how the measurements tool and time were used to determine the strain rate in the Cine Viewer are discussed in the High Speed Camera Method section.

The measuring tool was also used to determine the velocity of the falling drop hammer. For the 8 ft drop hammer tests the average velocity was 21.2 ft/sec. For the 16 ft drop hammer tests the average velocity was 30.9 ft/sec.

Partner™ Material Testing

The program Partner™ Material Testing for Windows was used to operate and record data from the Satec™ Series Instron®. Partner records the load and corresponding time of the tests. By inputting the proper areas considering ASTM standard C496/C496M-04e1 for tension tests[3] and C39/C39M -09a for compression tests[4], the compressive strength and strain were calculated. The data recorded could be exported to an excel file, which could be used for further analysis. This was done to determine the strain rates and to verify the compressive strength using the initial raw data of measured load and time.

Data Analysis

Three main methods of determining the strain rate were explored: the high speed camera method, the load cell method and the strain gauge method. Each method was reviewed to decide which method to consider.

High Speed Camera Method

During the July 2011 tests, high speed cameras were used to record the tests of each specimen. The high speed videos of the tests made it possible to visually see how the cylinder responded to dynamic loading. The breaking pattern for the different specimen types were better understood from the video recordings. The visual data collected provided information that was used in the high speed camera method of determining strain rates.

The strain rates were calculated by measuring the change in size of the specimen as it was tested. For the tension tests, measurements of the cylinder diameter were taken for each recorded frame, which occurred approximately every 10^{-4} seconds. The change in diameter as the cylinder broke apart was divided by the time in which the change occurred, giving the strain rate. For the compression tests, the same procedure was used by measuring the change in height of the cylinder as it decreased while being loaded dynamically.

The strain rates were computed until the specimen crushed to a point where the diameter or height could no longer be measured. On average, this lasted $1.5 * 10^{-3}$ seconds. Individual strain rates were computed over this time range for each specimen. That is, a strain rate was computed every 10^{-4} seconds for $1.5 * 10^{-3}$ seconds. The maximum strain rate, which was considered to be the strain rate of the concrete specimen, generally occurred within $0.75 * 10^{-3}$ seconds.

The high speed camera method introduces some error when measuring the width or height of the specimen. This was especially true for the compression tests which were difficult to measure

because the drop weight obstructed the image of the cylinder. Also, the strain rate will be different depending on which location on the cylinder the measurement is made. Generally, the center of the specimen was found to better represent the specimen; however, it is difficult to guarantee that you are measuring the same portion of the cylinder as it breaks. Measuring the change in length on the end (considered for tension tests) or side (considered for compression tests) of the specimen corresponds to a local strain rate. Therefore, the high speed camera method does not represent the overall strain rate of the specimen.

Load Cell Method

The load cell method considers the data collected from the load cells and then applies elastic theory to determine the strain rate for each specimen. The first step in this method is to determine the loading rate. This was done by plotting the filtered load data. For example, Figure 26 shows the filtered load versus time data for a fiber reinforced specimen tested in tension at a drop height of 16 ft (TF16). The load versus time data for the July 2011 tests are given in Appendix C, and for the April 2012 tests in Appendix D. These figures show the individual loads for each load sensor, the total load for all load sensors and the filtered load, which was considered during analysis. The only portion of the graph considered was from initial loading to peak load. The point of initial loading was not always definitive and required some judgment as to where it should begin.

To determine the loading rate, various methods were explored. First, the loading rate in-between each data point was determined. For this approach, the loading rate was considered to be the average of the individual loading rates. Second, a linear regression line was computed, in which the loading rate was taken as the slope of the regression line. Lastly, only the maximum value of the individual loading rates in-between each data point was determined. The first two methods depend on the point of initial loading; the last method does not, making it a more standardized approach. Using the maximum value also proved to be the most consistent among the various tests, therefore, this was the approach used to determine the loading rate for all specimens.

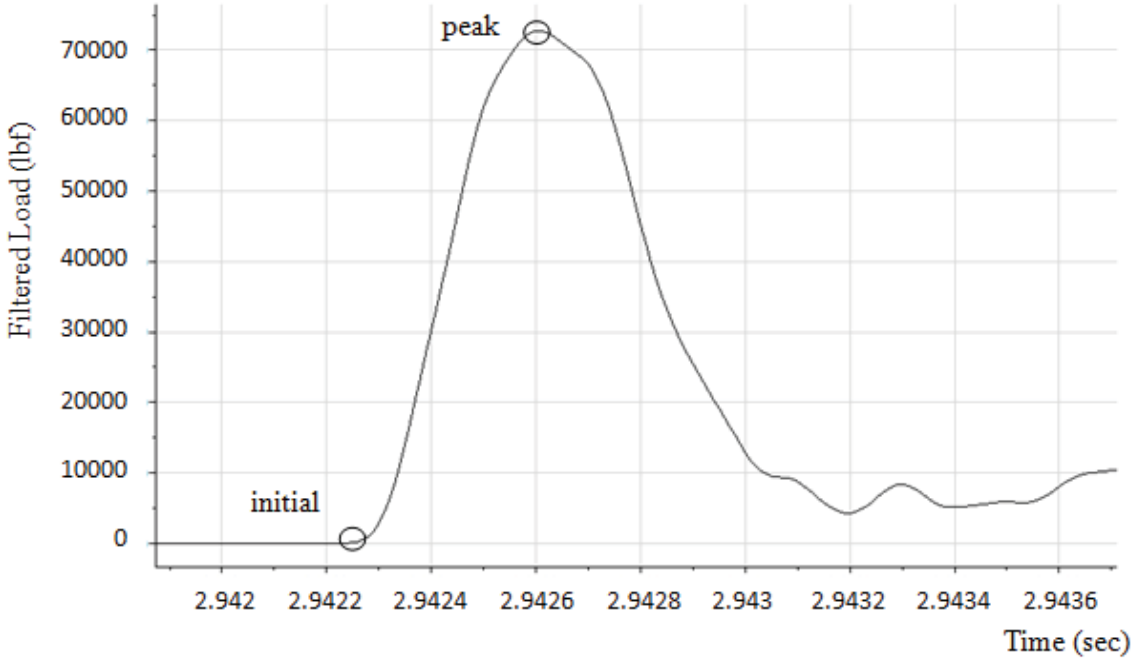

Figure 26 - TF16 Load Data

Once the loading rate (P_R) was determined, elasticity theory was applied. This method assumes that the relationship between stress and strain is linear. To compute the strain rate the compressive strength (f_c') was determined for NWC and FRC specimens. For the July 2011 tests the average compressive strength for CN and CF static tests were computed. For the April 2012, the average compressive strength for CF0-R and CN0-R were computed. These compressive strengths are from the room temperature, compressive static tests, which are most representative of the concrete material and can be used to determine the modulus of elasticity. Assuming the weight of concrete to be normal weight (145 pcf), and f_c' is given in ksi units, Equation (7) was used to determine the modulus of elasticity for NWC and FRC for both July 2011 and April 2012 tests. This equation is used with the assumption that elastic properties of concrete under dynamic loads are similar to those under static loads.

$$E_c = 1746\sqrt{f_c'} \tag{7}$$

The stress rate was then determined using the measured loading rate and the appropriate area according to ASTM standard C496/C496M-04e1 Standard Test Method for Splitting Strength of Cylindrical Concrete Specimens[3] and C39/C39M -09a Standard Test Method for Compressive Strength of Cylindrical Concrete[4]. The area used for tension is half of the side surface area as sown in Figure 27 (a). The area used for compression is the cross sectional area of the cylinder as shown in Figure 27 (b). The stress rate was then determined using the calculated modulus of elasticity and appropriate area. Equation (8) was used for the tension tests and Equation (9) was used for the compression tests. For both equations, D is the cylinder diameter and L is the cylinder height; these equations give the stress rate in (ksi/in.). Finally, stress-strain properties were used to determine the strain rate in (in./in./sec) using Equation (10).

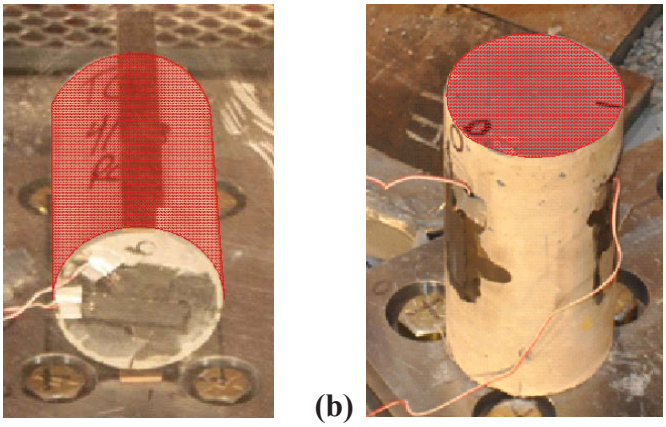

Figure 27 - Area Considered for (a) Tension and (b) Compression

$$\sigma_{R,Tension} = \frac{P_R}{A_{Tension}} = \frac{P_R}{(\pi * D * L)/2} \tag{8}$$

$$\sigma_{R,Compression} = \frac{P_R}{A_{Compression}} = \frac{P_R}{(\pi * D^2)/4} \quad (9)$$

$$\varepsilon_R = \frac{\sigma_R}{E_c} \quad (10)$$

Strain Gauge Method

Depending on the specimen type, compression versus tension test and 16 ft versus 8 ft drop, the strain gauge data varied greatly. Examples of different plots of strain versus time are shown in Figure 28 through Figure 32. Appendix E shows strain graphs for each specimen type.

Some approaches initially taken included: using a moving average from the initial strain to the peak, using an average of the moving average of the first and second portions (shown in Figure 28), using an overall average from initial to peak strain, and using the average of the two slopes where the plot changes from the first to the second portion. In some tests, different approaches were taken depending on the type of data available. The various methods used produced drastically different results within a single specimen and were not repeatable for any given specimen type.

After considering the load cell and high speed camera methods, it was observed that the peak plateau seen in a majority of the strain data was a result of the strain gauge reaching capacity. It was also determined that the data collected, after the strain began to decrease, was representative of the strain rate. For this reason, two new methods for determining the strain rate were considered. First, the strain rate was taken from the point in time when the strain began increasing significantly, all the way to the peak strain. Similarly, the strain rate was determined using the strain rate of the decreasing strain after the plateau was reached. The average of the absolute value of the two strain rates before and after the plateau was then considered to be the true strain rate.

The second method also considered the strain rates before and after the plateau. However, it considered the absolute average of single strain rates one data point prior to and after the plateau. That is, it only considered the second portion of the data. Both of these methods required judgment to determine which time values should be considered and which peak values were most appropriate in cases where the strain gauge did not reach capacity (when there was no plateau). There were also graphs that varied greatly as was shown in Figure 28 through Figure 32. This made it difficult to take a singular and consistent approach in the analysis of the data. However, the first approach had the most consistent results and was determined to be the best method; it was used to determine the strain rate.

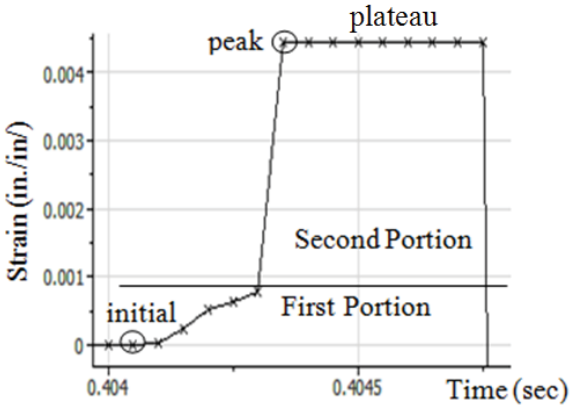

Figure 28 – TF16 Strain Data

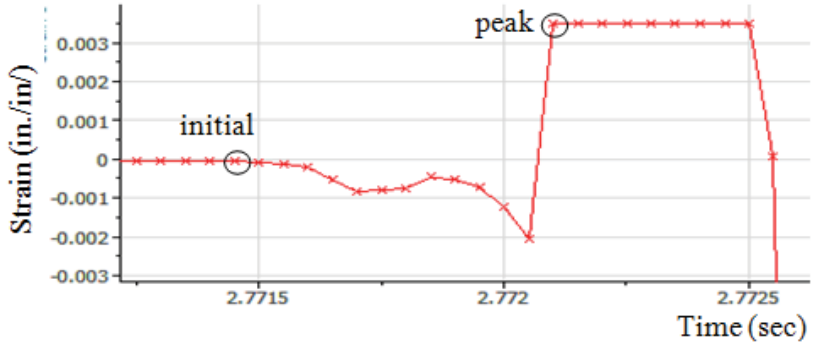

Figure 29 - CF16 Strain Data

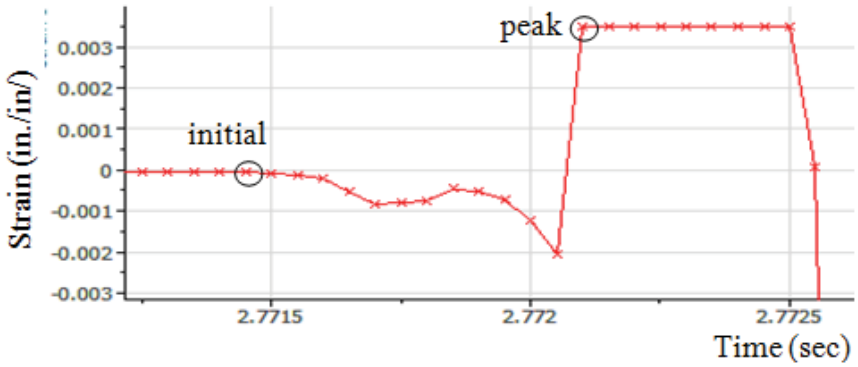

Figure 30 - CF16 Strain Data

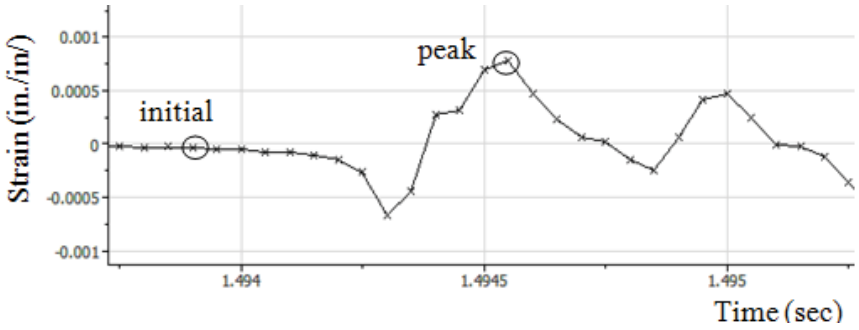

Figure 31 - CN16 Strain Data

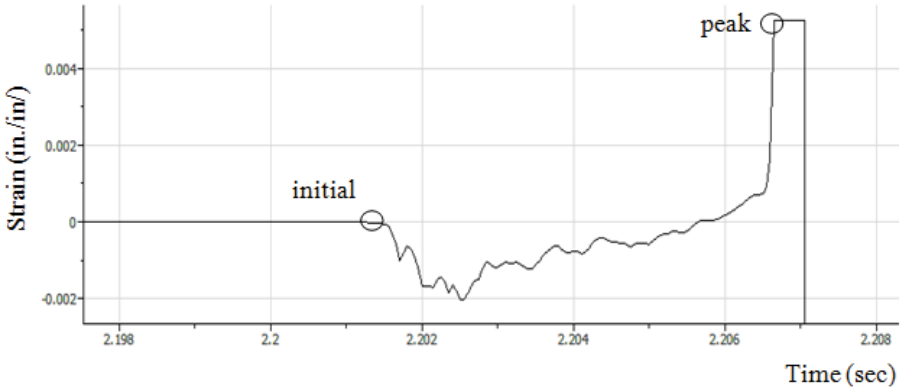

Figure 32 - CF8 Strain Data

Once refined, comparisons between the three methods of determining strain rates were made. Values determined for each method are shown in Table 9 for tests with an 8 ft test height. Tests done with a 16 ft test height are shown in Table 8. These results are also shown graphically in Figure 33, which is a plot of strain rates versus the ratio of dynamic to static load.

From Figure 33 it can be seen that the strain gauge and high speed camera methods for determining the strain rate produced very similar results. This is expected, since both methods represent a local strain rate measured at a similar location on the cylinder. The load cell method had strain rates that were significantly lower than the other two methods. It was also the method that best represented the cylinder as a whole. As a whole, the cylinder would be able to better resist the dynamic impact, thus having a lower strain rate.

For the purpose of these tests, a global representation of the dynamic impact effect is desired. Therefore, the load cell method was used to further analyze the effects of reinforcement and temperature under dynamic loading.

Table 9 – Comparison of Strain Rate Methods for 8 ft Drop Height

	Strain Rates (1/sec)				
Specimen	**Camera**	**Strain Gauge 0**	**Strain Gauge 1**	**Load Cells**	**Maximum Filtered Load vs. Average Static Load**
TF8-1	94	N.A.	N.A.	N.A.	N.A.
TF8-2	95	385	201	1.411	2.432
TF8-3	65	199	199	1.165	2.305
TF8-4	63	386	318	1.115	2.303
TF8-5	95	390	751	1.159	2.348
TF8-6	62	197	N.A.	0.868	1.922
TF8-7	95	N.A.	206	1.105	1.932
TF8-8	63	64	388	1.103	1.812
TF8-9	95	387	N.A.	1.223	1.852
CF8-1	51	308	N.A.	2.206	1.738
CF8-2	25	378	N.A.	4.152	1.528
CF8-3	47	N.A.	202	4.961	1.740
TN8-1	94	208	208	0.512	1.500
TN8-2	126	193	193	0.548	1.987
TN8-3	119	192	192	0.610	2.670
TN8-4	94	200	200	0.872	2.563
TN8-5	95	386	385	0.610	2.768
TN8-6	158	202	202	0.697	2.211
TN8-7	95	198	198	0.883	2.553
TN8-8	94	389	387	0.941	2.546
CN8-1	N.A.	216	N.A.	0.886	0.933
CN8-2	47	392	N.A.	3.152	1.193
CN8-3	31	235	235	1.881	1.205

Table 10 – Comparison of Strain Rate Methods for 16 ft Drop Height

	Strain Rates (1/sec)				
Specimen	**Camera**	**Strain Gauge 0**	**Strain Gauge 1**	**Load Cells**	**Maximum Filtered Load vs. Average Static Load**
TF16-1	95	201	204	0.619	1.621
TF16-2	95	196	N.A.	1.274	2.384
TF16-3	127	386	N.A.	1.225	2.243
TF16-4	96	386	200	1.541	2.694
TF16-5	95	383	198	1.096	2.307
TF16-6	94	202	368	1.237	2.109
TF16-7	95	389	391	0.755	1.766
CF16-1	47	191	191	5.293	2.013
CF16-2	19	252	N.A.	9.429	2.328
CF16-3	48	209	243	5.551	1.893
TN16-1	157	388	N.A.	0.845	2.310
TN16-2	126	202	235	1.780	4.031
TN16-3	95	202	392	1.231	4.124
TN16-4	94	379	193	1.599	3.757
TN16-6	157	N.A.	N.A.	N.A.	N.A.
TN16-7	119	214	209	N.A.	N.A.
TN16-8	95	217	204	1.339	2.970
TN16-9	125	199	200	1.112	3.262
CN16-1	46	209	N.A.	3.761	1.536
CN16-2	24	543	203	4.945	1.979
CN16-3	47	342	363	5.259	1.977

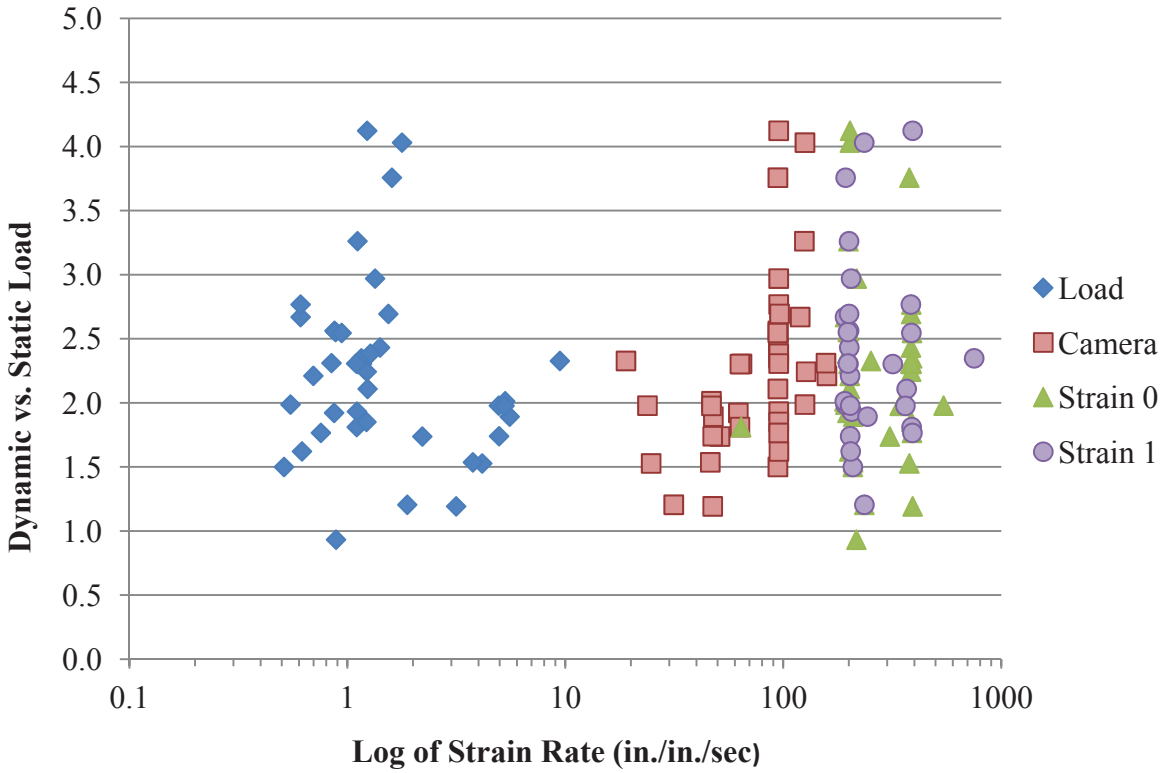

Figure 33 – Comparison of Strain Rate Methods

Results

In several cases, comparisons had to be made between tests when different drop weights were used. For example, the drop weight for CN8 was 92 lbf in July 2011, whereas it was 223 lbf in April 2012. To evaluate the effect of the drop weight, the NWC room temperature tests from July 2011 were compared to the same tests performed in April 2012. For all tests the drop weights were increased from July 2011 to April 21012. It is important to know the significance of the change in drop weight to determine if proper comparisons can be made where only one variable is a consideration.

The compression tests in July 2011 had a compressive strength of 10,900 psi, whereas the April 2012 tests had a compressive strength of 11,000 psi. Similarly, the tension test strengths were 520 psi in July 2011 and 470 psi in April 2012. The strength of the concrete did not change significantly between the two test dates and is therefore not considered to be a variable. Similar results were also found for the FRC specimens.

The CN8 test drop weights increased from 92 lbf in July 2011 to 223 lbf in April 2012. The average DIF increased from 1.1 during July 2011 to 1.5 during April 2012. For the CN16 specimens the drop weight increased from 70.5 to 136 lbf in April 2012. The average DIF increased from 1.8 to 2.8.

The changes in drop weight for the tension tests were less extensive than the compression tests. For TN8 tests the drop weight increased from 70.5 to 92 lbf. This decreased the average DIF

from 2.4 to 1.4. For the TN16 tests the drop weight increased from 49.5 to 53.5 lbf. This decreased the DIF from 3.4 to 2.2.

The result of increasing the drop weight by 142% for the CN8 tests had a similar effect as increasing the drop weight by 8% for the TN16 tests. Since a direct correlation between drop weights and resulting DIF and strain rates were not observed between the July 2011 and April 2012, test types with different drop weight are believed to be comparable. To better compare test results and demonstrate the testing conditions the drop energy in terms of kinetic energy is given along with the test results.

To summarize the dynamic test results, the DIFs are compared visually with the strain rates in Figure 34 for the July 2011 tests and in Figure 35 for the April 2012 tests. Similar drop hammer research has been conducted to determine the relationship between strain rate and DIF, a summary of which is shown in Figure 36. Malvar and Ross[7] summarized and compared the results from several dynamic impact tests using different loading procedures on various specimen sizes. Mellinger and Birkimer tested 10.25 in. long by 2 in. diameter specimens, Birkimer tested 35 in. long by 2 in. diameter specimens, and Ross tested specimens with diameters ranging from 0.75 to 2 in. and length ranging from 2 to 3 in.

In addition, Millar, Molyneaux and Barnett[8] performed dynamic flexural and shear tests on 11.0 x 2.8 x 2.8 in. beams and 13.8 x 3.9 x 2.0 in. beams. A summary of their results is shown in Figure 37. All previous research found regarding dynamic impact factors on concrete used various specimen sizes. No other drop hammer tests used 4 in. diameter by 8 in. long cylinders. Models for determining DIFs based on strain rates have been produced by Malvar and Ross[7] and the Comité Euro-International du Béton (CEB)[9]. One model for compression was formulated by the CEB and is shown graphically along with compression test results from July 2011 and April 2012 in Figure 38. For the tension tests, two models were given: the CEB model and the Modified CEB model by Ross. Both of these models, as well as the tension results for July 2011 and April 2012, are given in Figure 39.

For the tension tests, it can be seen that the majority of the data follows closely the trend of the Modified CEB model for tension. The Modified CEB model is a much better representation of the results than the CEB Model. The Modified CEB model conservatively predicts lower DIF than those determined from the test results. This is true with the exception of several heated test specimens. A couple of TN16-400 and TN8-400 specimens had lower DIF than what was predicted by the model. However, it can be seen that specimens of these same categories had DIF well above the model prediction. This shows the wide variability of results produced by the heated cylinders. A single TF8-400 specimen even had a DIF lower than 1.0, which in this case is considered to be an outlier.

The results of the dynamic compression tests, when compared to the static compression tests performed without steel caps, follow the trend of increasing DIF with increasing strain rate given by the CEB model for compression. The results show that the CEB model is much more conservative than the Modified CEB model for tension. However, in some instances, at lower strain rates, the model is slightly un-conservative. The single CN8 specimen with a DIF less than 1.0 is considered to be an outlier.

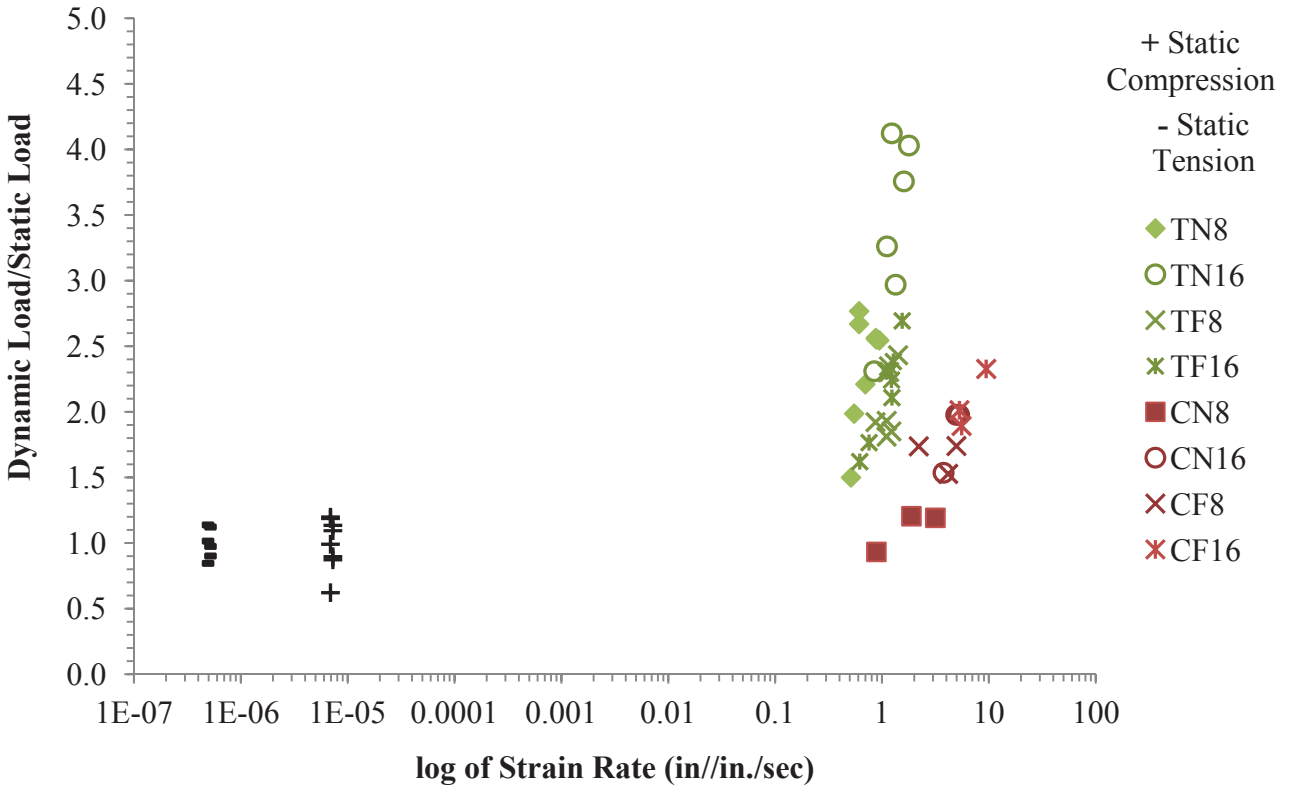

Figure 34 - Dynamic Increase Factor vs. Strain Rate for July 2011

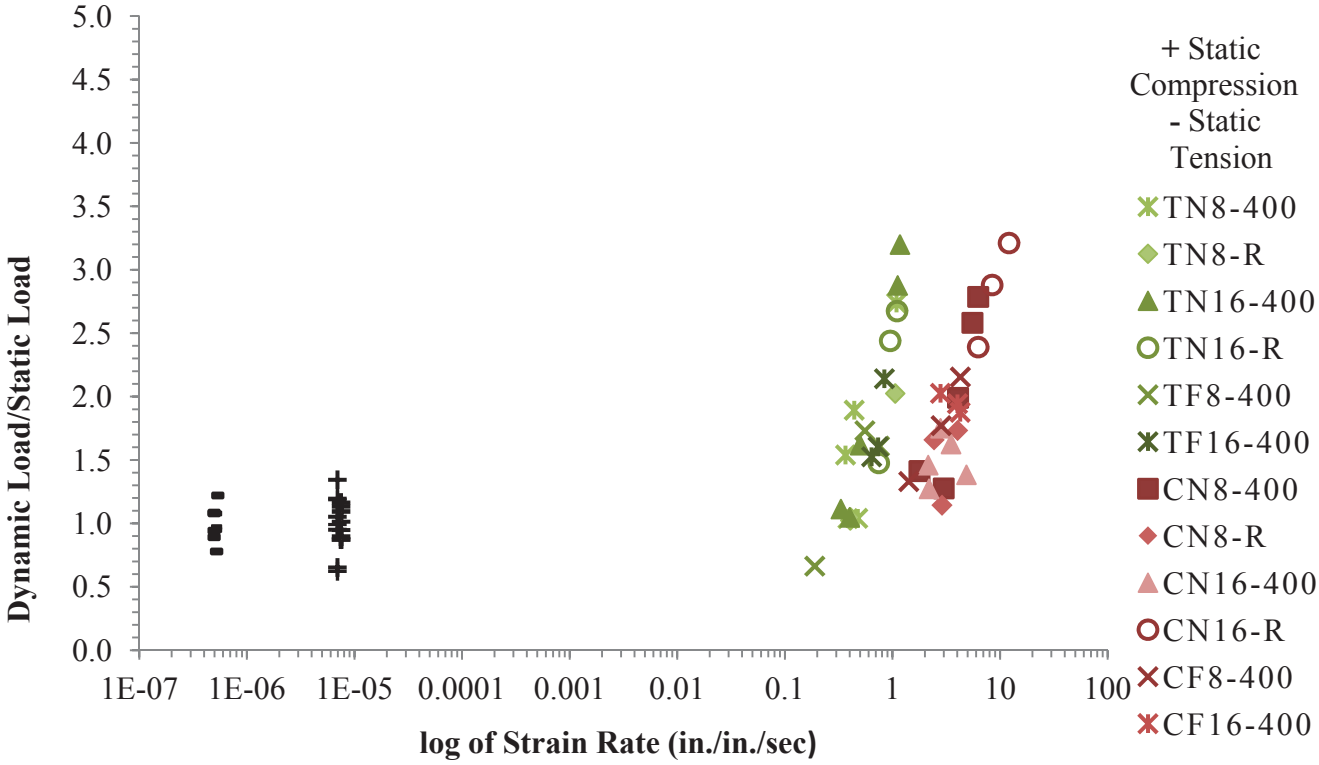

Figure 35 - Dynamic Increase Factor vs. Strain Rate for April 2012

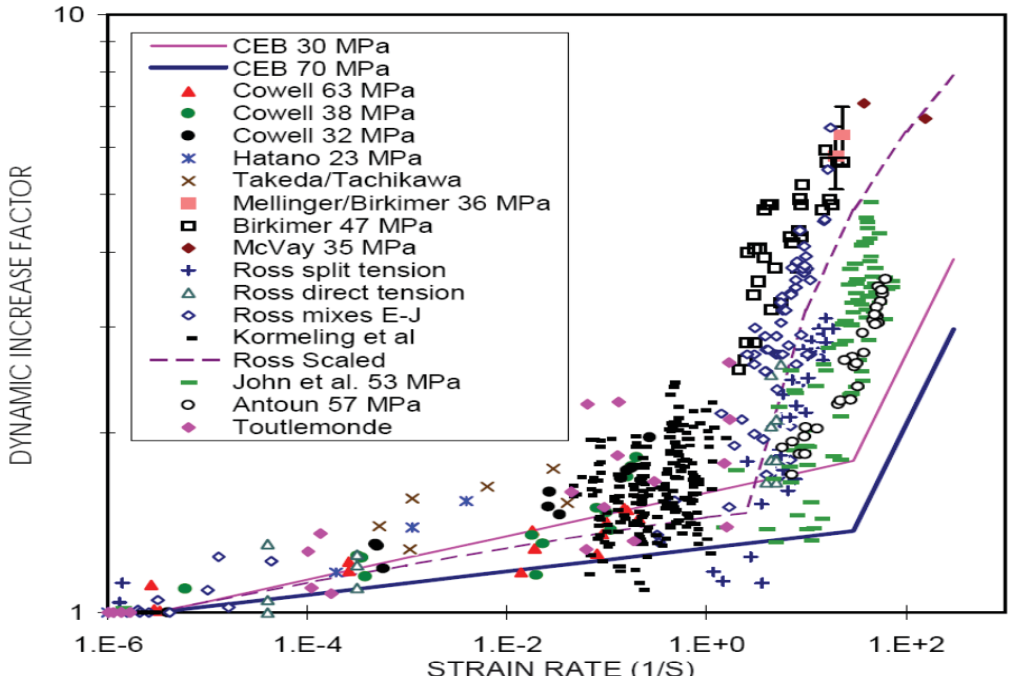

Figure 36 – Malvar and Ross's Comparison of Strain Rate Effects for Concrete in Tension[7]

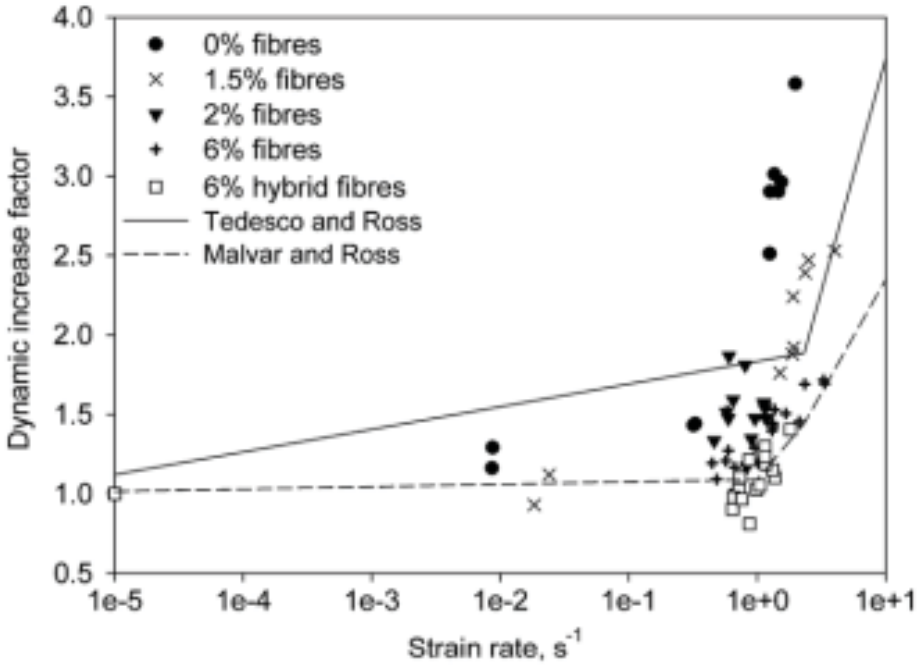

Figure 37 – Millard, Molyneaux and Barnett's Dynamic Increase Factor of Maximum Load with Strain[8]

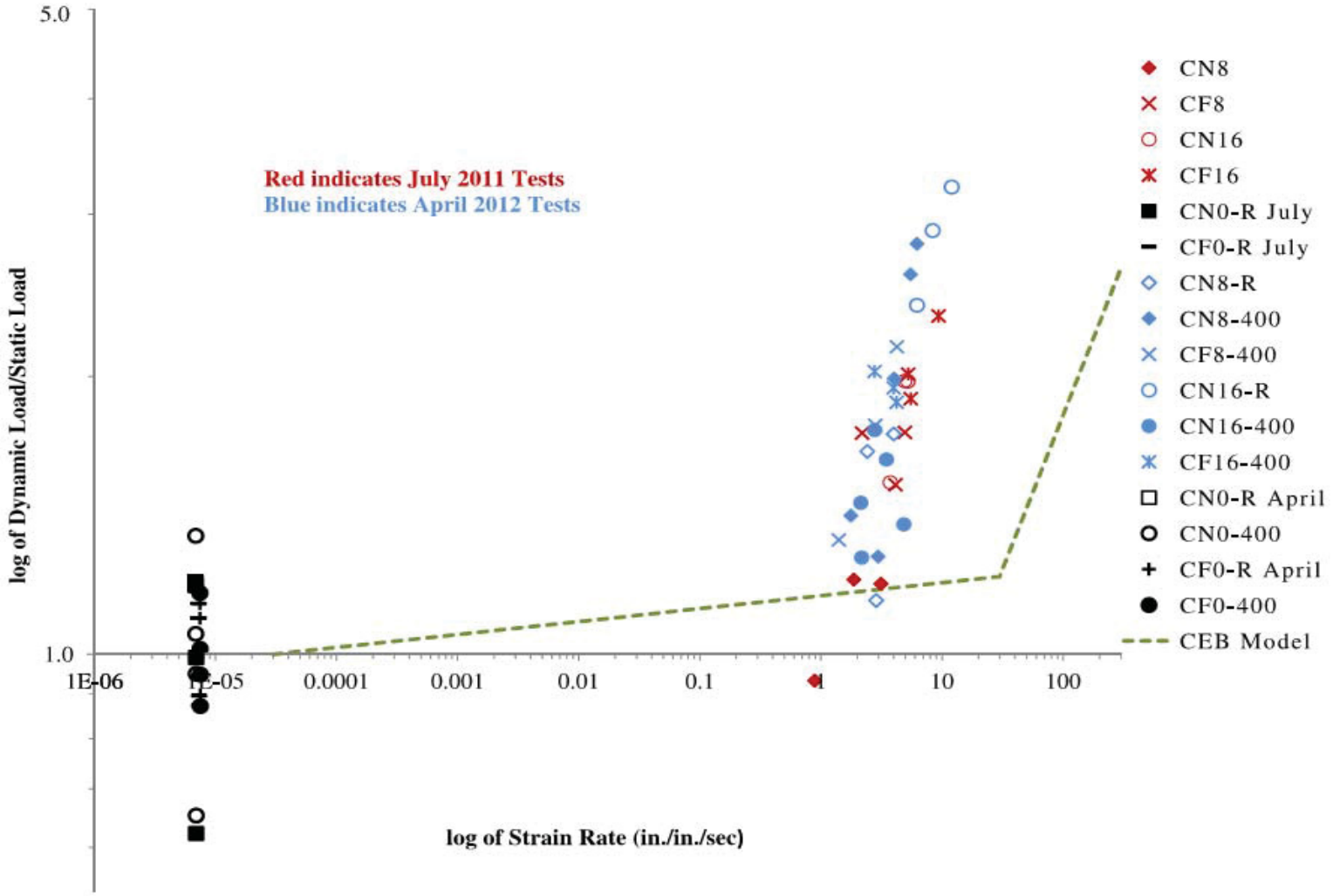

Figure 38 - Compression Dynamic Increase Factor vs. Strain Rate

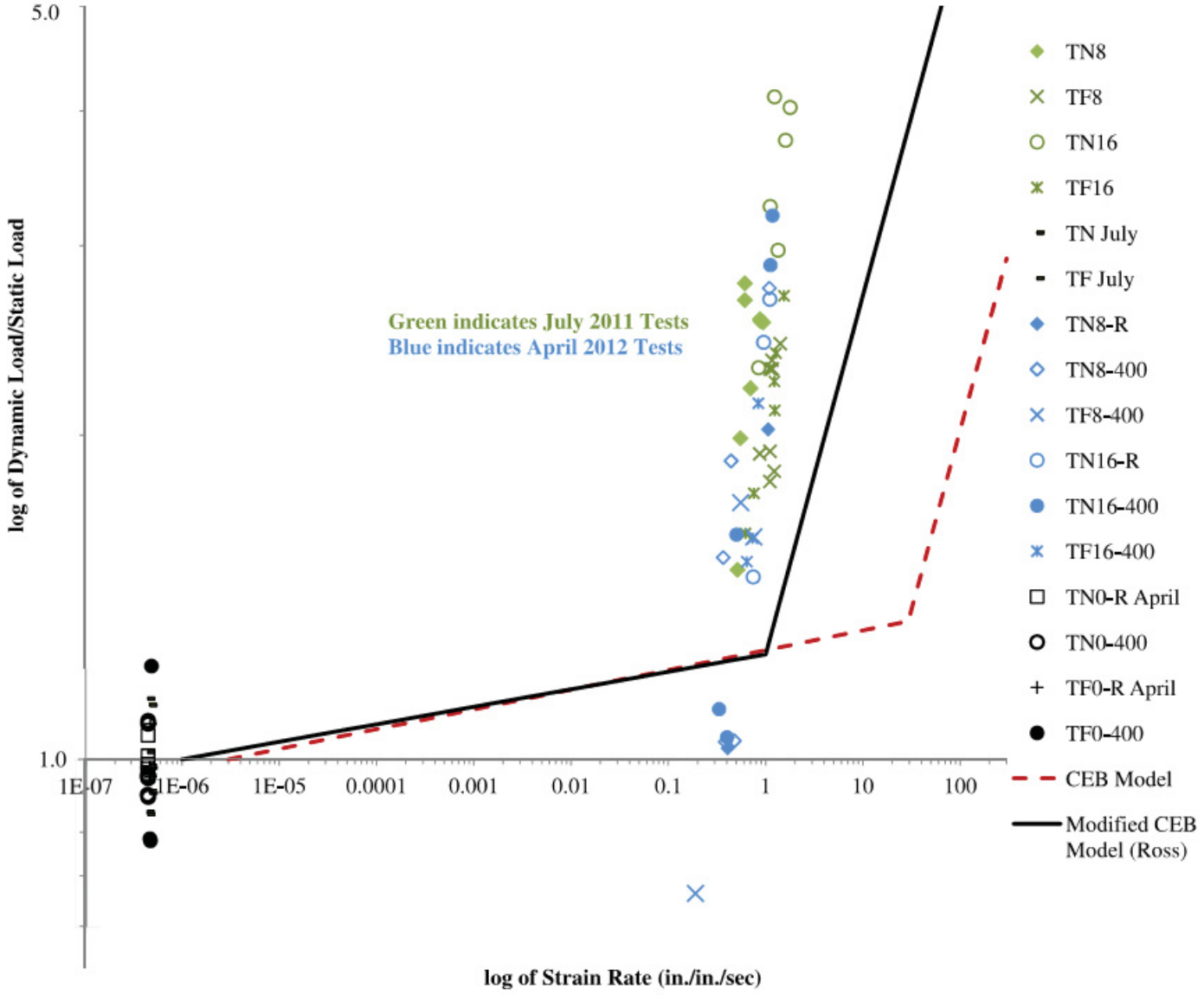

Figure 39 - Tension Dynamic Increase Factor vs. Strain Rate

Additional DIF versus strain rate graphs are shown in Appendix F. These graphs are shown to better compare the results of individual variables. For example, a plot of the tension tests at 400°F is given to compare the results of NWC and FRC, thus comparing the effects of fiber reinforcement at elevated temperatures. These graphs can be used to better understand the results for each individual variable. These graphs also show the CEB and Modified CEB (Ross) models for further comparison with former research results.

To review the results of the drop hammer tests more extensively, comparisons were made between drop heights of 8 ft and 16 ft for NWC and FRC at room temperature and between drop height of 8 ft and 16 ft for NWC and FRC at elevated temperatures. Comparisons were also made between NWC and FRC at room temperature and between NWC and FRC at elevated temperatures. Finally, comparisons were made between room and elevated temperatures for both NWC and FRC. For each dynamic tests specimen type, load versus time data is shown in Appendix C for July 2011 and in Appendix D for April 2012 tests. Appendix A and B also provide visual results for July 2011 and April 2012 static and dynamic tests.

Drop Height at Room Temperature

Results for the July 2011 tests are shown in Table 11 for static tests, and

Table 12 for dynamic tests with an 8 ft drop height and

Table 13 for dynamic tests with a 16 ft drop height. When comparing results, average DIFs are reported for each specimen type. Note that in some cases this average is taken from the results of only three tests. Therefore, the range of values can be significant; refer to the results tables for more comprehensive results.

The impact energy, as previously discussed, is a function of drop height and drop weight. It is used to better understand and compare the test parameters for each specimen type. To determine the effect of the impact energy on DIF at room temperature, results from NWC specimens are compared. The TN8 specimens, having an impact energy of 492 ft-lbf, had an average DIF of 2.4. For the TN16 specimens, which had an impact energy of 734 ft-lbf, the average DIF increased to 3.4 in./in./sec.

The CN8 specimens, having an impact energy of 643 ft-lbf, had an average DIF of 1.1. For the CN16 specimens, which had an impact energy of 1046 ft-lbf, the average DIF increased to 1.8.

The DIF for tension increased by 45% when the impact energy increased by 49%. Likewise, the DIF for compression increased by 65% when the impact energy increased by 62%. From these

results, it can be seen that the increase in DIF is nearly equivalent to the increase in impact energy for both compression and tension NWC specimens.

The change in impact energy is also compared for FRC specimens. The TF8 specimens, having an impact energy of 643 ft-lbf, had an average DIF of 2.1. The TF16 specimens, having an impact energy of 734 ft-lbf, had a similar average DIF of 2.2. The increase in impact energy from the TF8 to the TF16 specimens was about 14%, which, as can be seen had little effect on the DIF. From these results it can be concluded that similar impact energies produce similar results. Thus, it is important to consider both drop height and drop weight when comparing results of drop hammer tests.
The CF8 specimens, having an impact energy of 1104 ft-lbf, had an average DIF of 1.7. For the CF16 specimens, which had an impact energy of 1364 ft-lbf, the average DIF increased to 2.1 in./in./sec. The increase in impact energy from the CF8 to the CF16 specimens was about 24%; this resulted in a 25% increase in the average DIF. Similar to the NWC results, the increase in impact energy is nearly equivalent to the increase in DIF for FRC compression specimens. In Figure 40 and Figure 41 plots of impact energy versus DIF are given for compression and tension tests respectively. These plots summarize the relationships that have been discussed in the section.

Table 11 - July 2011, Static Test Results

Specimen ID	Strain Rates (in/in/sec)	Strength (psi)	Maximum Load (lbf)	Equivalent 4x8 Maximum Load (lbf)	Maximum Load/Maximum Average Load
TF-1	4.70E-07	592	29737	N.A.	0.975
TF-2	4.70E-07	682	34260	N.A.	1.123
TF-3	4.70E-07	548	27531	N.A.	0.902
Average		**607**	**30509**		
CF-1	-	9706	-	-	-
CF-2	-	9863	-	-	-
CF-3	-	10207	-	-	-
Average		**9926**			
CF0-R-6-1*	7.27E-06	4042	114290	50796	1.095
CF0-R-6-2*	7.27E-06	3312	93636	41616	0.897
CF0-R-6-3*	7.27E-06	4191	118504	52669	1.135
CF0-R-6-4*	7.27E-06	3225	91194	40531	0.873
Average		**3693**	**104406**	**46403**	
TN-1	4.46E-07	399	20071	N.A.	0.846
TN-2	4.46E-07	479	24093	N.A.	1.015
TN-3	4.46E-07	538	27024	N.A.	1.139
Average		**472**	**23729**		
CN-1	-	11130	-	-	-
CN-2	-	10951	-	-	-
CN-3	-	11008	-	-	-

Average		11030			
CN0-R-6-1*	6.89E-06	4563	129014	57340	1.198
CN0-R-6-2*	6.89E-06	2370	67007	29781	0.622
CN0-R-6-3*	6.89E-06	3776	106774	47455	0.992
CN0-R-6-4*	6.89E-06	4520	127804	56802	1.187
Average		3807	107650	47844	

Table 12 - July 2011, 8 ft Test Results

Specimen ID	Strain Rate (in./in./sec)	Maximum Dynamic Load (lbf)	Average Maximum Static Load (lbf)	Dynamic/Static Load
TF8-1	N.A.	N.A.	30509	N.A.
TF8-2	1.411	74207		2.432
TF8-3	1.165	70312		2.305
TF8-4	1.115	70267		2.303
TF8-5	1.159	71637		2.348
TF8-6	0.868	58642		1.922
TF8-7	1.105	58950		1.932
TF8-8	1.103	55272		1.812
TF8-9	1.223	56488		1.852
CF8-1	2.206	80629	46403	1.738
CF8-2	4.152	70883		1.528
CF8-3	4.961	80755		1.740
TN8-1	0.512	35595	23729	1.500
TN8-2	0.548	47150		1.987
TN8-3	1.111	63353		2.670
TN8-4	0.872	60822		2.563
TN8-5	0.610	65674		2.768
TN8-6	0.697	52474		2.211
TN8-7	0.883	60578		2.553
TN8-8	0.941	60412		2.546
CN8-1	0.886	44634	47844	0.933
CN8-2	3.152	57063		1.193
CN8-3	1.881	57661		1.205

Table 13 - July 2011, 16 ft Test Results

Specimen ID	Strain Rate (in./in./sec)	Maximum Dynamic Load (lbf)	Average Maximum Static Load (lbf)	Dynamic/Static Load
TF16-1	0.619	49465	30509	1.621
TF16-2	1.274	72727		2.384
TF16-3	1.225	68444		2.243
TF16-4	1.541	82205		2.694
TF16-5	1.096	70384		2.307
TF16-6	1.237	64349		2.109
TF16-7	0.755	53882		1.766
CF16-1	5.293	93409	46403	2.013
CF16-2	9.429	108006		2.328
CF16-3	5.551	87833		1.893
TN16-1	0.845	54825	23729	2.310
TN16-2	1.780	95652		4.031
TN16-3	1.231	97850		4.124
TN16-4	1.599	89158		3.757
TN16-6	N.A.	N.A.		N.A.
TN16-7	N.A.	N.A.		N.A.
TN16-8	1.339	70477		2.970
TN16-9	1.112	77400		3.262
CN16-1	3.761	73496	47844	1.536
CN16-2	4.945	94661		1.979
CN16-3	5.259	94585		1.977

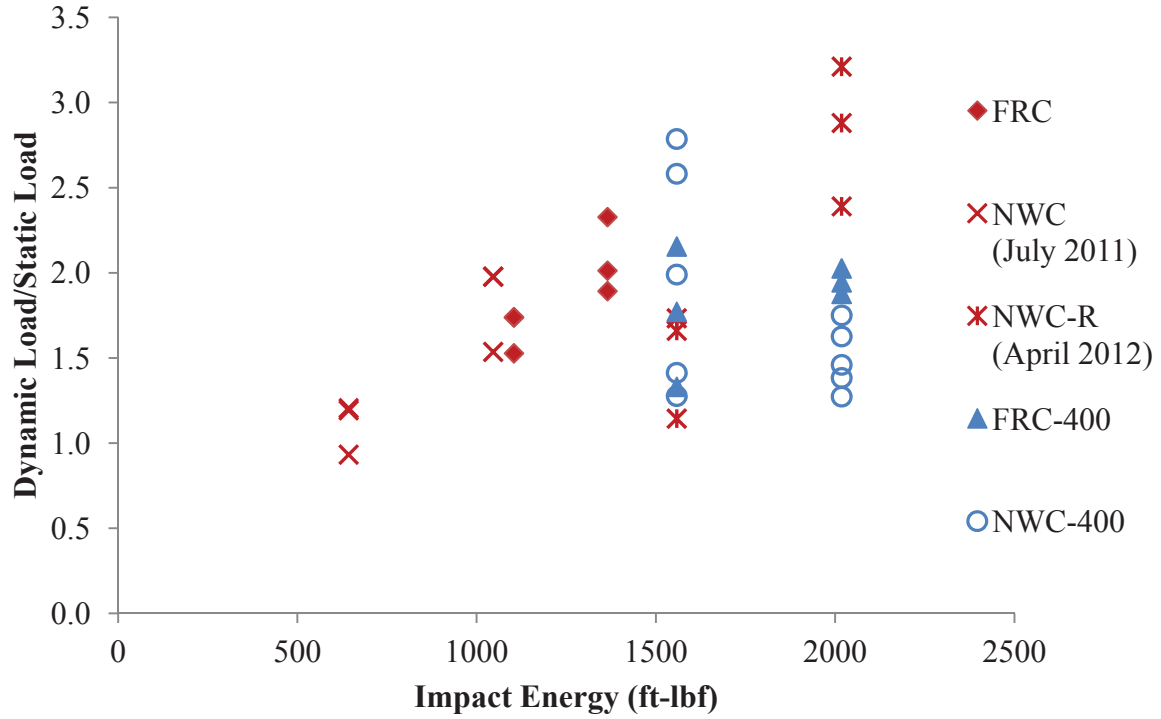

Figure 40 – Compression Dynamic Increase Factor vs. Impact Energy

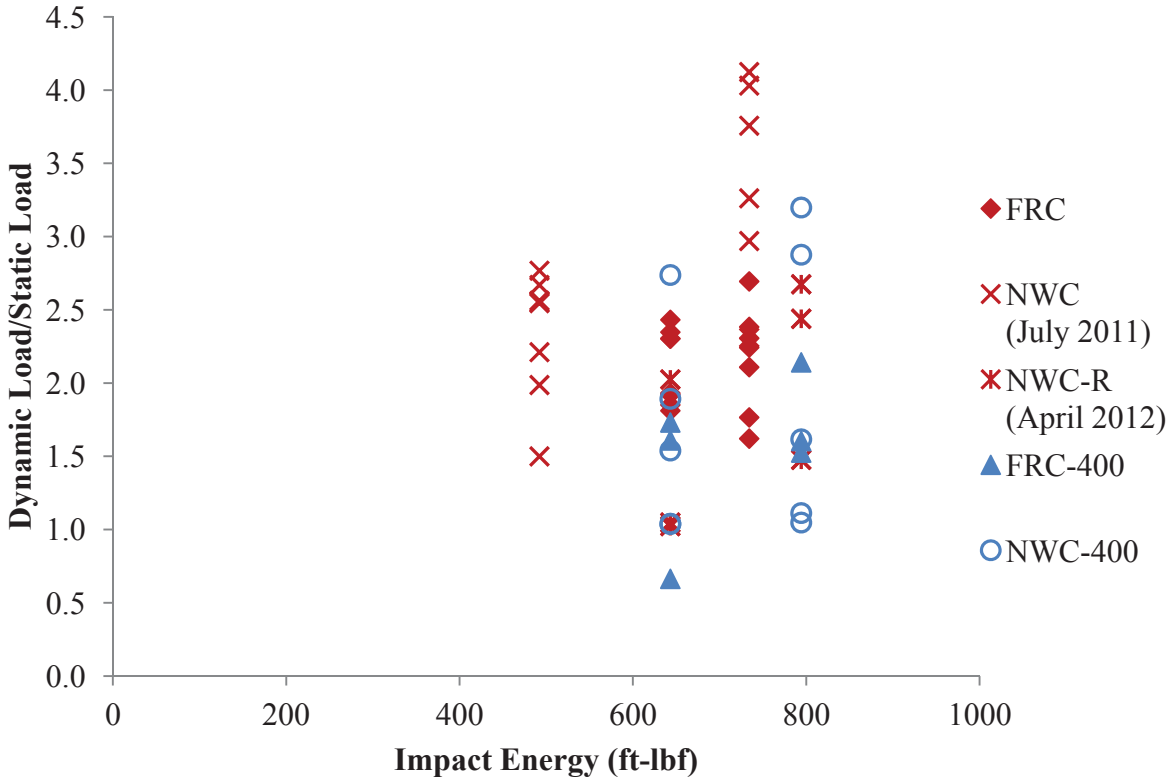

Figure 41 - Tension Dynamic Increase Factor vs. Impact Energy

Drop Height at Elevated Temperature

Results for the April 2012 tests are shown in Table 14 and Table 15 for static tests, and Table 16 for dynamic tests with an 8 ft drop height and Table 17 for dynamic tests with a 16 ft drop height. To determine the effects of the drop height at elevated temperature, NWC concrete specimens are compared. The TN8-400 specimens, which had an impact energy of 643 ft-lbf, had an average DIF of 1.7. For the TN16-400 specimens which had an impact energy of 79 ft-lbf, the average DIF increased to 2.0.

The CN8-400 specimens, which had an impact energy of 1558 ft-lbf, had an average DIF of 2.0. For the CN16-400 specimens, which had an impact energy of 2018 ft-lbf impact energy, the average DIF decreased to 1.5 in./in./sec.

For heated NWC tension specimens, a 24% increase in impact energy resulted in a 20% increase in DIF. The increase in DIF was similar to the increase in impact energy for the room temperature NWC tension specimens. In contract, for the heated NWC compression specimens, the DIF decreased by 25% when the impact energy increase by 30%. Therefore, it can be concluded that heated NWC, when tested in compression, has lower strength results at higher impact energies.

The change in drop height is also compared for elevated temperature FRC specimens. The TF8-400 specimens, having an impact energy of 643 lbf, had an DIF of 1.3. For the TF16-400 specimens, which had an impact energy of 794 ft-lbf, the average DIF increased to 1.8.

The CF8-400 specimens, having an impact energy of 1558 ft-lbf, had an average DIF of 1.8. For the CN16-400 specimens, which had an impact energy of 2018 ft-lbf the average DIF increased slightly to 1.9 in./in./sec.

For heated FRC tension specimens, a 24% increase in impact energy resulted in a 32% increase in average DIF. For the heated FRC compression specimens, a 30% increase in average impact energy resulted in a 11% increase in DIF. In comparison, when similar increases in impact energy were applied, the strength results for the heated FRC tension specimens increased at a higher percentage than the compression specimens. This was also true for the NWC, which actually had a reduction in strength results.

Comparing test drop heights, and thus impact energies, is another way of comparing the effects of strain rate. The results explained in these last two sections on the effect of impact energy are similar to explaining how the strain rate affects the DIF. The CEB, and modified CEB models, as shown in Figure 38 and Figure 39, provide a correlation between strain rates and DIFs for both compression and tension. In addition, Figure 42 and Figure 43 show the relationship of strain rate versus impact energy for compression and tension tests respectively.

Table 14 - April 2012, Static Test Results for Fiber Reinforced Concrete

Specimen ID	Strain Rates (in/in/sec)	Strength (psi)	Maximum Load (lbf)	Equivalent 4x8 Maximum Load (lbf)	Maximum Load/Maximum Average Load
TF0-400-4-1	4.85E-07	541	27173	N.A.	1.221
TF0-400-6-1	4.72E-07	345	39028	17346	0.779
Average		**443**	**33101**	**22259**	
TF0-R-6-1	4.72E-07	588	66462	29539	0.972
TF0-R-6-2	4.72E-07	574	64951	28867	0.949
TF0-R-6-3	4.72E-07	653	73822	32810	1.079
Average		**605**	**68412**	**30405**	
CF0-400-4-1	-	5107	-	-	-
CF0-400-4-2	-	5316	-	-	-
CF0-400-6-1	-	5336	-	-	-
Average		**5253**			
CF0-400-6-1**	7.49E-06	2166	61251	27223	1.014
CF0-400-6-2**	7.49E-06	1863	52687	23416	0.872
CF0-400-6-3**	7.49E-06	2026	57272	25454	0.948
CF0-400-6-4**	7.49E-06	2490	70403	31290	1.166
Average		**2136**	**60403**	**26846**	
CF0-R-6-1	-	9468	-	-	-
CF0-R-6-2	-	9791	-	-	-
CF0-R-6-3	-	8756	-	-	-
Average		**9338**			
CF0-R-6-1*	7.49E-06	4042	114290	50796	1.095
CF0-R-6-2*	7.49E-06	3312	93636	41616	0.897
CF0-R-6-3*	7.49E-06	4191	118504	52669	1.135
CF0-R-6-4*	7.49E-06	3225	91194	40531	0.873
Average		**3693**	**104406**	**46403**	

*Tested without steel caps in December 2012
**Tested without steel caps in February 2013

Table 15 - April 2012, Static Test Results for Normal Weight Concrete

Specimen ID	Strain Rates (in/in/sec)	Strength (psi)	Maximum Load (lbf)	Equivalent 4x8 Maximum Load (lbf)	Maximum Load/Maximum Average Load
TN0-400-4-1	4.48E-07	430	21637	N.A.	1.086
TN0-400-4-2	4.48E-07	374	18811	N.A.	0.944
TN0-400-4-3	4.48E-07	428	21505	N.A.	1.079
TN0-400-4-4	4.48E-07	353	17764	N.A.	0.891
Average		**396**	**19929**		
TN0-R-4-1	4.48E-07	525	26375	N.A.	1.008
TN0-R-4-2	4.48E-07	548	27554	N.A.	1.053
TN0-R-4-3	4.48E-07	513	25786	N.A.	0.985
TN0-R-4-4	4.48E-07	496	24956	N.A.	0.954
Average		**521**	**26168**		
CN0-400-4-1	-	8270	-	-	-
CN0-400-4-2	-	8154	-	-	-
CN0-400-4-3	-	7021	-	-	-
CN0-400-4-4	-	8174	-	-	-
Average		**7905**			
CN0-400-6-1**	6.93E-06	3051	86264	38340	1.053
CN0-400-6-2**	6.93E-06	1892	53493	23775	0.653
CN0-400-6-3**	6.93E-06	3897	110187	48972	1.344
CN0-400-6-4**	6.93E-06	2754	77873	34610	0.950
Average		**2899**	**81954**	**36424**	
CN0-R-4-1	-	9939	-	-	-
CN0-R-4-2	-	10872	-	-	-
CN0-R-4-3	-	11145	-	-	-
CN0-R-4-4	-	11718	-	-	-
Average		**10919**			
CN0-R-6-1*	6.93E-06	4563	129014	57340	1.198
CN0-R-6-2*	6.93E-06	2370	67007	29781	0.622
CN0-R-6-3*	6.93E-06	3776	106774	47455	0.992
CN0-R-6-4*	6.93E-06	4520	127804	56802	1.187
Average		**3807**	**107650**	**47844**	

*Tested without steel caps in December 2012
**Tested without steel caps in February 2013

Table 16 - April 2012, 8 ft Test Results

Specimen ID	Strain Rate (in./in./sec)	Maximum Dynamic Load (lbf)	Average Maximum Static Load (lbf)	Dynamic/Static Load
TF8-400-4-1	0.757	35821	22259	1.609
TF8-400-4-2	0.189	14770		0.664
TF8-400-4-3	0.553	38541		1.731
CF8-400-4-1	2.829	47549	26846	1.771
CF8-400-4-2	1.415	35723		1.331
CF8-400-4-3	4.271	57847		2.155
TN8-400-4-1	0.366	30687	19929	1.540
TN8-400-4-2	0.385	20689		1.038
TN8-400-4-3	0.441	37728		1.893
TN8-400-4-4	0.475	20738		1.041
TN8-400-4-5	1.090	54574		2.738
TN8-R-4-1	0.405	26799	26168	1.024
TN8-R-4-2	1.059	52990		2.025
TN8-R-4-3	0.406	27420		1.048
CN8-400-4-1	6.251	101491	36424	2.786
CN8-400-4-2	1.781	51476		1.413
CN8-400-4-3	5.530	94046		2.582
CN8-400-4-4	4.060	72496		1.990
CN8-400-4-5	2.987	46496		1.277
CN8-R-4-1	2.880	54744	47844	1.144
CN8-R-4-2	4.024	82929		1.733
CN8-R-4-3	2.430	79404		1.660

Table 17 - April 2012, 16 ft Test Results

Specimen ID	Strain Rate (in./in./sec)	Maximum Dynamic Load (lbf)	Average Maximum Static Load (lbf)	Dynamic/Static Load
TF16-400-4-1	0.735	35715	22259	1.605
TF16-400-4-2	0.840	47664		2.141
TF16-400-4-3	0.639	33964		1.526
CF16-400-4-1	2.792	54394	26846	2.026
CF16-400-4-2	4.250	50369		1.876
CF16-400-4-3	4.012	52201		1.944
TN16-400-4-1	0.400	20896	19929	1.049
TN16-400-4-2	0.331	22187		1.113
TN16-400-4-3	1.172	63753		3.199
TN16-400-4-4	0.500	32222		1.617
TN16-400-4-5	1.117	57333		2.877
TN16-R-4-1	0.951	63837	26168	2.440
TN16-R-4-2	0.744	38653		1.477
TN16-R-4-3	1.102	69992		2.675
CN16-400-4-1	4.865	50390	36424	1.383
CN16-400-4-2	3.495	59244		1.626
CN16-400-4-3	2.184	46375		1.273
CN16-400-4-4	2.147	53176		1.460
CN16-400-4-5	2.794	63759		1.750
CN16-R-4-1	12.103	153630	47844	3.211
CN16-R-4-2	6.254	114367		2.390
CN16-R-4-3	8.429	137804		2.880
CN16-cooled-4-1	4.006	87321	N/A	N/A
CN16-cooled-4-2	4.843	109316		N/A
CN16-cooled-4-3	4.794	98173		N/A

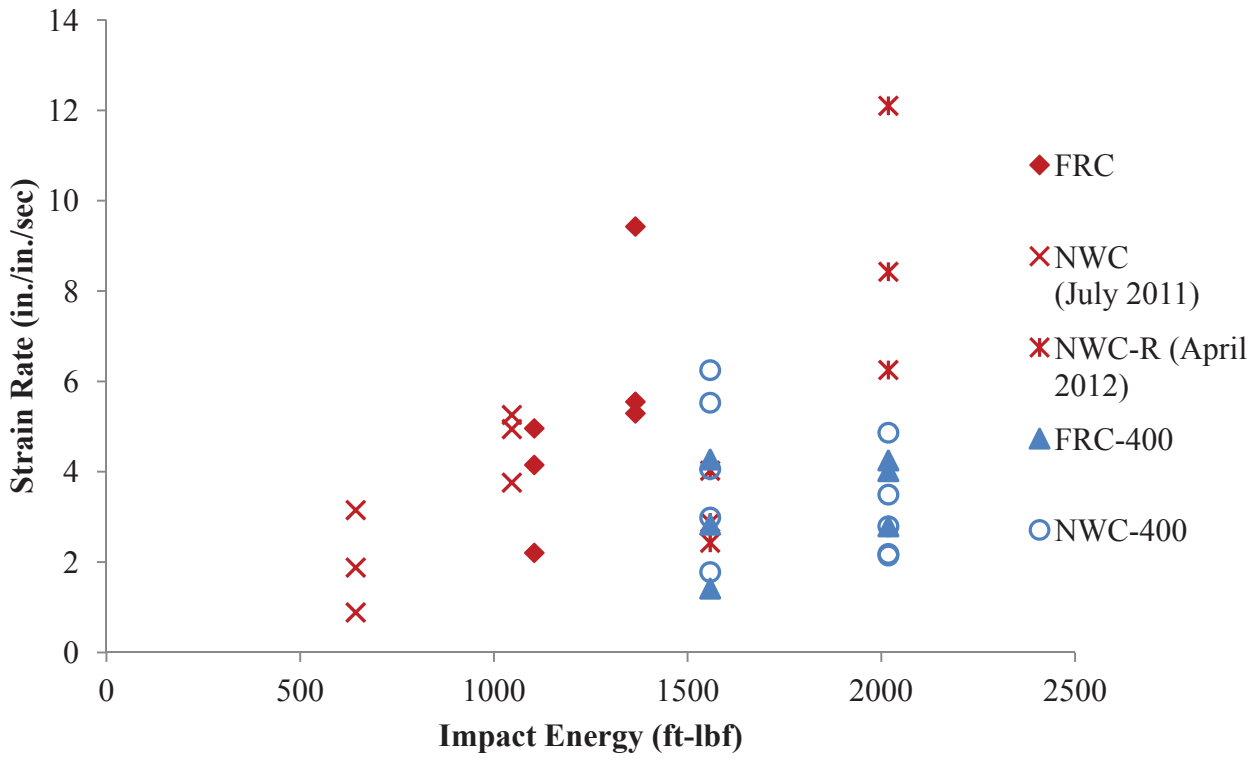

Figure 42 - Compression Strain Rate vs. Impact Energy

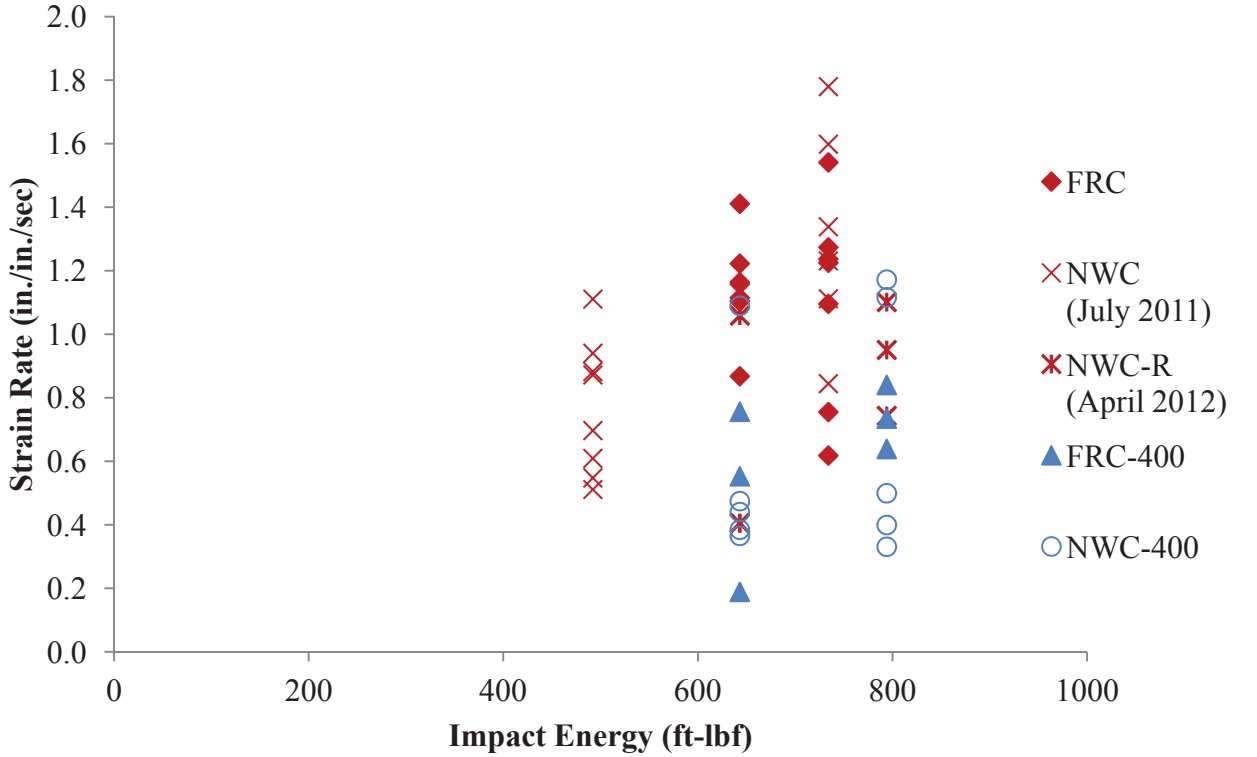

Figure 43 - Tension Strain Rate vs. Impact Energy

Concrete Composition at Room Temperature

To compare the results of FRC specimens with NWC specimens, compression tests performed at room temperature are evaluated. For CN8 specimens the average DIF was 1.1, which increased by 50% to 1.7 for CF8 specimens. This increase may in part be due to the increased impact energy from 643 ft-lb for NWC specimens to 1104 ft-lbf for FRC specimens; an increase of 72%.

The change in impact energy was less extensive for compression tests with a drop height of 16 ft. The impact energy increased from 1046 ft-lbf for CN16 specimens to 1365 ft-lbf for CF16; an increase of 30%.The CN16 specimens had an average DIF of 1.8 which increased by 14% to 2.1 for CF16 specimens.

To draw a conclusion regarding the effects of FRC when tested in compression, comparisons must be made between the percent increase in DIF and impact energy. In the case of the 8 ft drop height specimens, the DIF increased be only 50% from NWC to FRC, whereas the impact energy increased by 72%. In the case of the 16 ft drop height specimens, the DIF increased by only 14% from NWC to FRC, whereas the impact energy increased by 30%. In both cases the increase in DIF is less than the increase in impact energy. Therefore, it can be concluded that FRC specimens tested in compression have lower DIF than NWC specimens.

Comparisons regarding concrete composition are also made for tension specimens. The TN8 specimens had an impact energy of 492 ft-lbf, which increase by 31% to 643 ft-lbf for TF8 specimens. The TN8 specimens had an average DIF of 2.4 which decreased by 13% to 2.1 for TF8 specimens. This decrease in DIF is even more prominent when it is considered that the impact energy actually increased between tests.

The same impact energy of 734 ft-lbf was used for the TN16 and TF16 specimens. The TN16 specimens had an average DIF of 3.4 which decreased by 37% to 2.2 for TF16 specimens.

Overall, for tension tests the average DIF decreased when FRC was used in place of NWC. It is emphasized that the comparison between concrete composition results for both compression and tension specimens are not ideal since, in most cases, different impact energies were used.

Concrete Composition at Elevated Temperature

For elevated temperature compression tests an 8 ft drop height with a 1558 ft-lbf impact energy was used for both NWC and FRC. The average DIF decreased by 13% from 2.0 for CN8-400 to 1.8 for CF8-400. Additional elevated temperature compression tests were performed using a 16 ft drop height, which had an impact energy of 2018 ft-lbf. The average DIF increased by 30% from 1.5 for CN16-400 to 1.9 for CF16-400. Overall, when tested in compression at a lower impact energy, the addition of fibers to heated specimens caused a slight reduction in strength results. The opposite was true when tested at a higher impact energy, in which case the strength results increased with the addition of fibers.

For elevated temperature tension tests an 8 ft drop height with a 643 ft-lbf impact energy was used. The average DIF decreased by 19% from 1.7 for TN8-400 to 1.4 for TF8-400. For elevated

temperature tension tests with a 16 ft drop height a 794 ft-lbf impact energy was used. The average DIF decreased by 11% from 2.0 for TN16-400 to 1.8 for TF16-400.

Overall, for both impact energies, the FRC specimens had lower strength results than the NWC specimens when heated and tested in tension. The decrease in strength results for the specimens tested with the higher impact energy was slightly less than the specimens tested with the lower impact energy. This can be related to the results of the compression tests, which had an increase in strength when tested at a higher impact energy. Therefore, it is concluded that FRC specimens generate lower strength results than NWC when heated, but improve as the impact energy increases, especially when subjected to compressive forces.

Temperature Effects for Normal Weight Concrete

For NWC specimens tested in compression, the average static strength decreased by 28% from 10,919 psi at room temperature to 7,905 psi when heated to 400°F. For a list of all average static strengths from April 2012, refer to Table 18. More detailed static results are given in Table 11 for July 2011 tests and Figure 14 and Figure 15 for April 2012 tests.

Table 18 - Average Static Strength

		Strength (psi)	
Test Type	**Composition**	**Room Temperature**	**400°F**
Tension	FRC	605	443
Tension	NWC	521	396
Compression	FRC	9338	5253
Compression	NWC	10919	7905

For the dynamic tests, an 8 ft drop height having an impact energy of 1558 ft-lbf was used for elevated temperature compression tests on NWC. Heating the specimens increased the average DIF by 33% from 1.5 for CN8-R to 2.0 for CN8-400. For elevated temperature NWC compression tests with a 16 ft drop height a 2018 ft-lbf impact energy was used. Heating the specimen decreased the average DIF by 47% from 2.8 for CN16-R to 1.5 for CN16-400.

For NWC specimens tested in tension, the average static strength decreased by 24% from 521 psi at room temperature to 396 psi when heated to 400°F. An 8 ft drop height with an impact energy of 643 ft-lbf was used for dynamic tests on NWC tension specimens at elevated temperatures. Heating the specimens increased the DIF by 21% from 1.4 for TN8-R to 1.7 for TN8-400. For NWC tension tests at 16 ft drop heights a 794 ft-lbf impact energy was used. Heating these specimens decreased the average DIF by 10% from 2.2 for TN16-R to 2.0 for TN16-400.

In general, for NWC in compression the DIF increases when heated to 400°F for a lower impact energy (1558 ft-lbs), but decreases at a higher impact energy (2018 ft-lbs) when compared to room temperature results. The same is also true for tension, which had a lower impact energy of 643 ft-lbf and a higher impact energy of 794 ft-lbf.

A few additional compression tests with a drop height of 16 ft and a 2018 ft-lbf impact energy were performed on NWC specimens that were allowed to cool. Static tests were not performed on uncapped, cooled cylinders and therefore, DIF comparisons cannot be made. However, maximum dynamic load data is available for each CN16 specimen type. The average maximum dynamic load for the CN16-cooled, CN16-400 and CN16-R specimens was 98,270 lbf, 54,589 lbf, and 135,267 lbf respectively.

From the maximum dynamic load results it can be concluded that the cooled specimens perform better than the heated specimens, but do not perform as well as the room temperature specimens. It is recommended that additional cooled specimen tests be performed to determine the effects of additional variables, such as the use of FRC.

Temperature Effects for Fiber Reinforced Concrete

For FRC specimens tested in compression, the average static strength at room temperature was 9,338 psi. This strength decreased by 44% to 5,253 psi when heated to 400°F. For FRC specimens tested in tension, the average static strength decreased by 27% from 605 psi at room temperature to 443 psi when tested at 400°F.

For elevated temperature FRC dynamic tests, comparisons are made between July 2011 (room temperature) and April 2012 (heated) tests since no room temperature tests were done on FRC specimens in April 2012. Impact energies of 1104 and 1558 ft-lbf (a 41% difference) were used for CF8 and CF8-400 specimens respectively. The average DIF increased by 5% from 1.7 for CF8 to 1.8 for CF8-400. Impact energies of 1365 and 2018 ft-lbf (a 48% difference) were used for CF16 and CF16-400 specimens respectively. The average DIF decreased by 6% from 2.1 for CF16 to 1.9 for CF16-400.

For elevated temperature FRC tension tests, similar drop weights were used in July 2011 and April 2012. An impact energy of 643 ft-lbf was used for both TF8 and TF8-400. The average DIF decreased from 2.1 for TF8 to 1.3 for TF8-400, a decrease of 37%. Impact energies of 734 and 794 ft-lbf were used for TF16 and TF16-400 specimens, respectively. The average DIF decreased by 19% from 2.2 for TF16 to 1.8 for TF16-400. For FRC tension tests at elevated temperatures the DIF decreased for both 8 ft and 16 ft drop heights when compared with corresponding room temperature test results.

In general, for the compression tests not all of the comparisons are exact since different impact energies were used. For this reason, no definitive conclusion can be made. For the tension tests, similar impact energies were used when comparing the room temperature and heated specimens. It can be concluded that the increase in temperature reduces the DIF for tension members with fiber reinforcement.

Conclusions

To determine how concrete is affected by dynamic loads, 4 in. diameter by 8 in. high cylinders were tested with various concrete materials, loading types and drop heights. Dynamic impact factors and strain rates were calculated to compare the results of these tests.

To determine the appropriate strain rate, three methods were explored: the high speed camera method, the load cell method and the strain gauge method. The high speed camera method and load cell method gave strain rates that were up to 100% higher than the load cell method. These two methods are representative of a local strain rate, whereas the load cell method provides a more global result. To compare different specimen types, the load cell method was used to determine the strain rates.

Once the appropriate DIFs and strain rates were determined, they were compared with models based on previous research. The following conclusions and recommendations were drawn from the results:

- The combined effect of the drop weight and height can be summarized by calculating an impact energy, which is equivalent to the kinetic energy at impact. As a general trend of all data, for both compression and tension tests, increasing the impact energy results in an increase of DIF. This followed the trends proposed by the CEB and Modified CEB models. The results also show that tension tests are more affected by the increase in impact energy than compression tests.

- The strain rates were calculated using the modulus of elasticity determined from static compressive strength. Additional tests should be performed to determine the mechanical properties of concrete under dynamic loading. The possible change in modulus of elasticity only affects the strain rate; the DIF is independent of the test method used.

- A small number of tests were performed on NWC that had been heated and then cooled before testing. It was found that the maximum dynamic load increased when compared to the heated concrete, but was 27% less than the room temperature concrete. Additional testing may be performed to further analyze the effects of cooling on concrete specimens with both NWC and FRC under dynamic loading.

- For compression tests, different impact energies were used for FRC and NWC specimens. Because of this difference, it was difficult to determine how FRC concrete performed compared to NWC. However, by comparing the percent increase in impact energy to the percent increase in DIF, it is concluded that the FRC performed worse than NWC. For better comparisons, additional tests can be performed using the same impact energy for FRC and NWC specimens. The same can be said for the tension tests. However, for tension tests with a 16 ft drop height, the same impact energy was used. In this case, the same conclusion was drawn: FRC specimens had lower strength results than NWC specimens. This is opposite from static results, in which fibers generally add strength when tested in tension.

- For compression and tension tests at low impact energies, FRC specimens had lower DIFs than NWC when heated to 400°F. For tension tests, FRC specimens at high impact energies also had lower DIFs than NWC, but the decrease in DIFs was not as large as that experienced in the lower impact energy tests. For compression tests at high impact energies, the DIFs and strain rate actually increased when FRC was used in place of NWC. Therefore, FRC specimens generally have lower strength results compared to NWC when heated, but improve as the impact energy increases, especially when tested in compression.

- For NWC in compression the DIF increases when heated to 400°F for a lower impact energy (1558 ft-lbs), but decreases at a higher impact energy (2018 ft-lbs) when compared to room temperature results at the same impact energy. The same is also true for tension, which had a lower impact energy of 643 ft-lbf and a higher impact energy of 794 ft-lbf.

- The increase in temperature reduces the DIF for tension members with fiber reinforcement.

In summary, a standardized method for testing dynamic properties of concrete is needed. There are many contributing factors that need to be considered, including test specimen size, test configuration and the measurement of impact load and strain rate.

References

1. Garfield, T.T. (2011), "Performance of Reinforced Concrete Panels During Blast Loading," Master of Science Thesis, University of Utah, Salt Lake City, Utah.

2. PCB Piezotronic Inc. Force/Torque Division "Model 206C ICP® Dynamic Force Sensor Installation and Operation Manual."

3. American Society for Testing Material (2004), "ASTM C496/C496 M-04e1 Standard Test Method for Splitting Tensile Strength of Cylindrical Concrete Specimens." ASTM International, West Conshohocken.

4. American Society for Testing Material (2012). "ASTM C39/C39M-10 Standard Test Method for Splitting Compressive Strength of Cylindrical Concrete Specimens." ASTM International, West Conshohocken, PA.

5. DIAdem (2009). DIAdem Version 11.1, National Instruments Corp., Austin, TX.

6. Phantom (2012). Phantom Cine Viewer Version 2.0, Phantom Vision Research. Retrieved from http://www.visionresearch.com.

7. Malvar, L.J. and Ross, C.A. (1998), "Review of Strain Rate Effects for Concrete in Tension." ACI Materials Journal, 95(6), 735-739.

8. Millard, S.G., Molyneaux T.C.K. and Barnett, S.J. (2010), "Dynamic Enhancement of Blast-resistant Ultra High Performance Fibre-reinforce Concrete under Flexural and Shear Loading." International Journal of Impact Engineering, 37, 405-413.

9. Comite Euro-International du Beton. (1993). "*CEB-FIP Model Code 1990*." Redwood Books, Torewbridge, Wiltshire, UK.

APPENDIX A

July 2011 - Photographs of Tested Specimens

Figure A.1 - TF Specimens after Static Tests

Figure A.2 - TN Specimens after Static Test

Figure A.3 - Specimen TF8-2 after Dynamic Test

Figure A.4 – Specimen CF8-2 after Dynamic Test

Figure A.5 - Specimen TN8-2 after Dynamic Test

Figure A.6 - Specimen CN8-2 after Dynamic Test

Figure A.7 - Specimen TF16-2 after Dynamic Test

Figure A.8 - Specimen CF16-2 after Dynamic Test

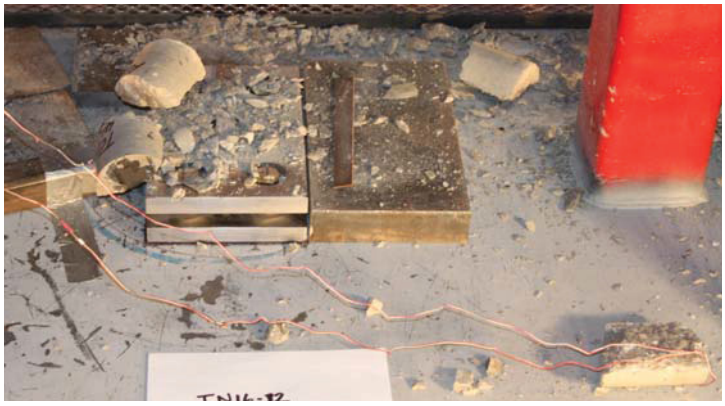

Figure A.9 - Specimen TN16-2 after Dynamic Test

Figure A.10 - Specimen CN16-2 after Dynamic Test

APPENDIX B

April 2012 – Photographs of Tested Specimens

Figure B.1 - CF0-0-4

Figure B.2 - CN0-0-4

Figure B.3 - TF0-400-4

Figure B.4 - CF0-400-4

Figure B.5 - TN0-400-4

Figure B.6 - CN0-400-4

Figure B.7 – Specimen TF8-400-4-1 after Dynamic Test

Figure B.8 – Specimen CF8-400-4-1 after Dynamic Test

Figure B.9 – Specimen TN8-400-4-1 after Dynamic Test

Figure B.10 - Specimen TN8-0-4-3 after Dynamic Test

Figure B.11 - Specimen CN8-400-4-4 after Dynamic Test

Figure B.12 - Specimen CN8-0-4-3 after Dynamic Test

Figure B.13 - Specimen TF16-400-4-1 after Dynamic Test

Figure B.14 – Specimen TF16-400-4-3 with Melted Fibers after Dynamic Test

Figure B.15 - Specimen CF16-400-4-1 after Dynamic Test

Figure B.16 – Specimen TN16-400-4-4 after Dynamic Test

Figure B.17 - Specimen TN16-0-4-1 after Dynamic Test

Figure B.18 – Specimen CN16-400-4-4 after Dynamic Test

Figure B.19 - Specimen CN16-0-4-1 after Dynamic Test

Figure B.20 - Specimen CN16-cooled-4-3

APPENDIX C

July 2011 – Load Data Graphs

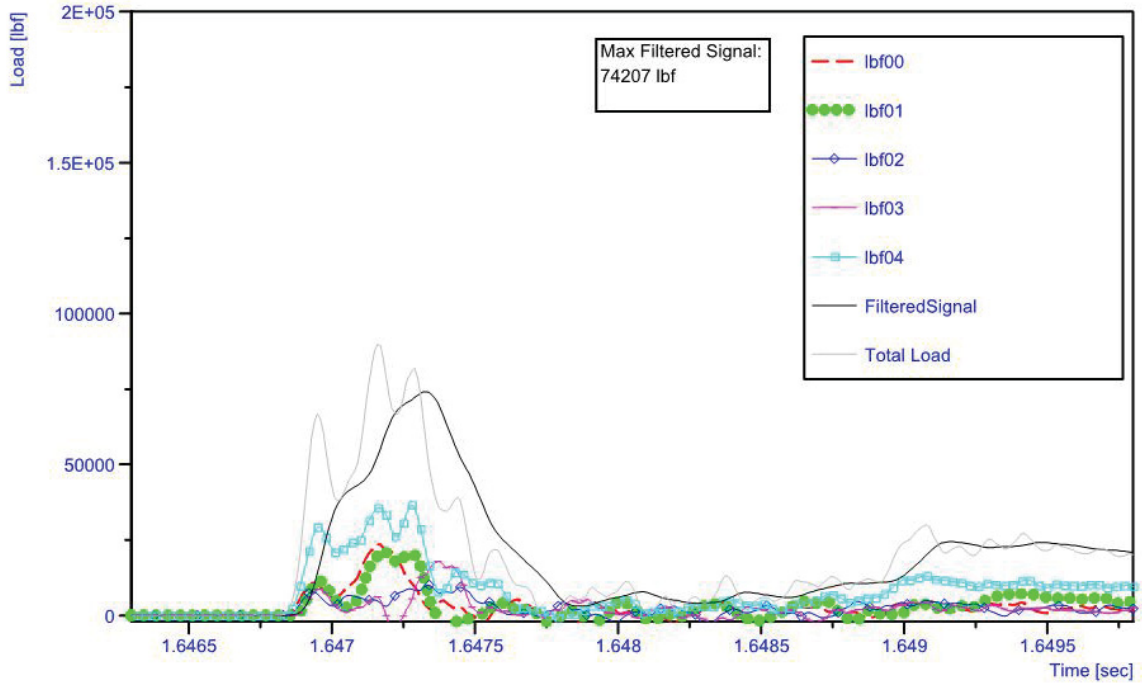

Figure C.1 – TF8-2 Load Data

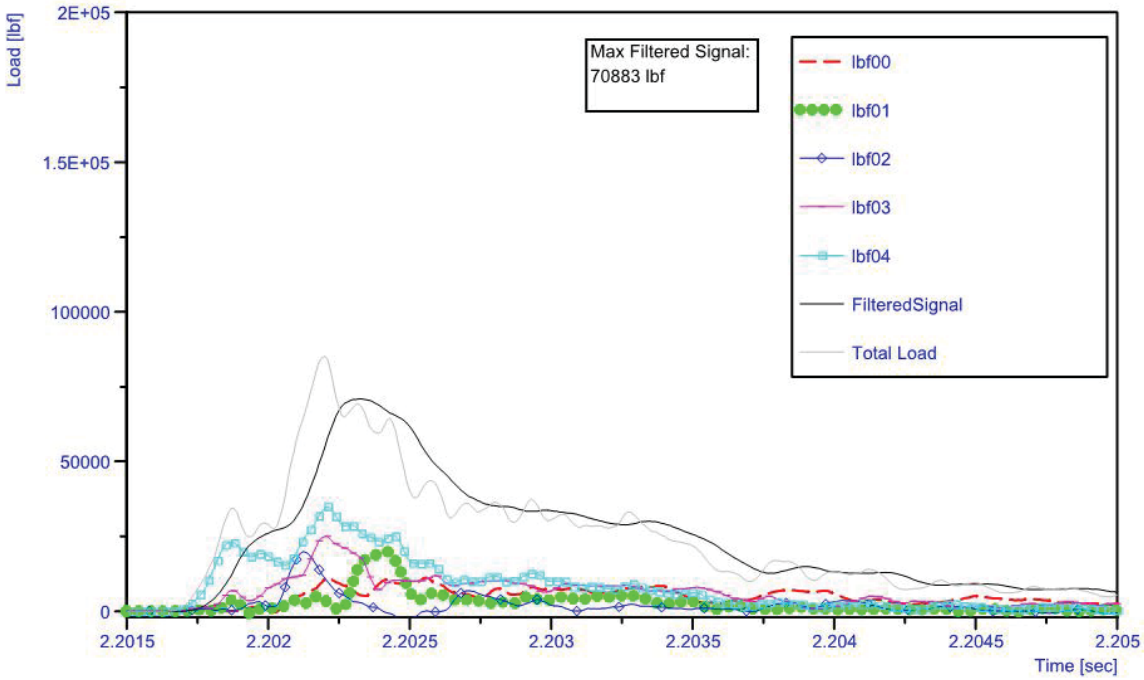

Figure C.2 - CF8-2 Load Data

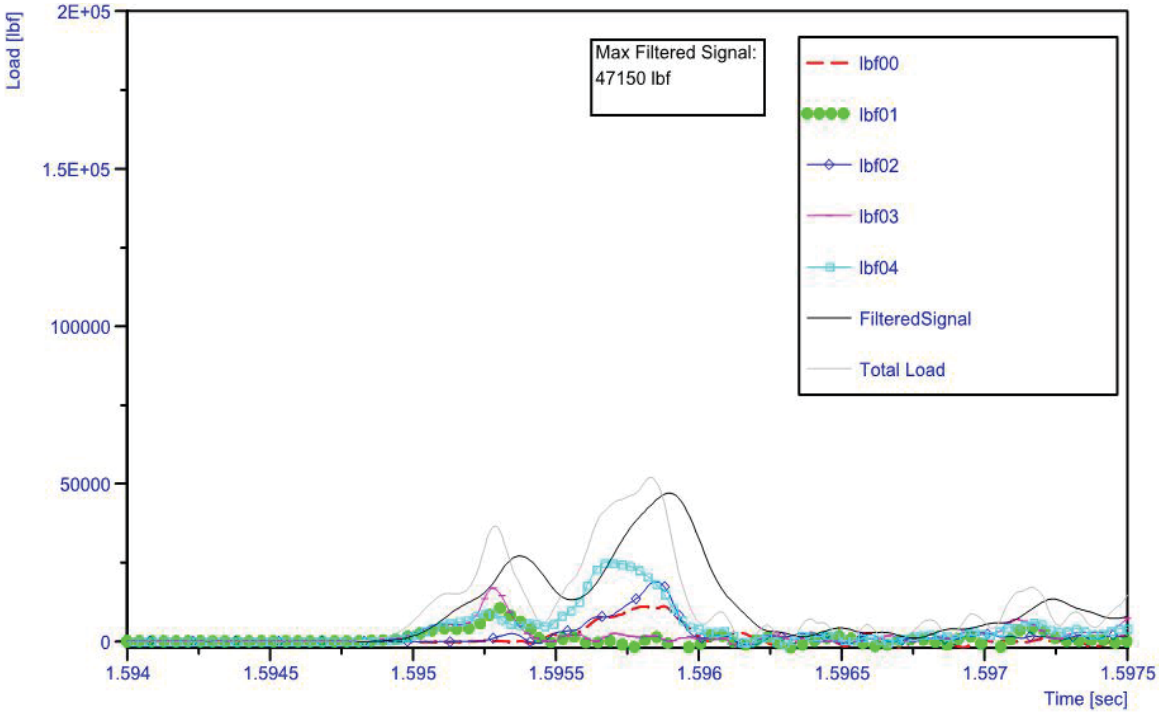

Figure C.3 - TN8-2 Load Data

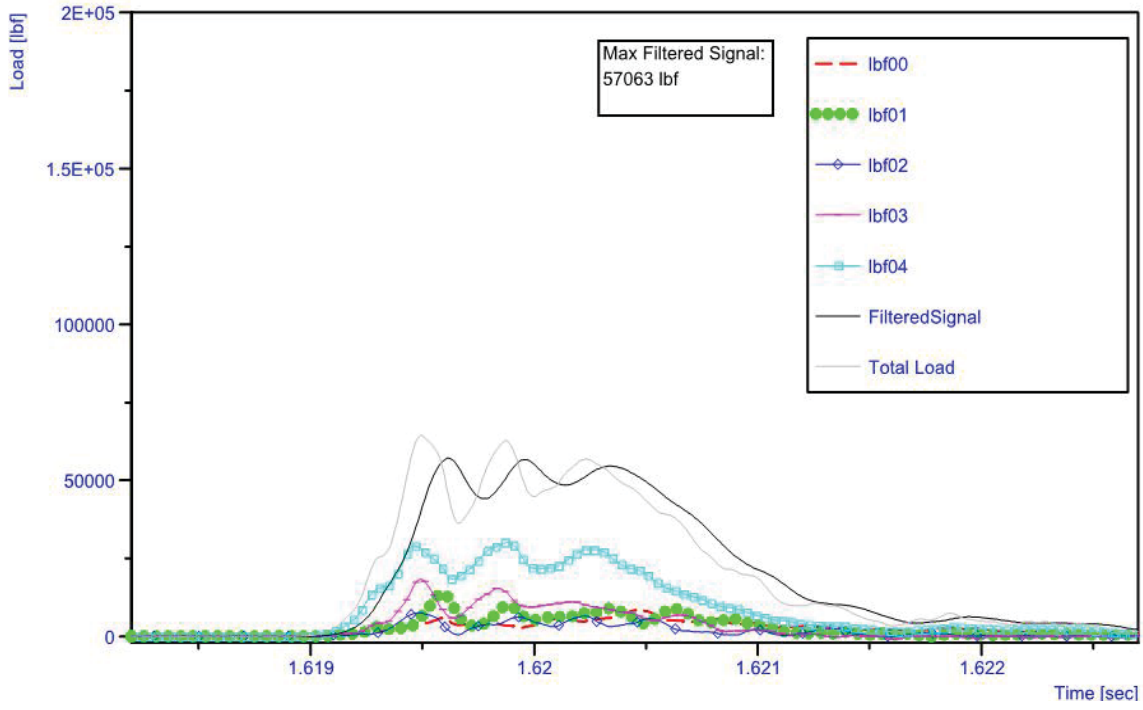

Figure C.4 - CN8-2 Load Data

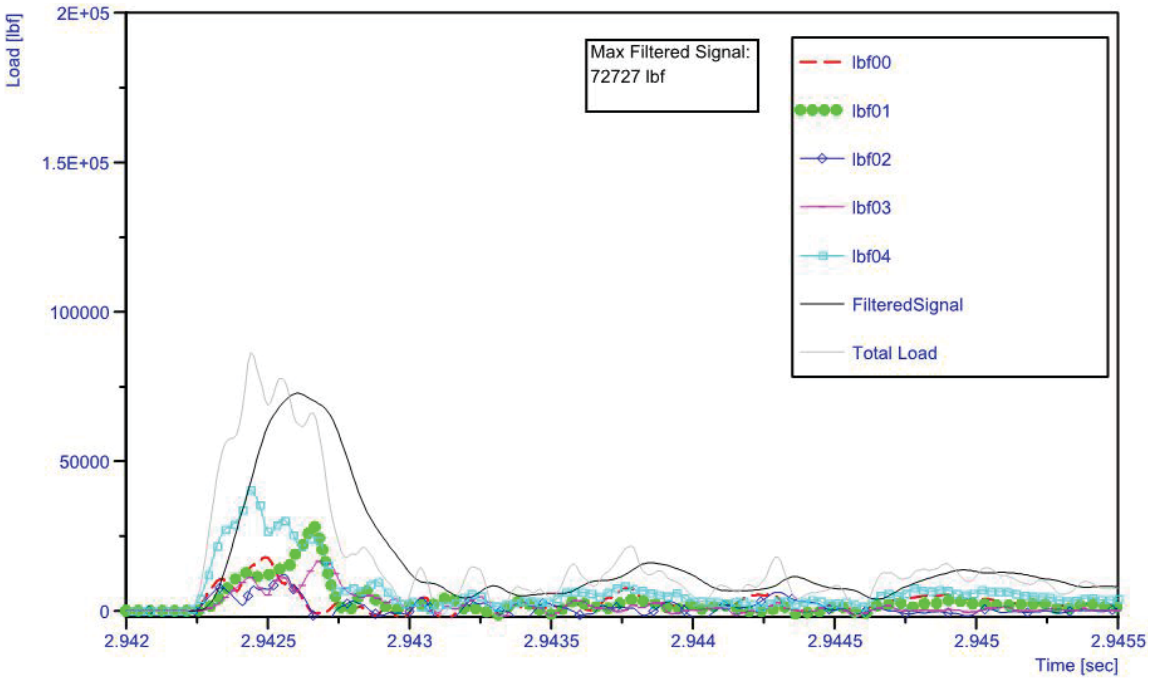

Figure C.5 - TF16-2 Load Data

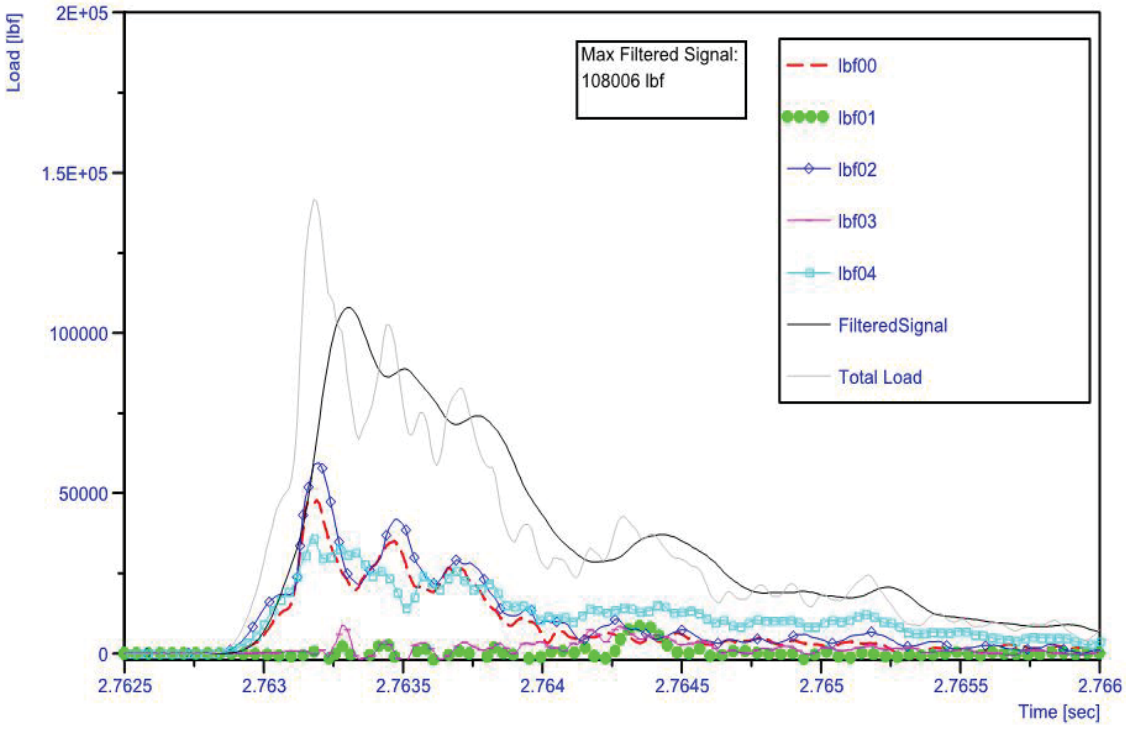

Figure C.6 - CF16-2 Load Data

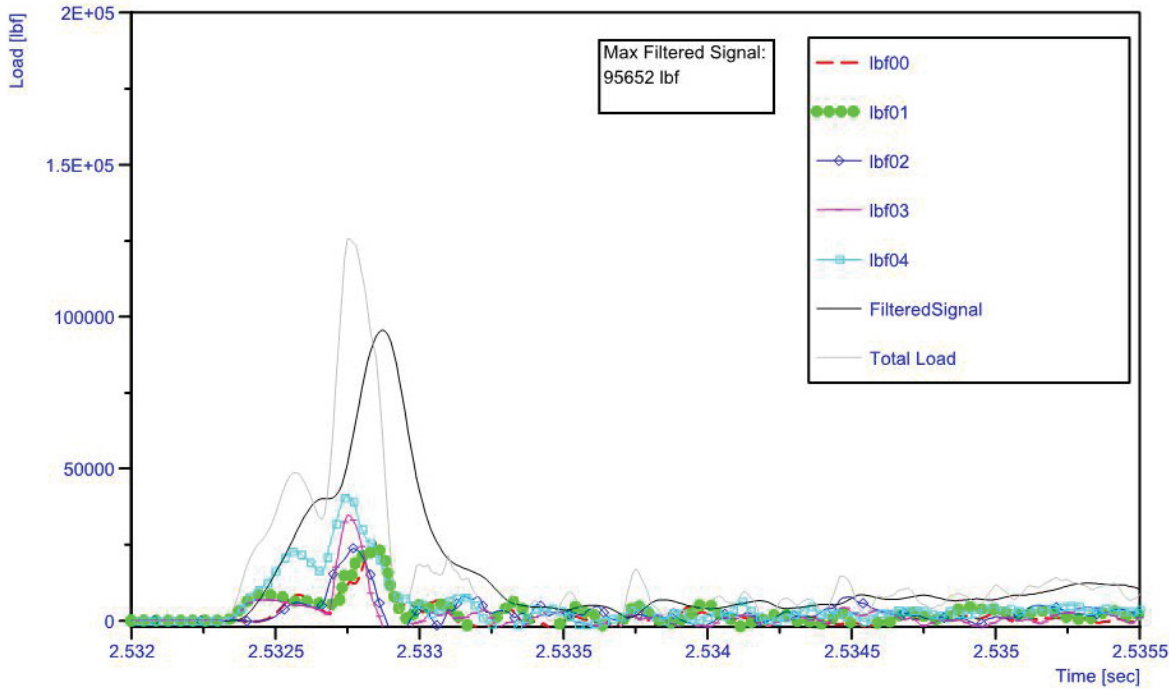

Figure C.7 - TN16-2 Load Data

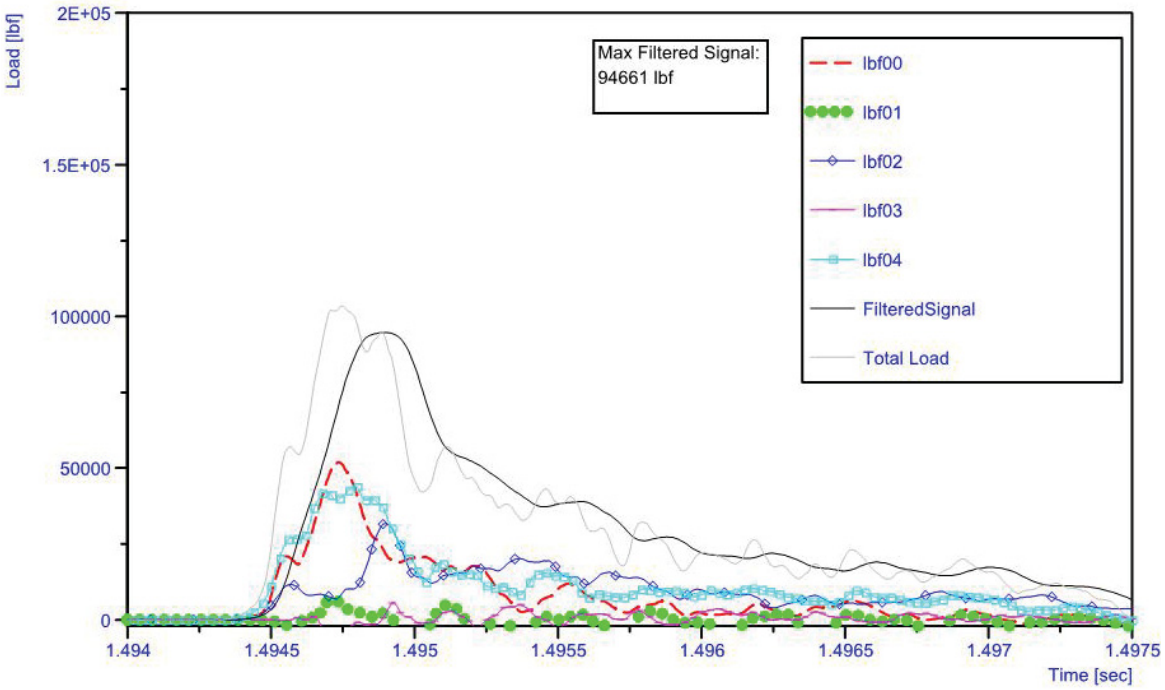

Figure C.8 - CN16-2 Load Data

APPENDIX D

April 2012 – Load Graphs

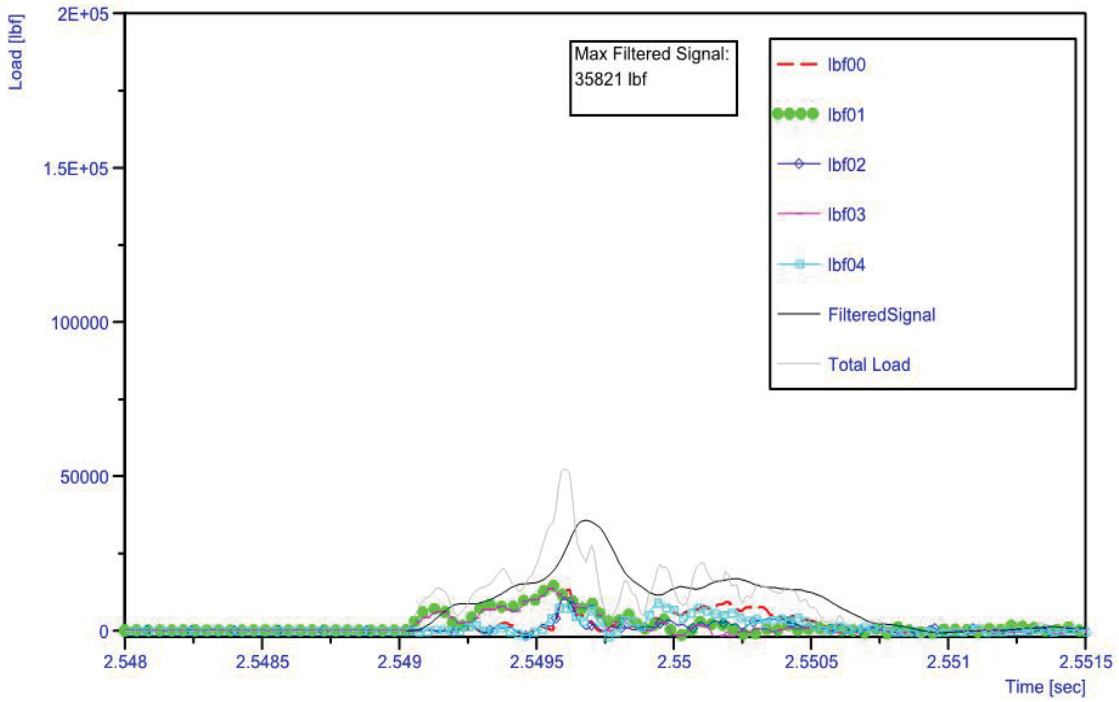

Figure D.1 - TF8-400-4-1 Load Data

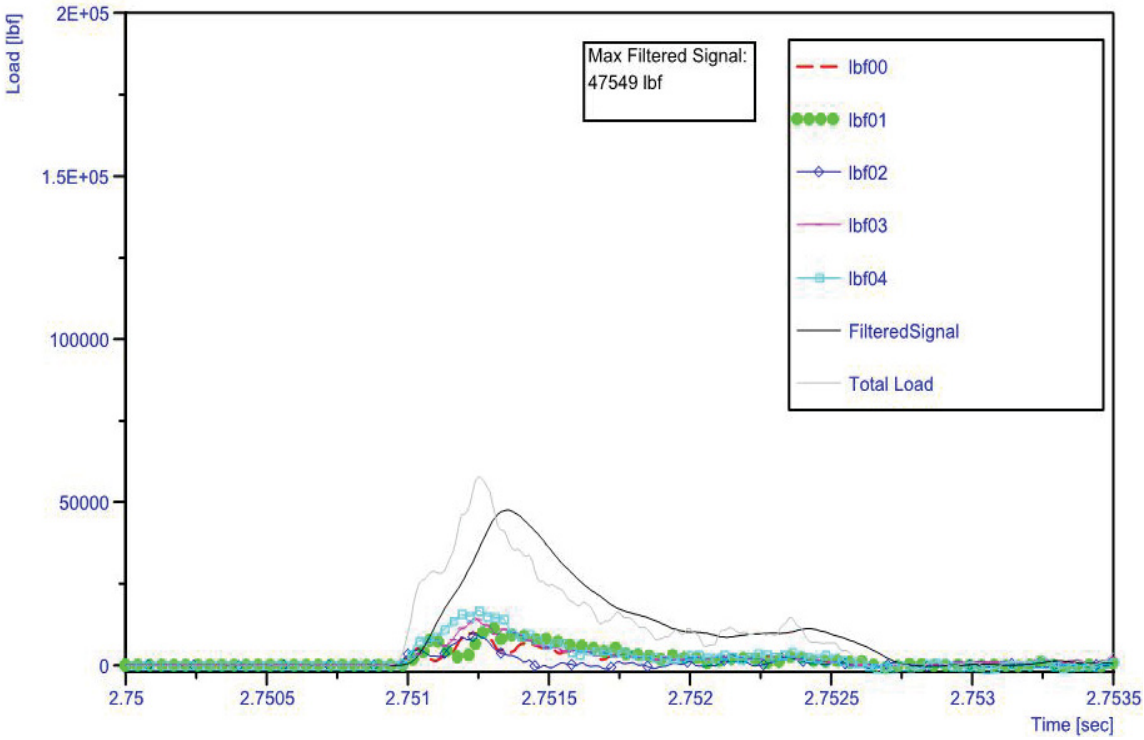

Figure D.2 - CF8-400-4-1 Load Data

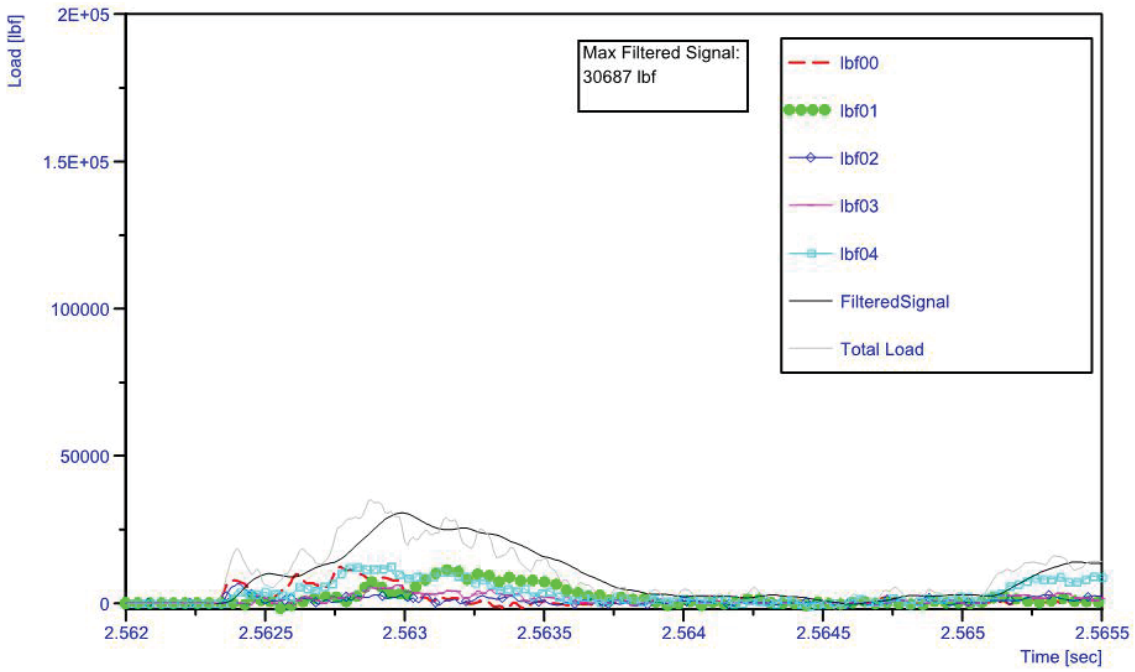

Figure D.3 - TN8-400-4-1 Load Data

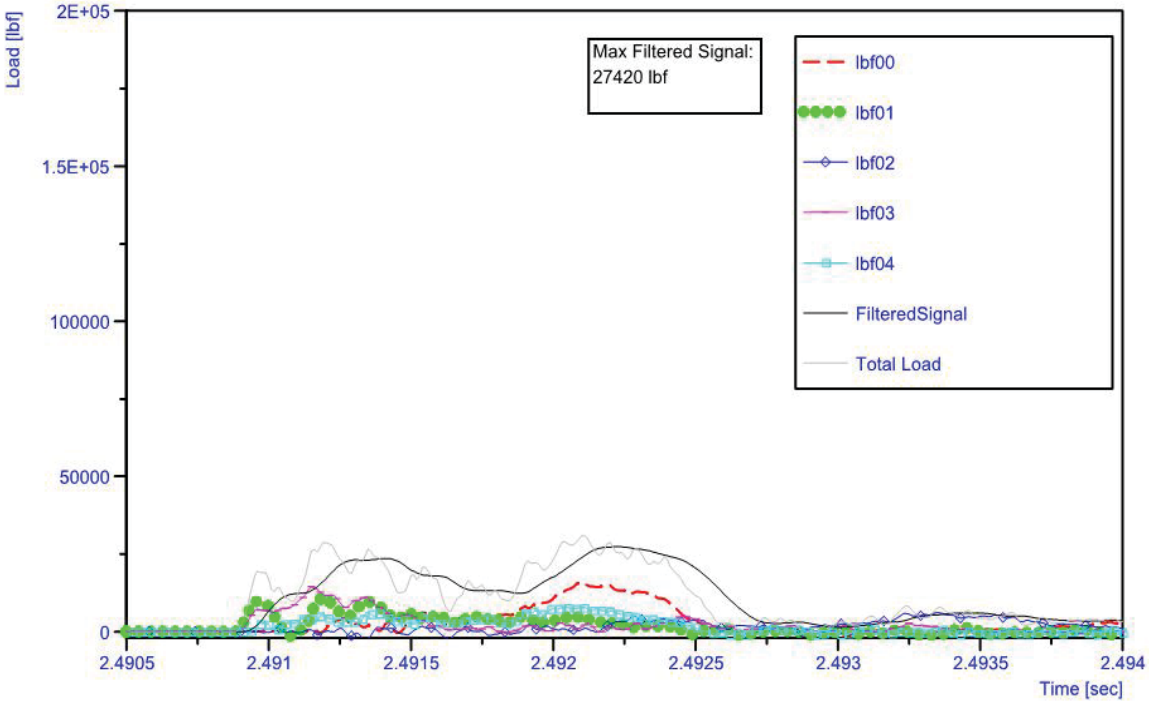

Figure D.4 - TN8-0-4-3 Load Data

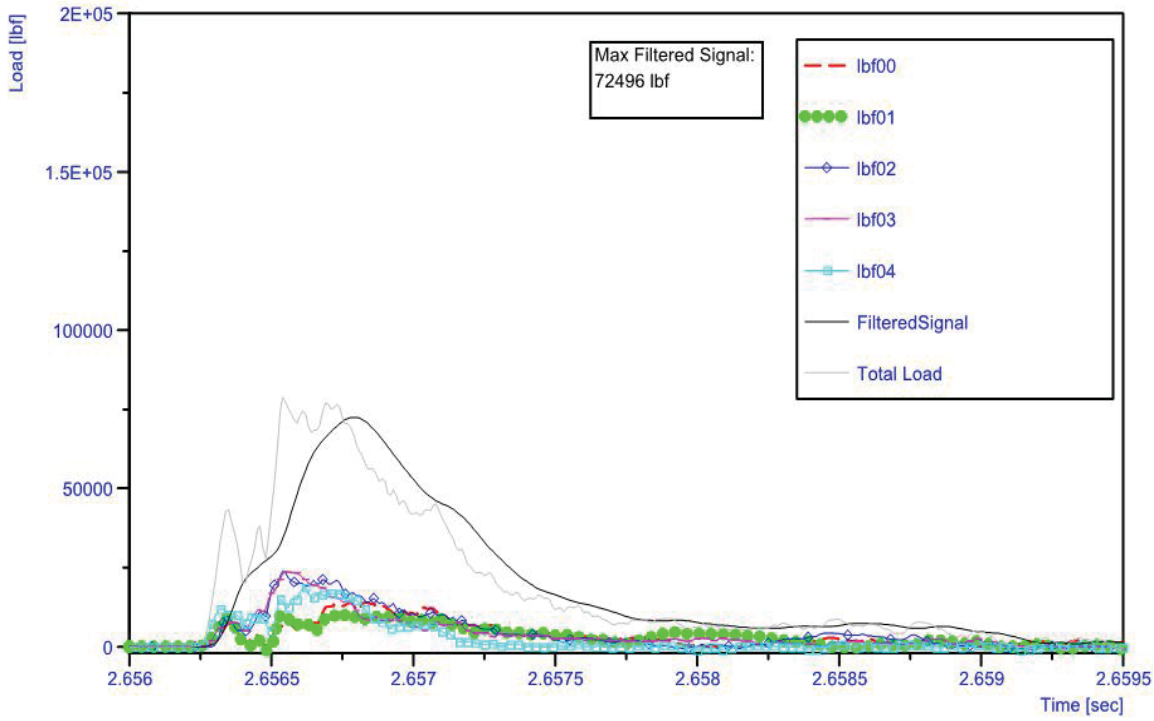

Figure D.5 - CN8-400-4-4 Load Data

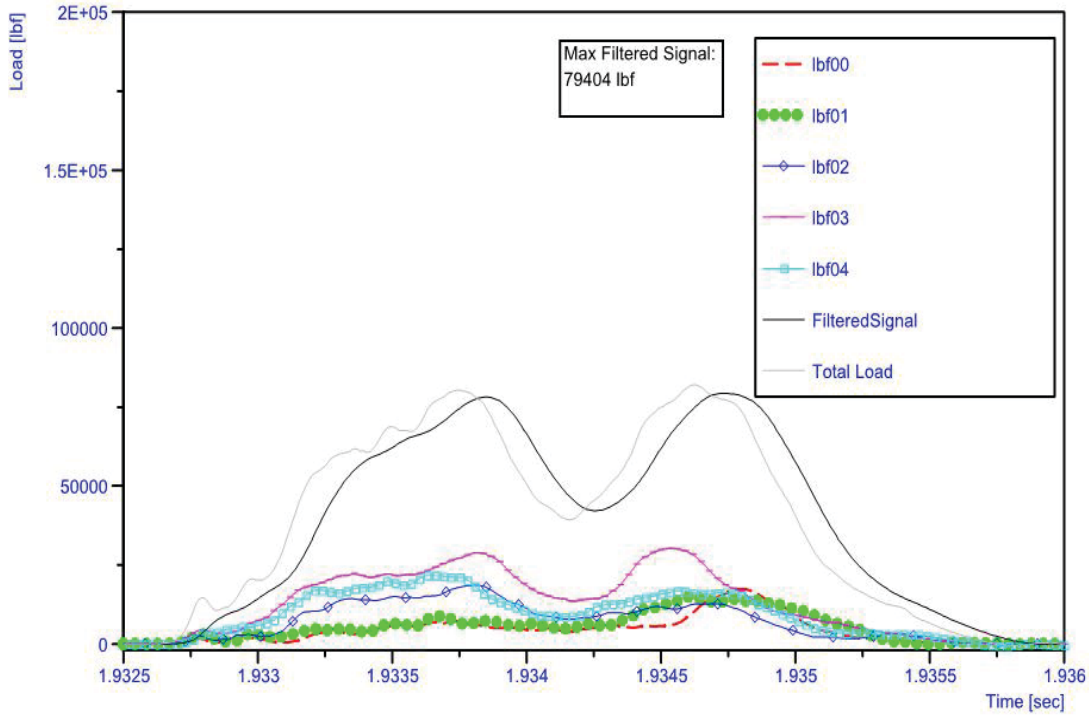

Figure D.6 - CN8-0-4-3 Load Data

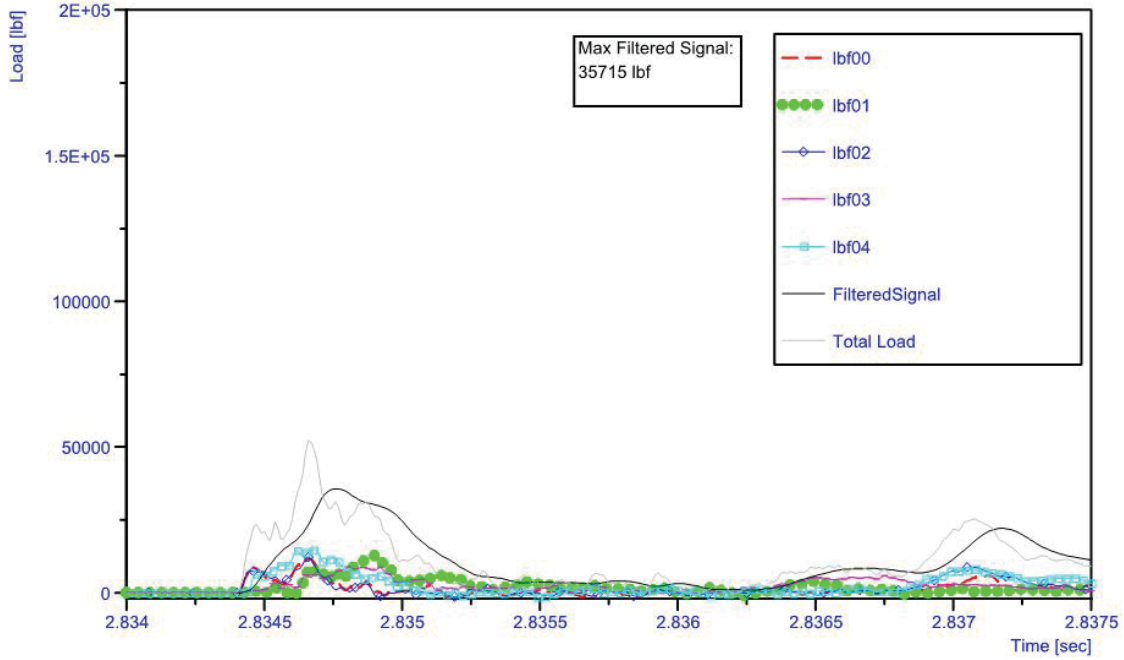

Figure D.7 - TF16-400-4-1 Load Data

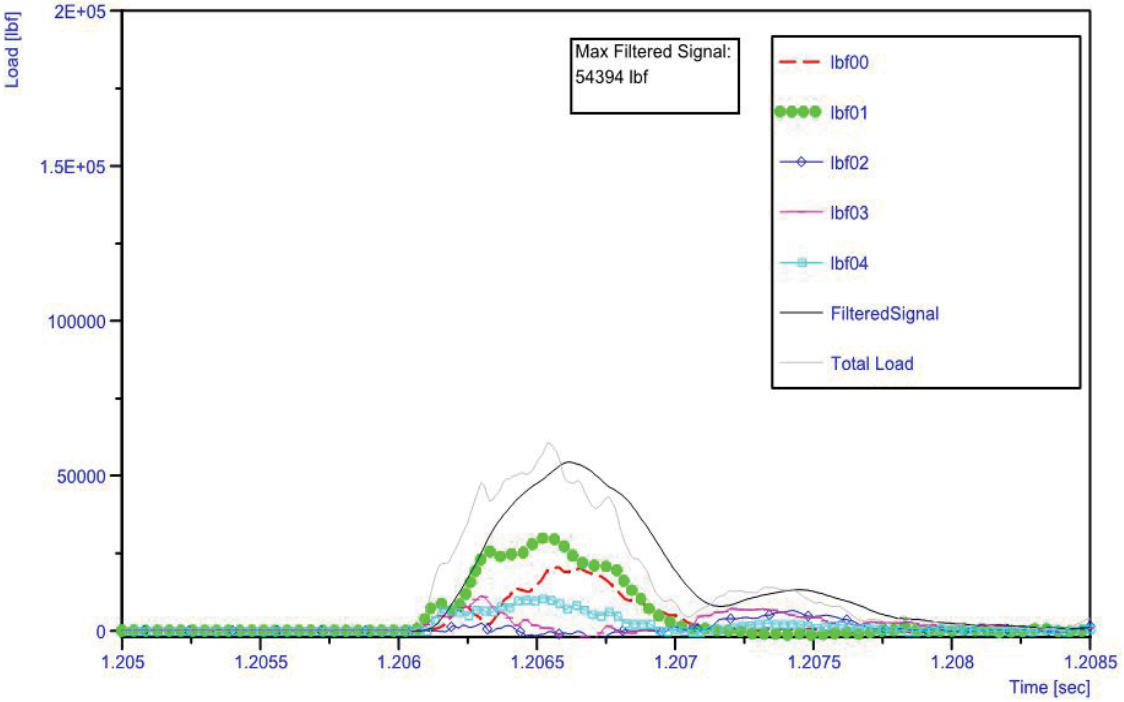

Figure D.8 - CF16-400-4-1 Load Data

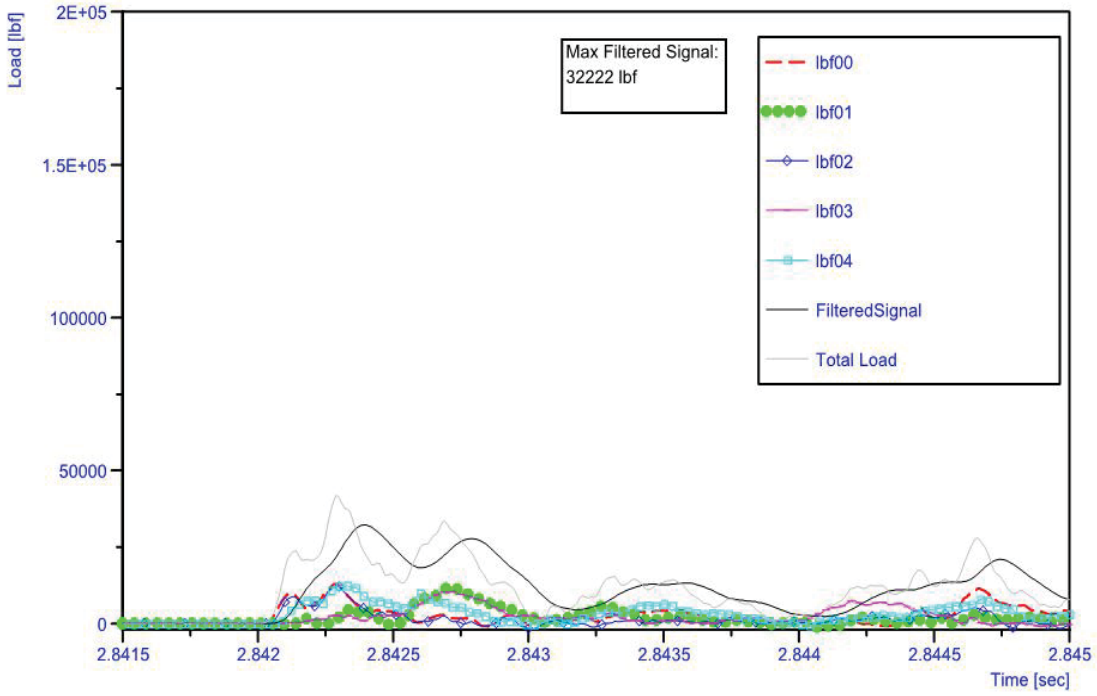

Figure D.9 - TN16-400-4-4 Load Data

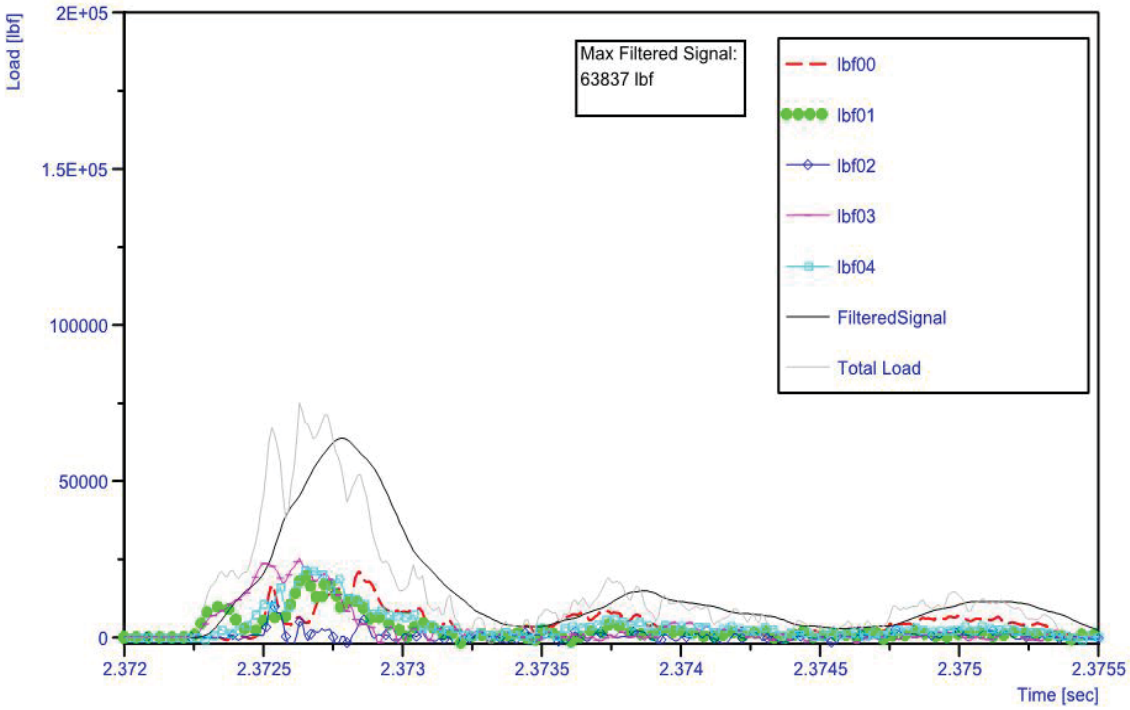

Figure D.10 - TN16-0-4-1 Load Data

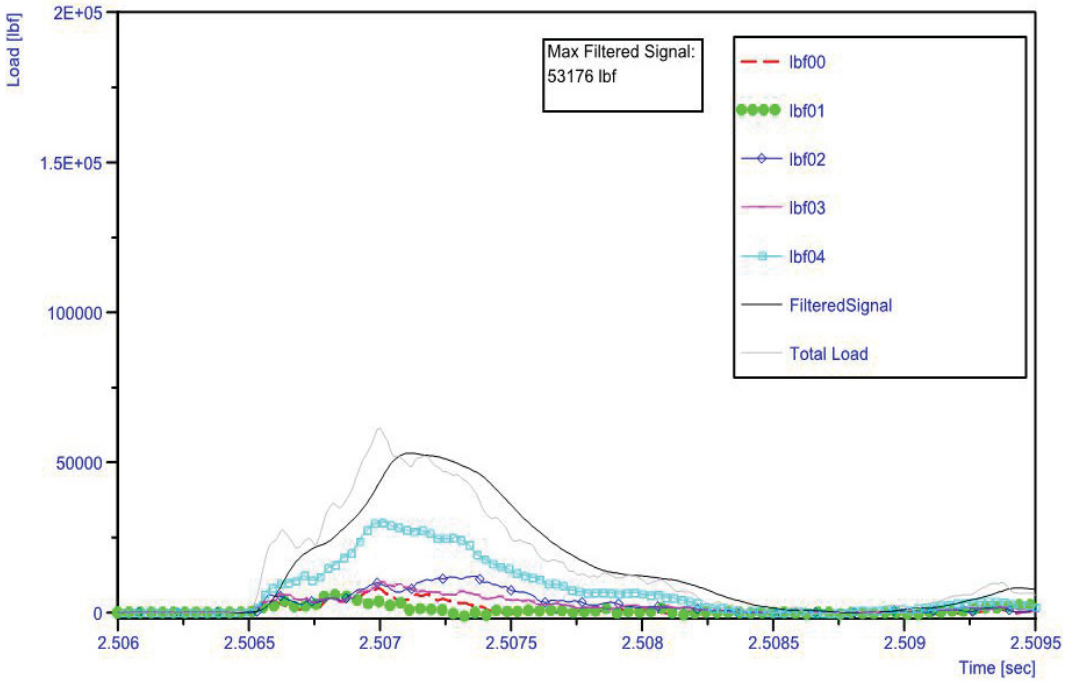

Figure D.11 - CN16-400-4-4 Load Data

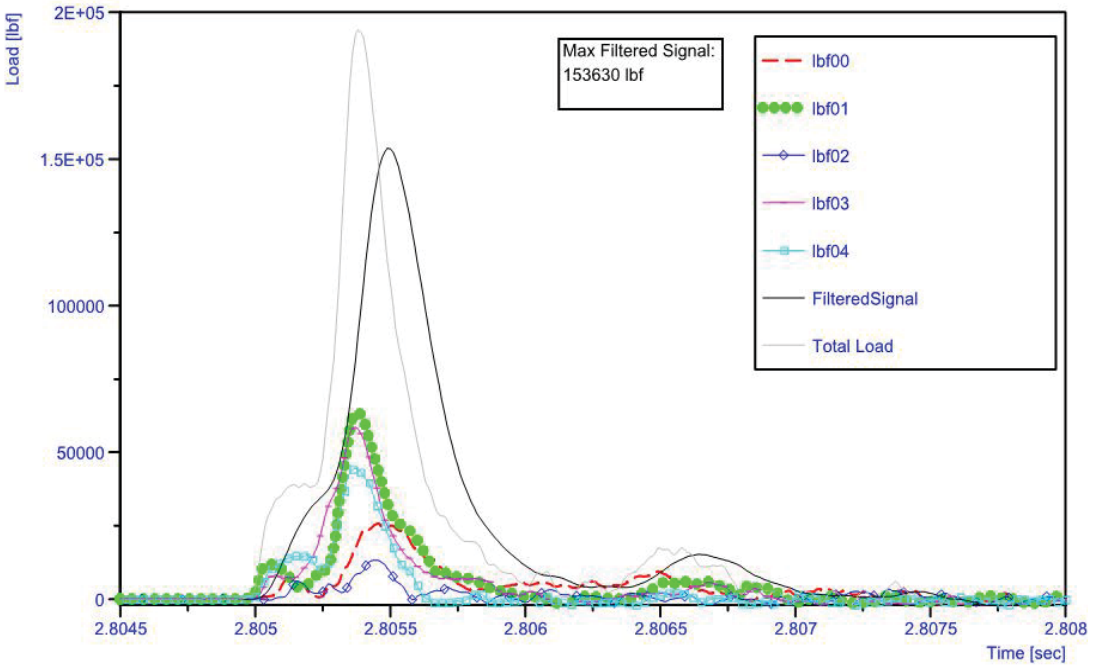

Figure D.12 - CN16-0-4-1 Load Data

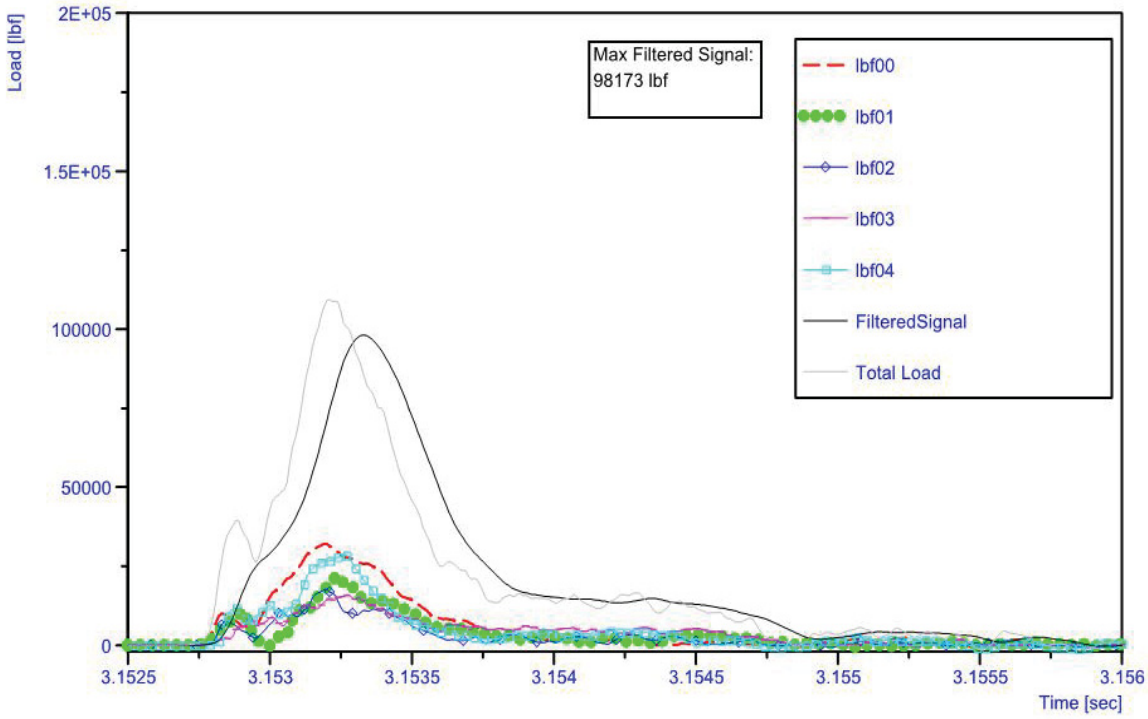

Figure D.13 - CN16-cooled-4-3 Load Data

APPENDIX E

July 2011 – Strain Data Graphs

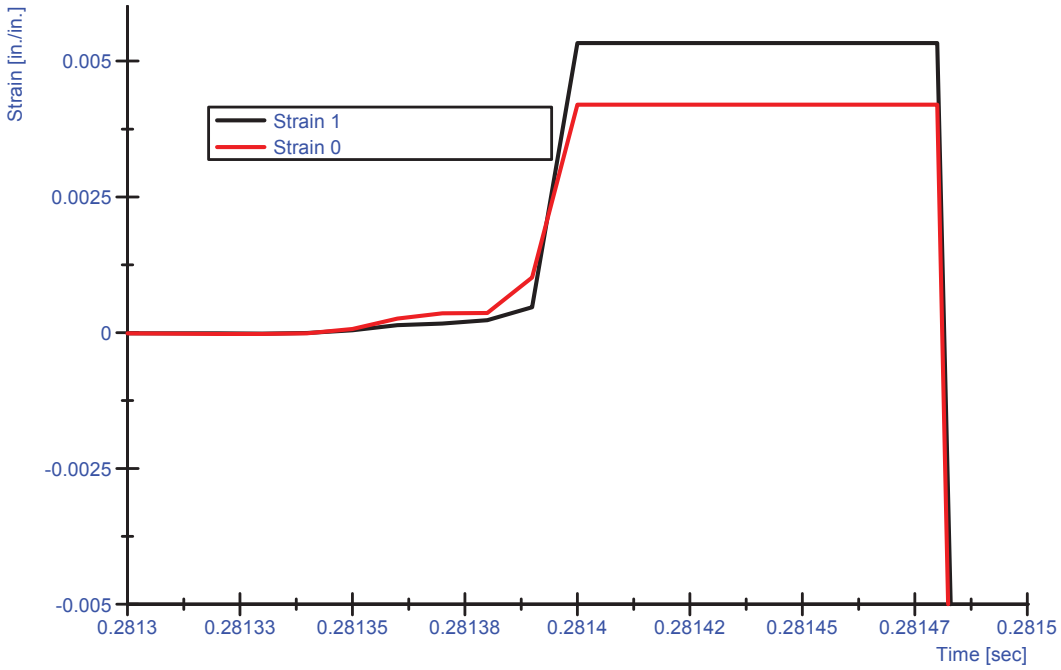

Figure E.1 – Specimen TN8-2 Strain Data for Dynamic Test

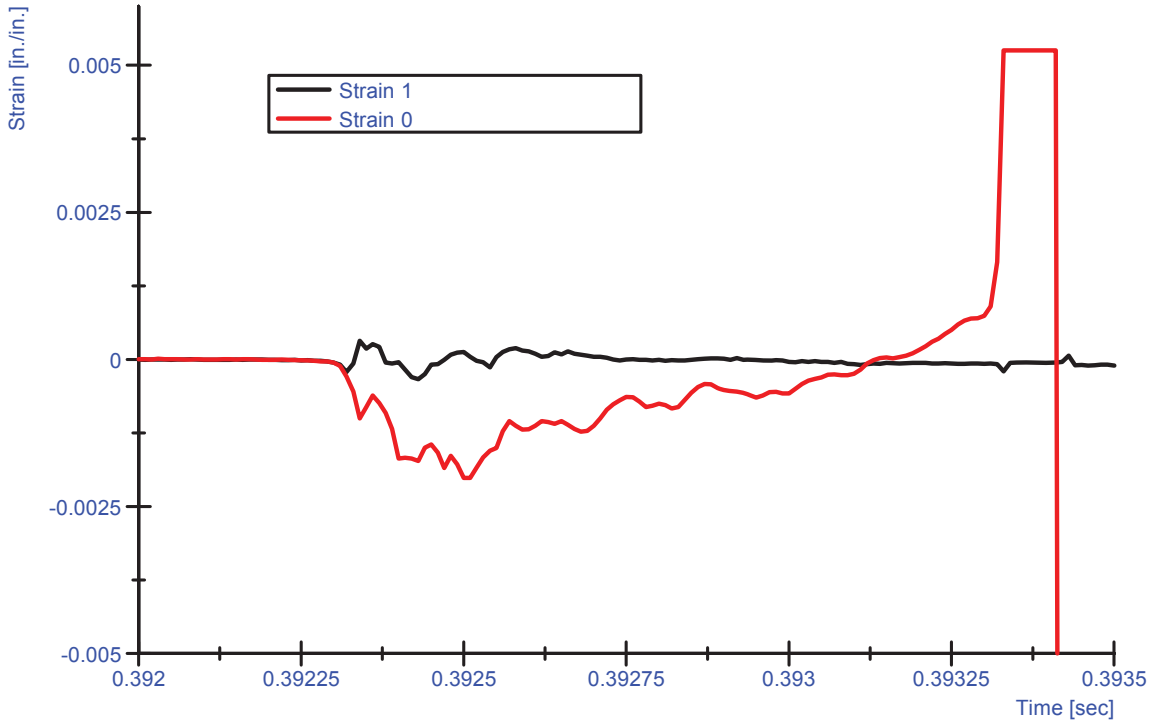

Figure E.2 – Specimen CF8-2 Strain Data for Dynamic Test

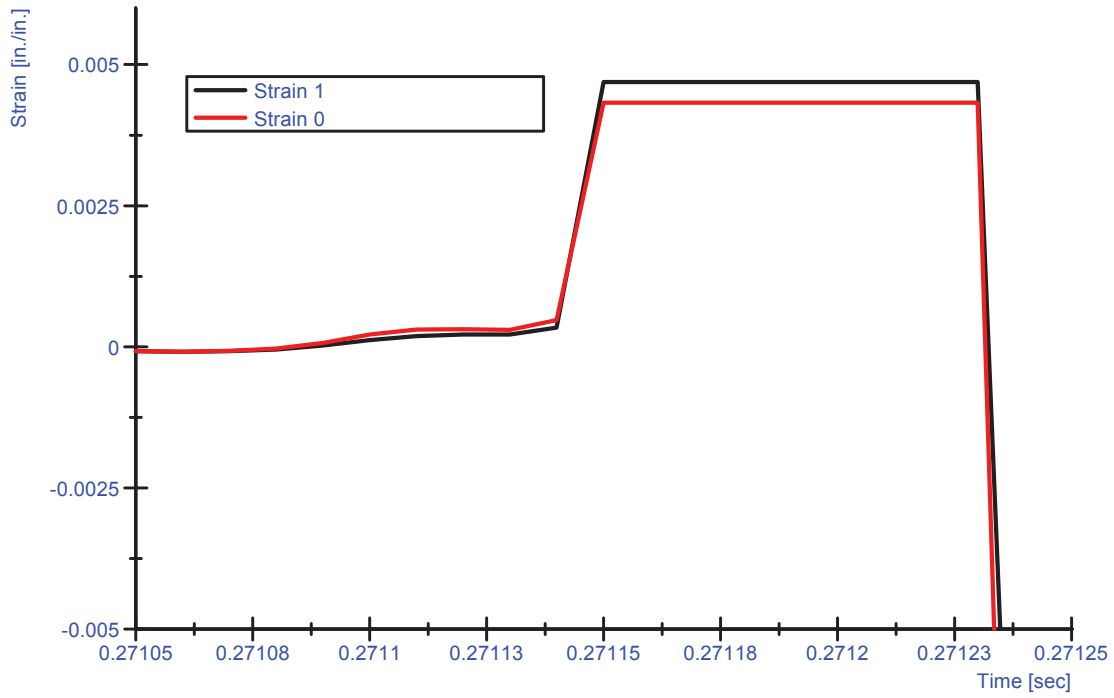

Figure E.3 – Specimen TN8-2 Strain Data for Dynamic Test

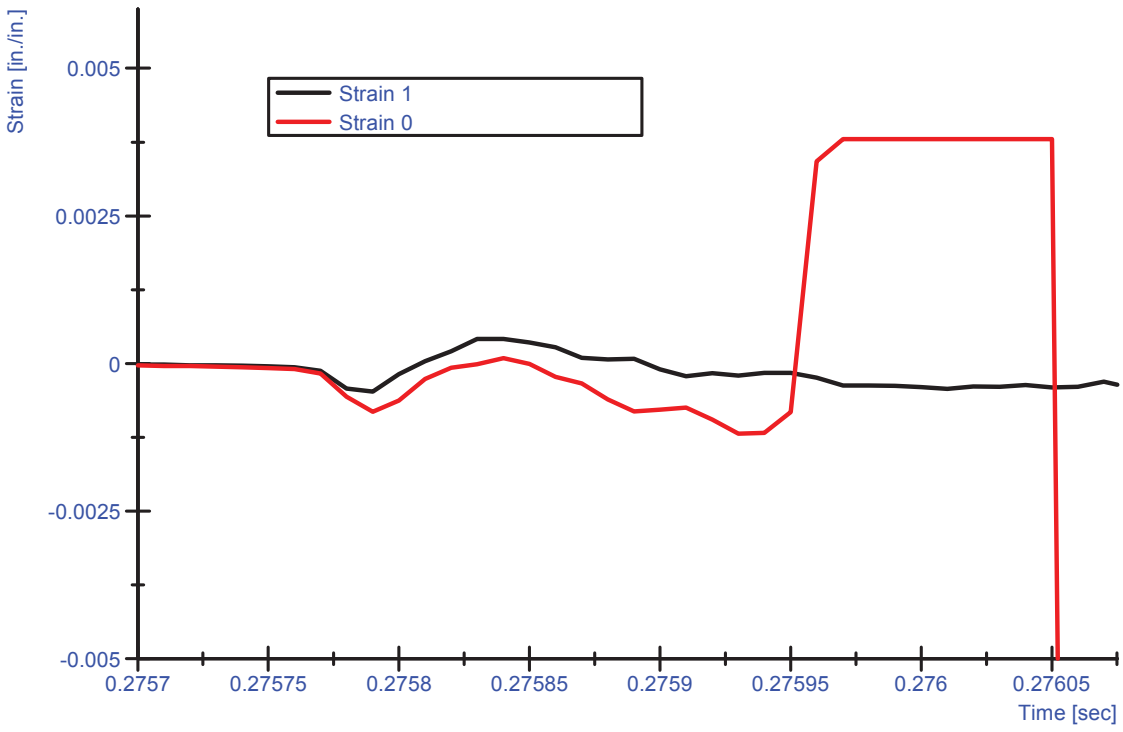

Figure E.4 – Specimen CN8-2 Strain Data for Dynamic Test

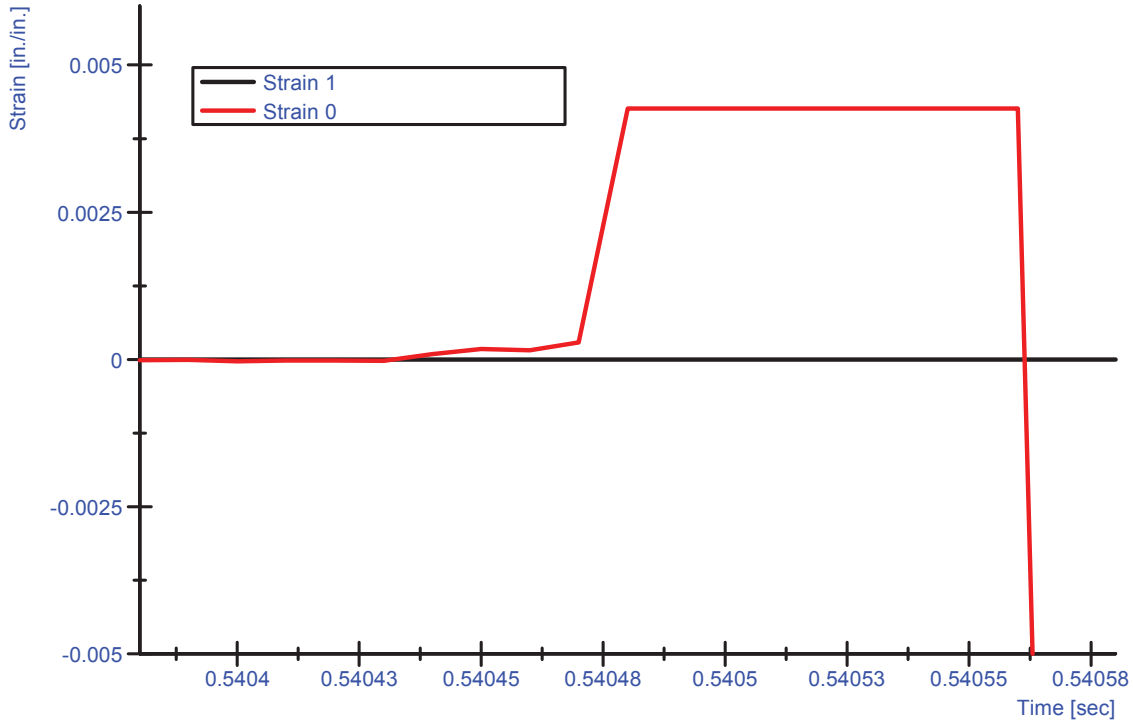

Figure E.5 – Specimen TF16-2 Strain Data for Dynamic Test

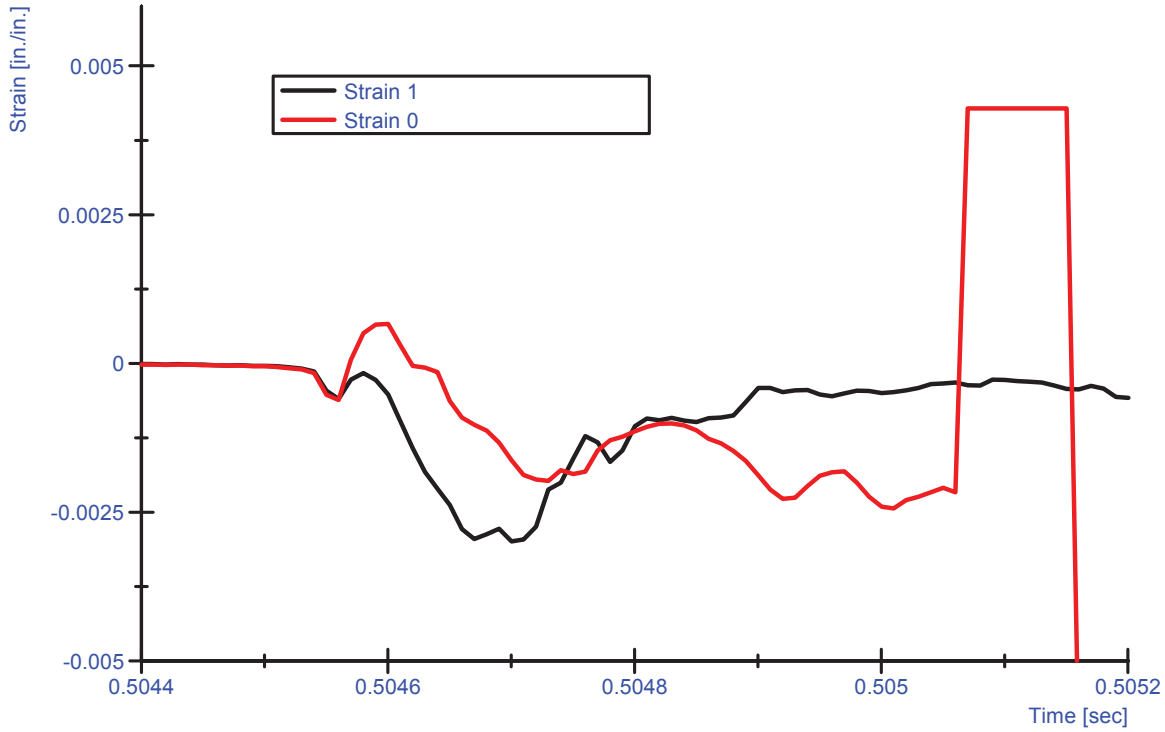

Figure E.6 – Specimen CF16-2 Strain Data for Dynamic Test

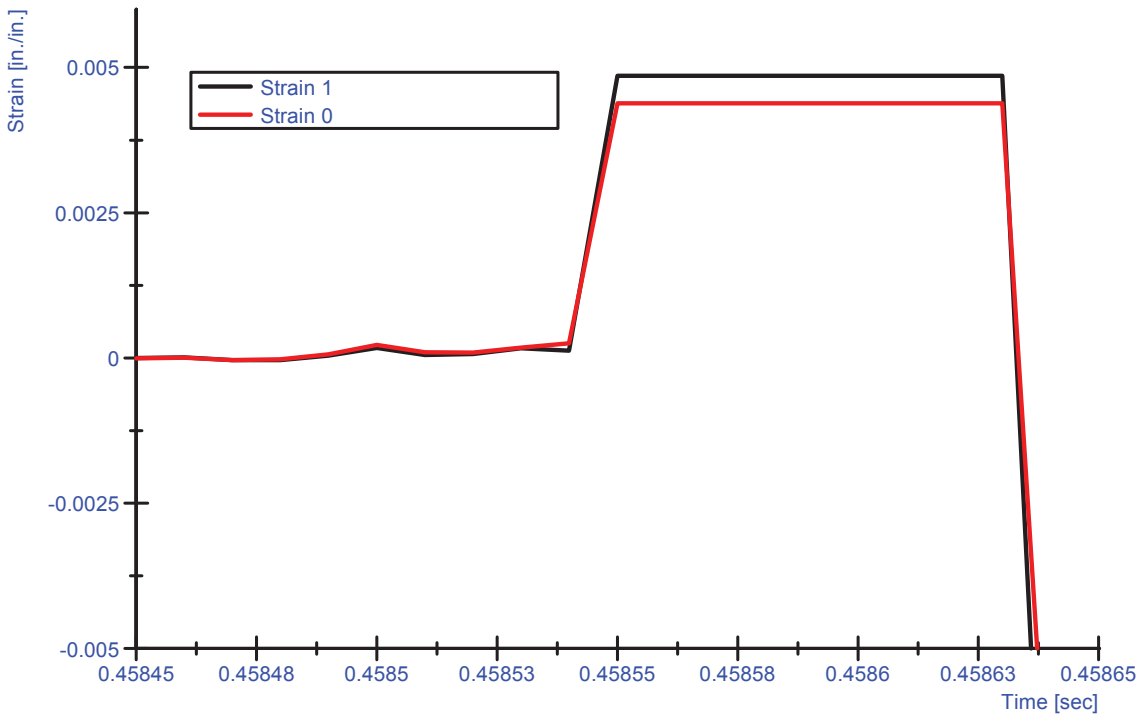

Figure E.7 – Specimen TN16-2 Strain Data for Dynamic Test

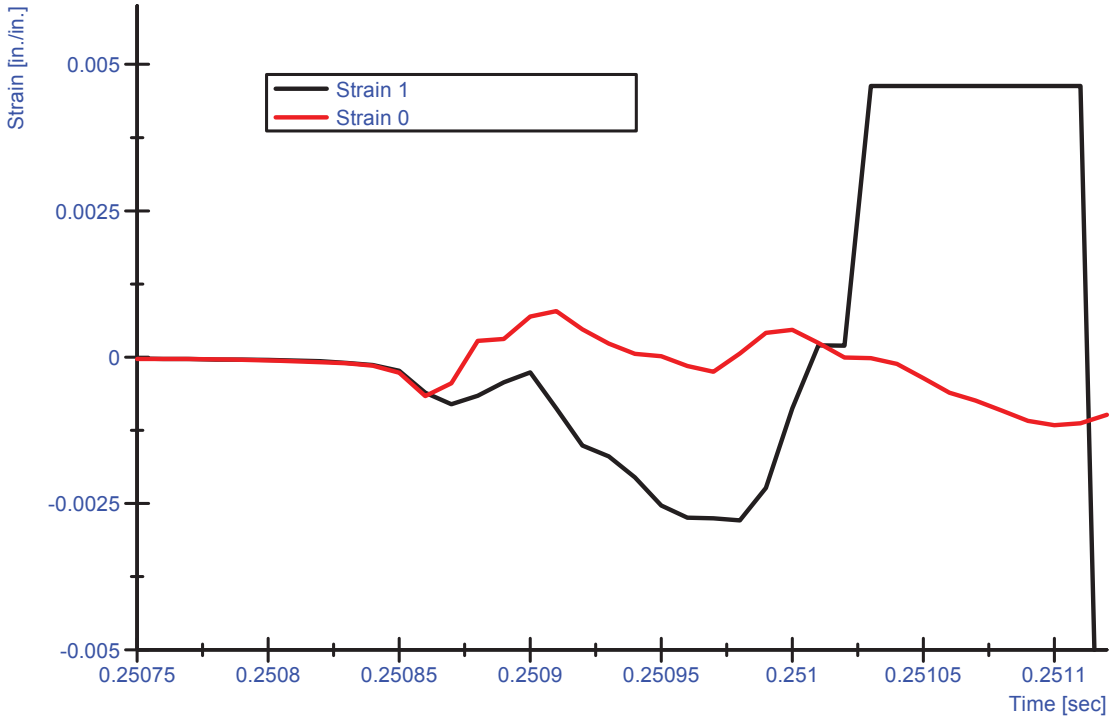

Figure E.8 – Specimen CN16-2 Strain Data for Dynamic Test

APPENDIX F

DIF verses Strain Rate Plots

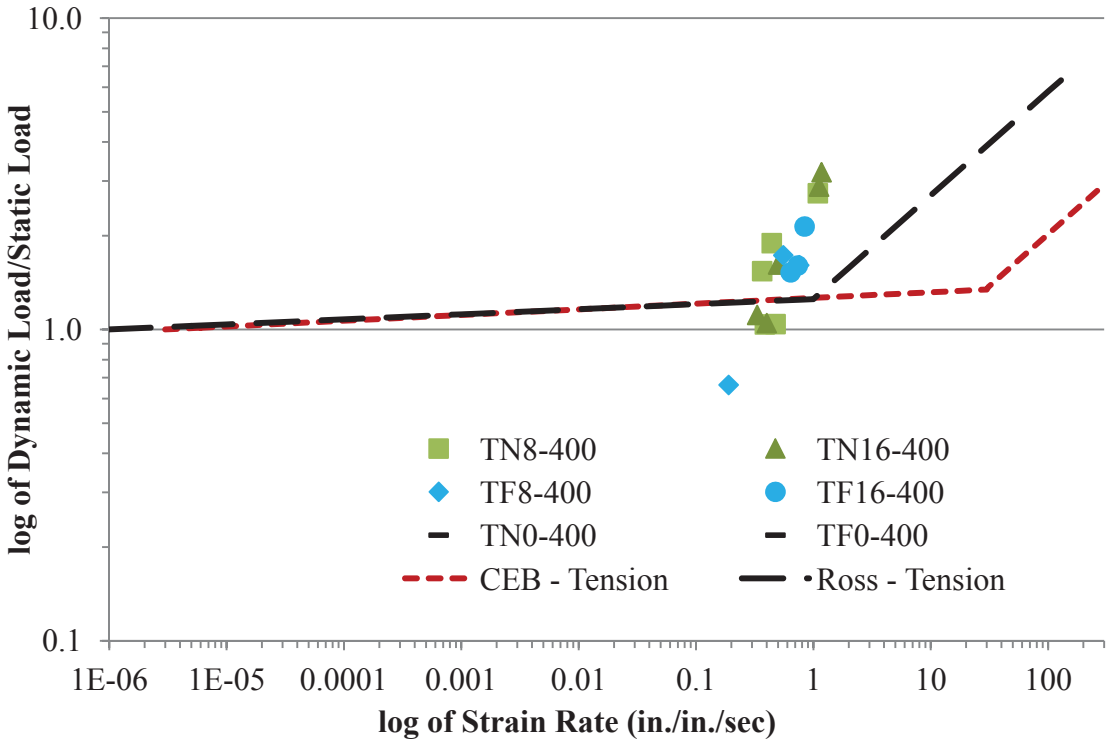

Figure F.1 – Tension at 400°F

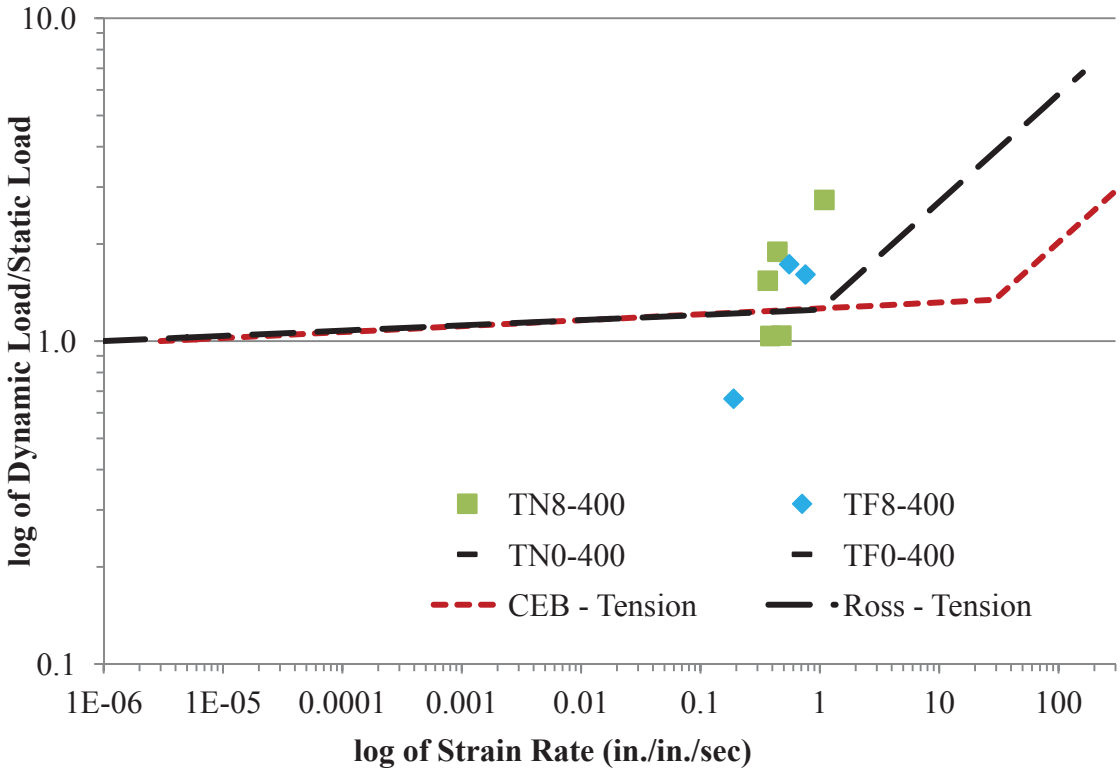

Figure F.2 – Tension, 8 ft at 400°F

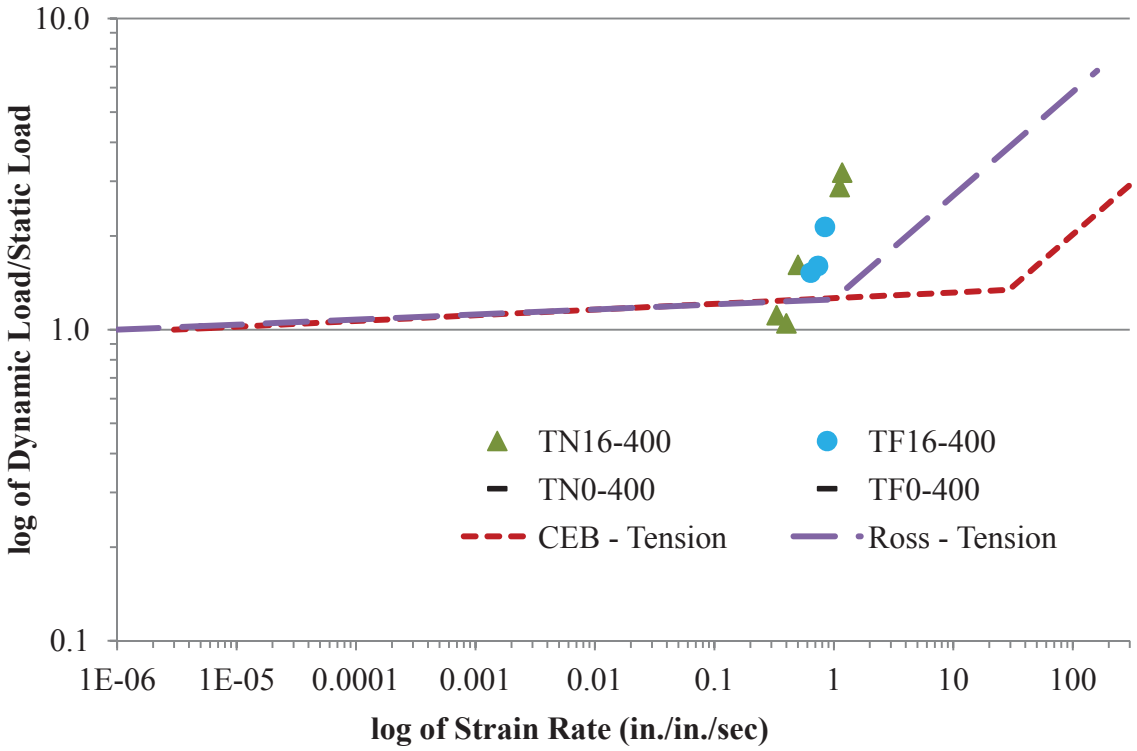

Figure F.3 – Tension, 16 ft at 400°F

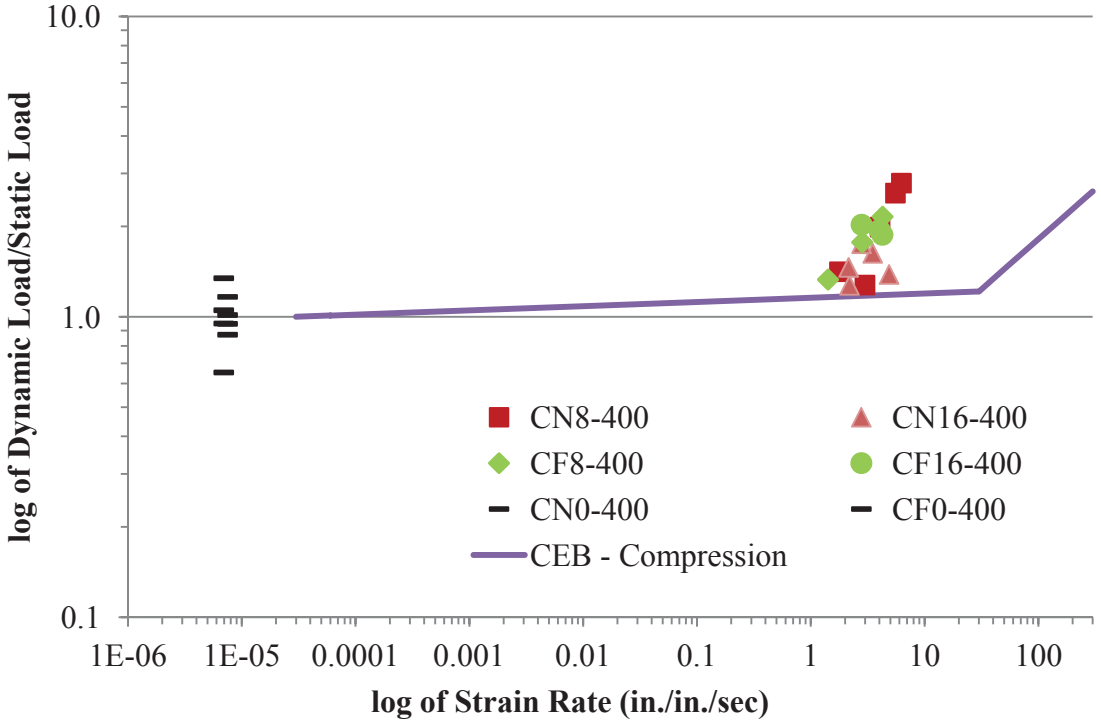

Figure F.4 – Compression at 400°F

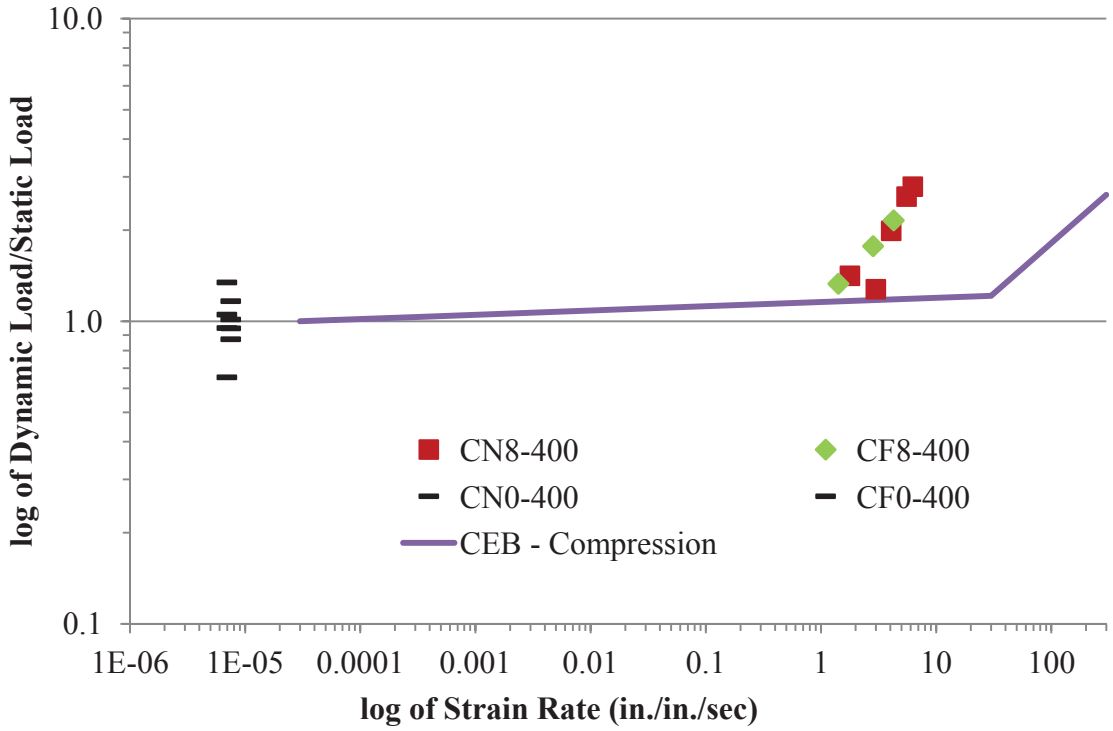

Figure F.5 – Compression, 8 ft at 400°F

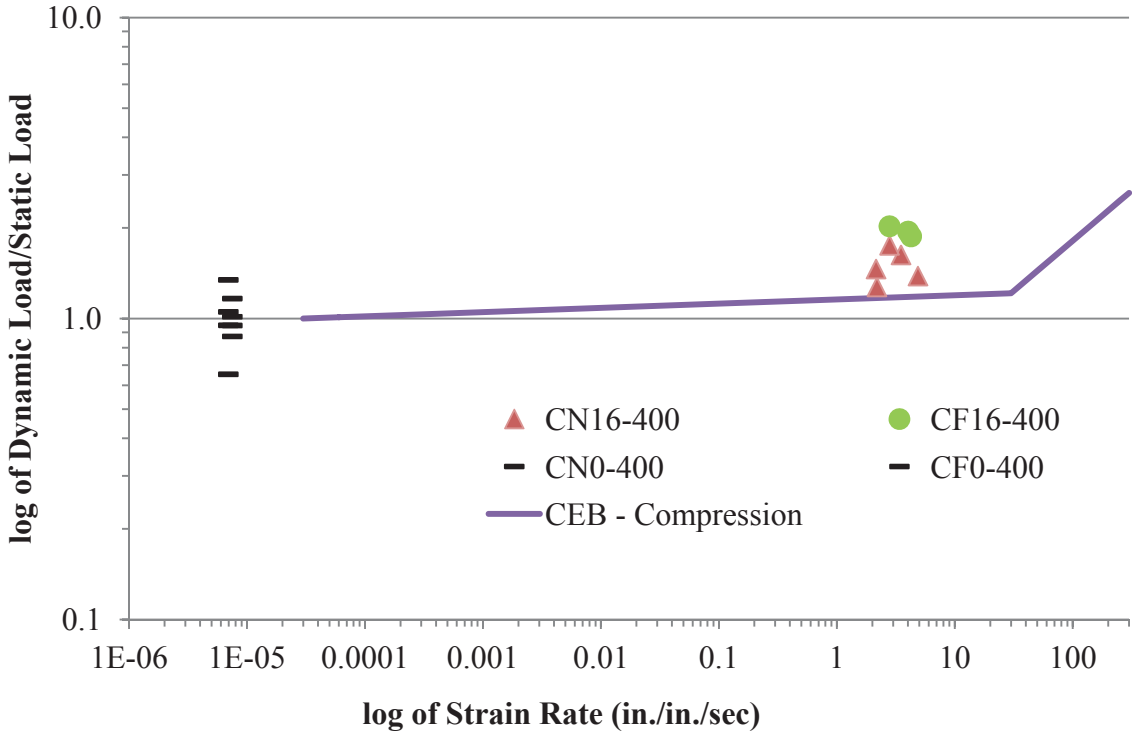

Figure F.6 – Compression, 16 ft at 400°F

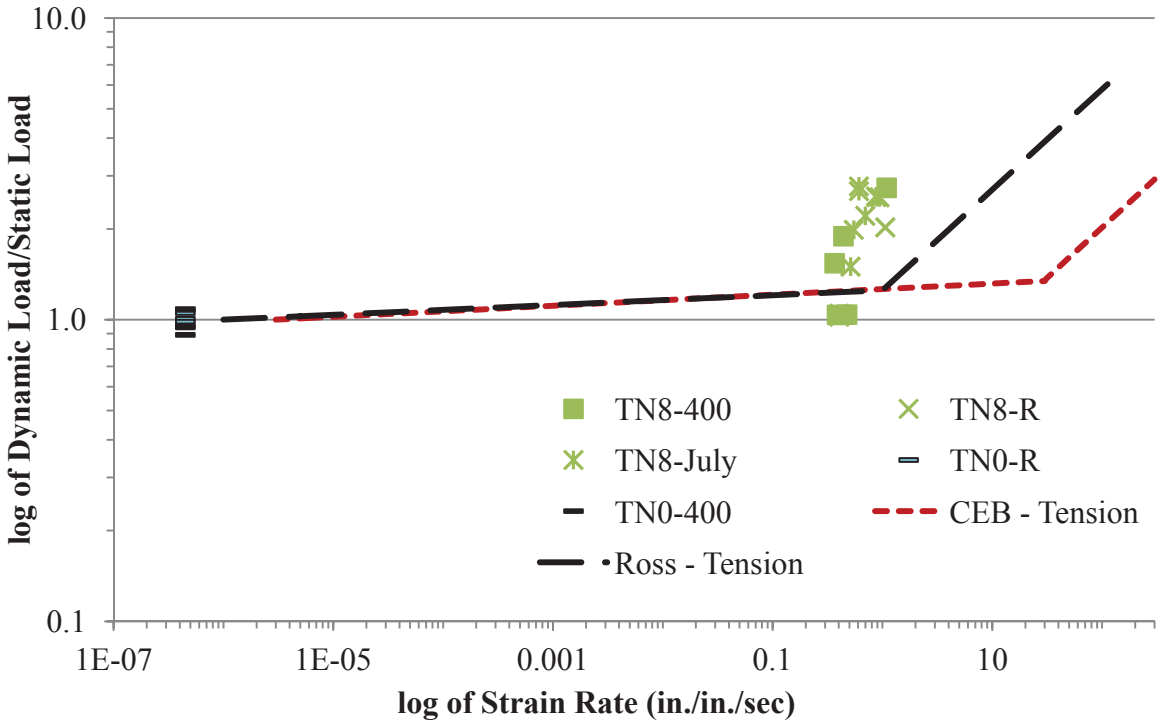

Figure F.7 – Tension, 8 ft – NWC at 400°F and Room Temperature

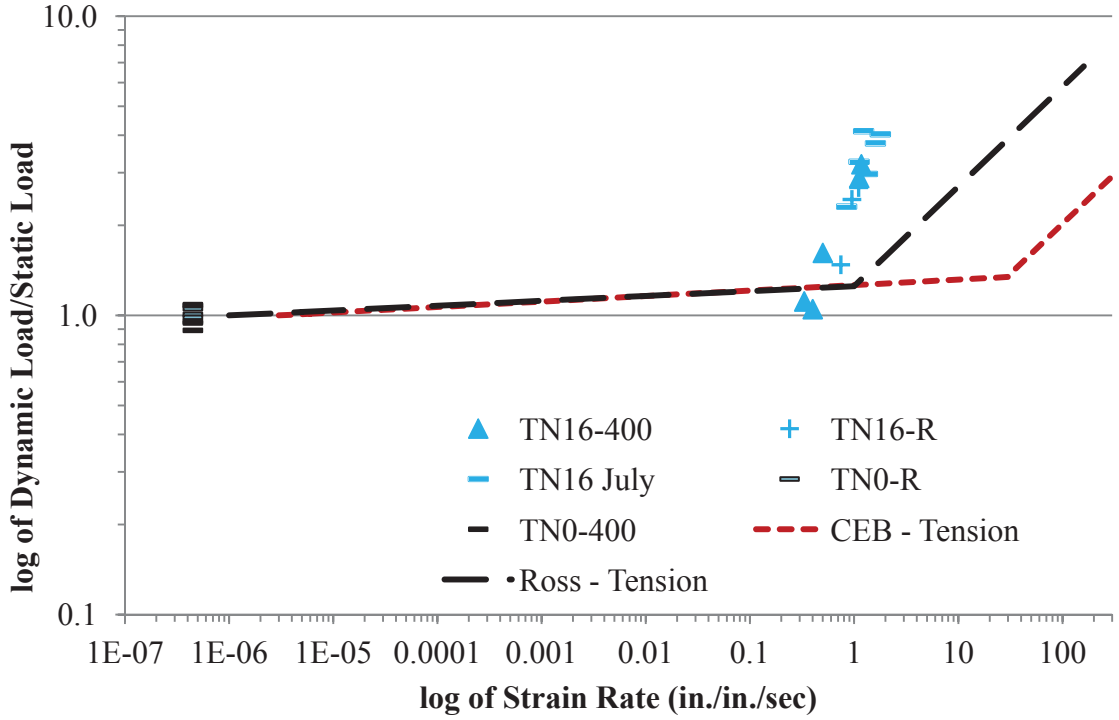

Figure F.8 – Tension, 16 ft – NWC at 400°F and Room Temperature

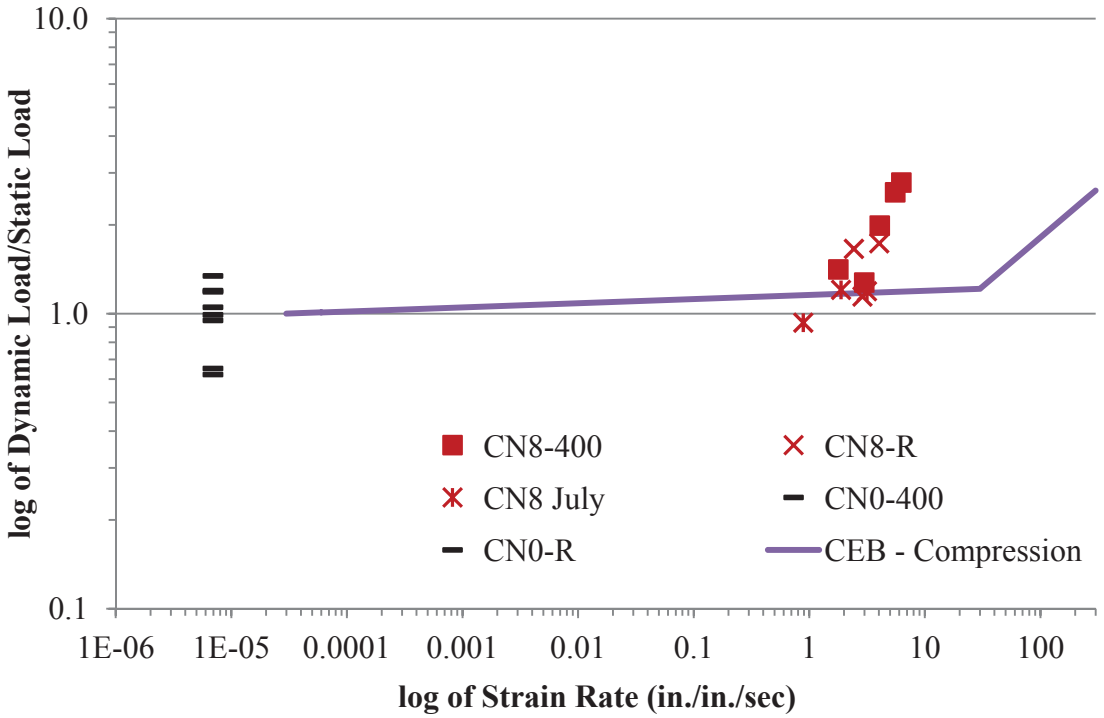

Figure F. 9 – Compression, 8 ft – NWC at 400°F and Room Temperature

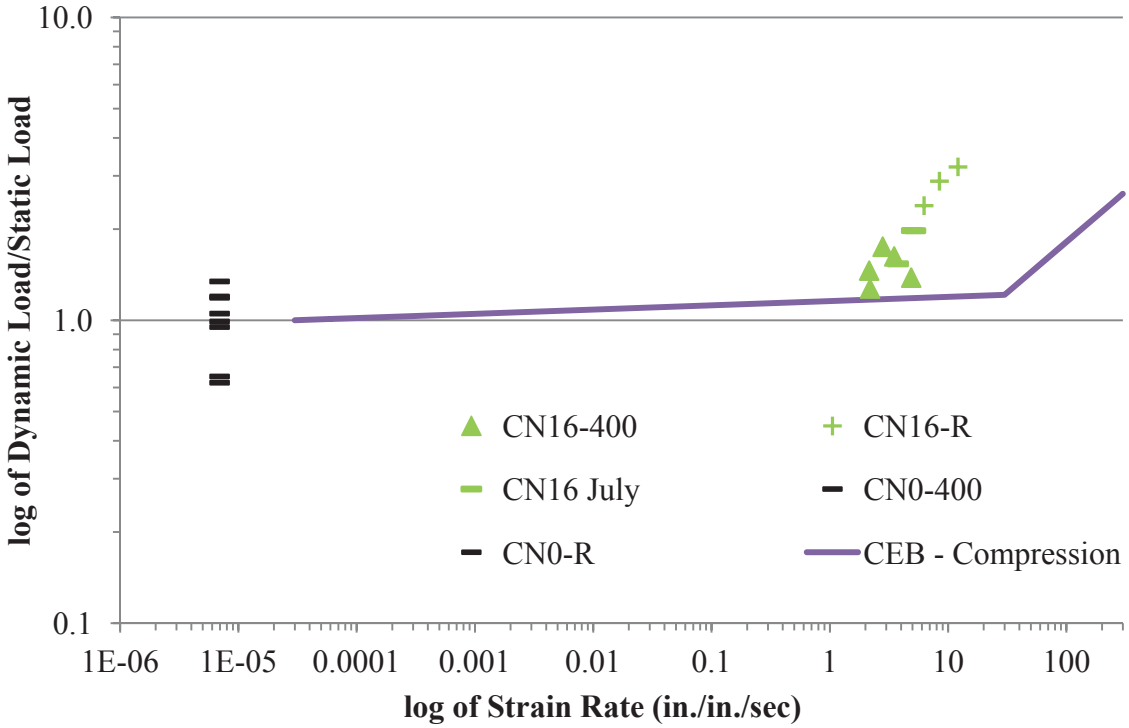

Figure F.10 – Compression, 16 ft – NWC at 400°F and Room Temperature

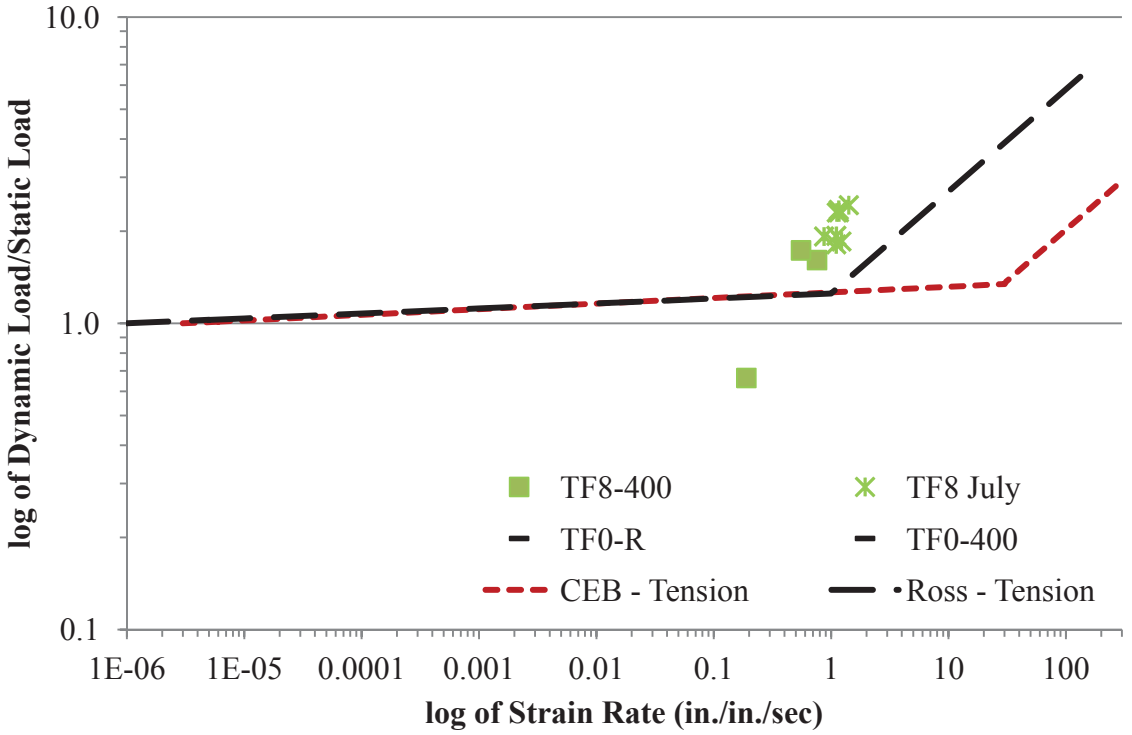

Figure F.11 – Tension, 8 ft – FRC at 400°F and Room Temperature

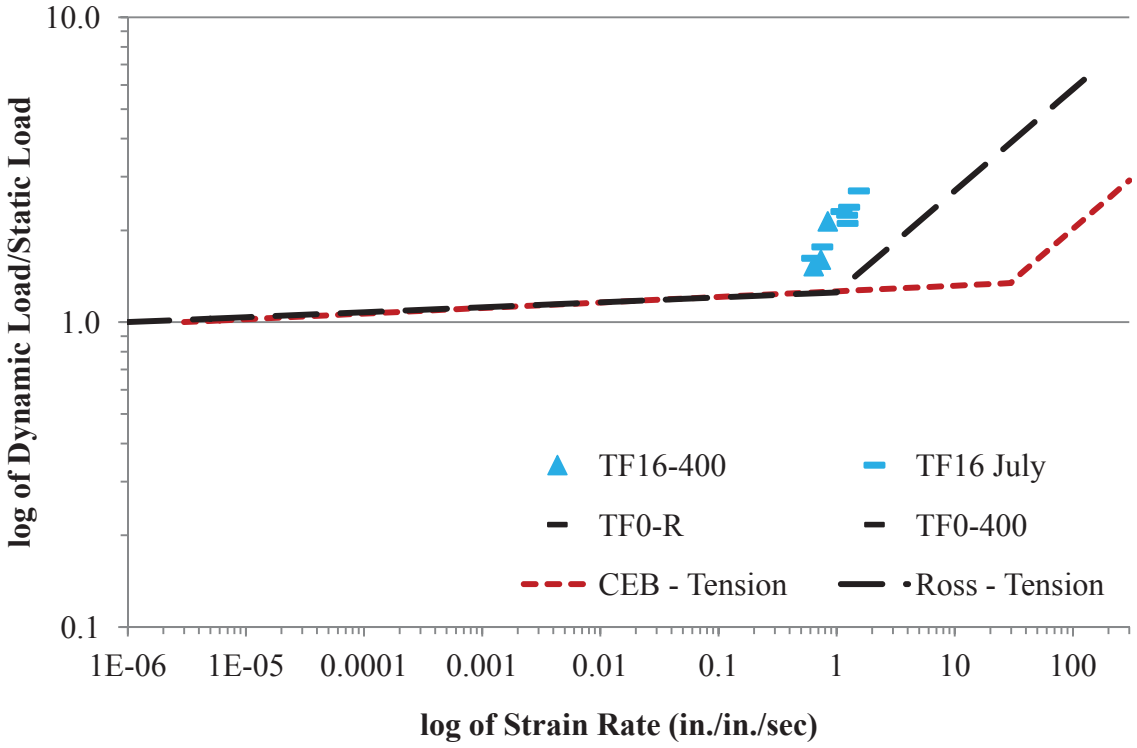

Figure F.12 – Tension, 16 ft – FRC at 400°F and Room Temperature

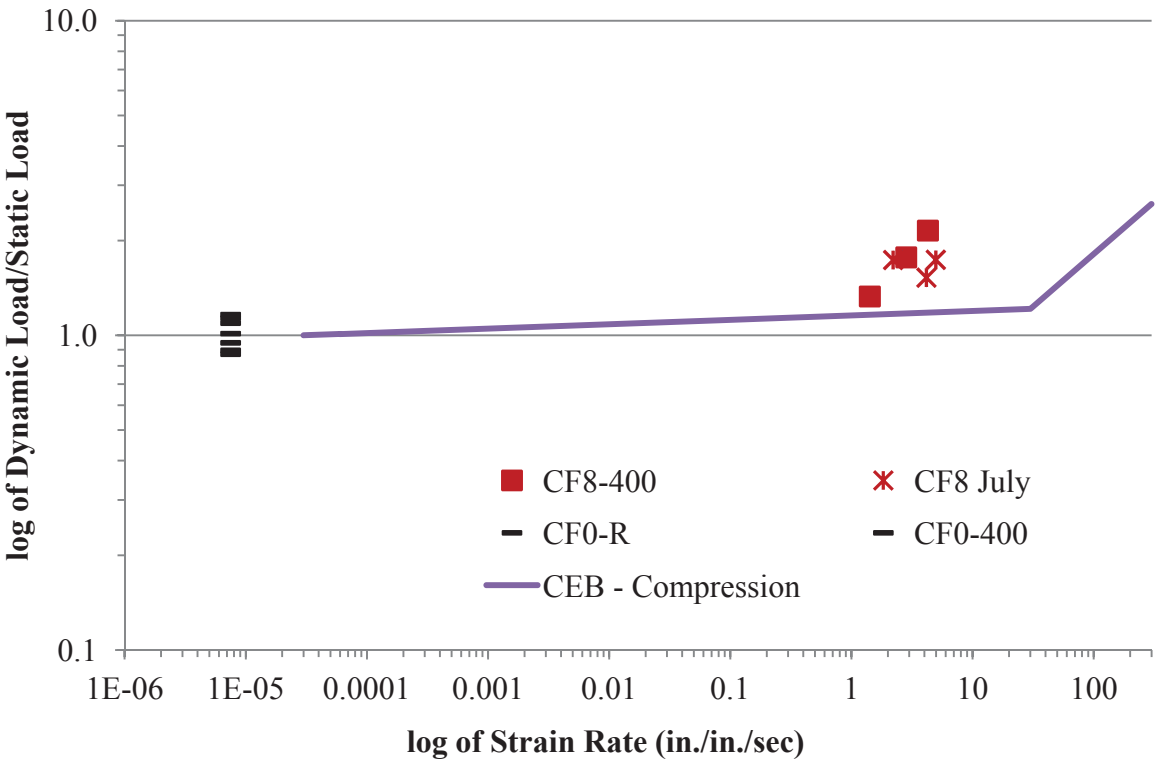

Figure F.13 – Compression, 8 ft – FRC at 400°F and Room Temperature

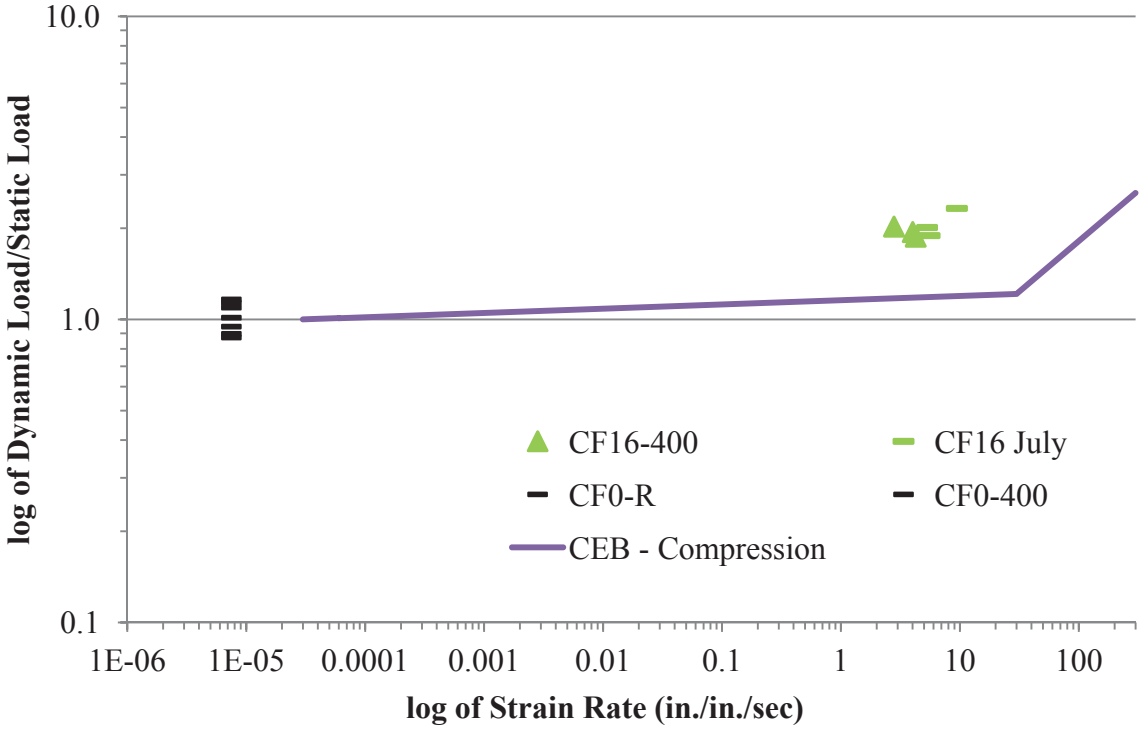

Figure F.14 – Compression, 16 ft – FRC at 400°F and Room Temperature

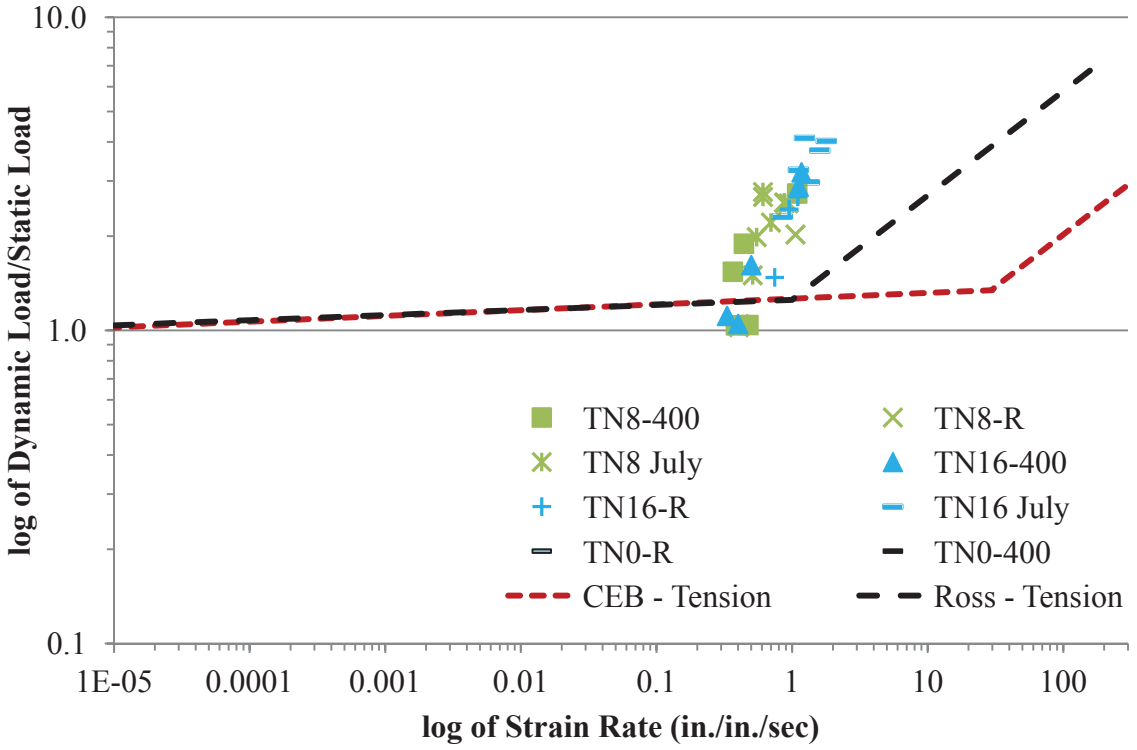

Figure F.15 – Tension – NWC at 400°F and Room Temperature

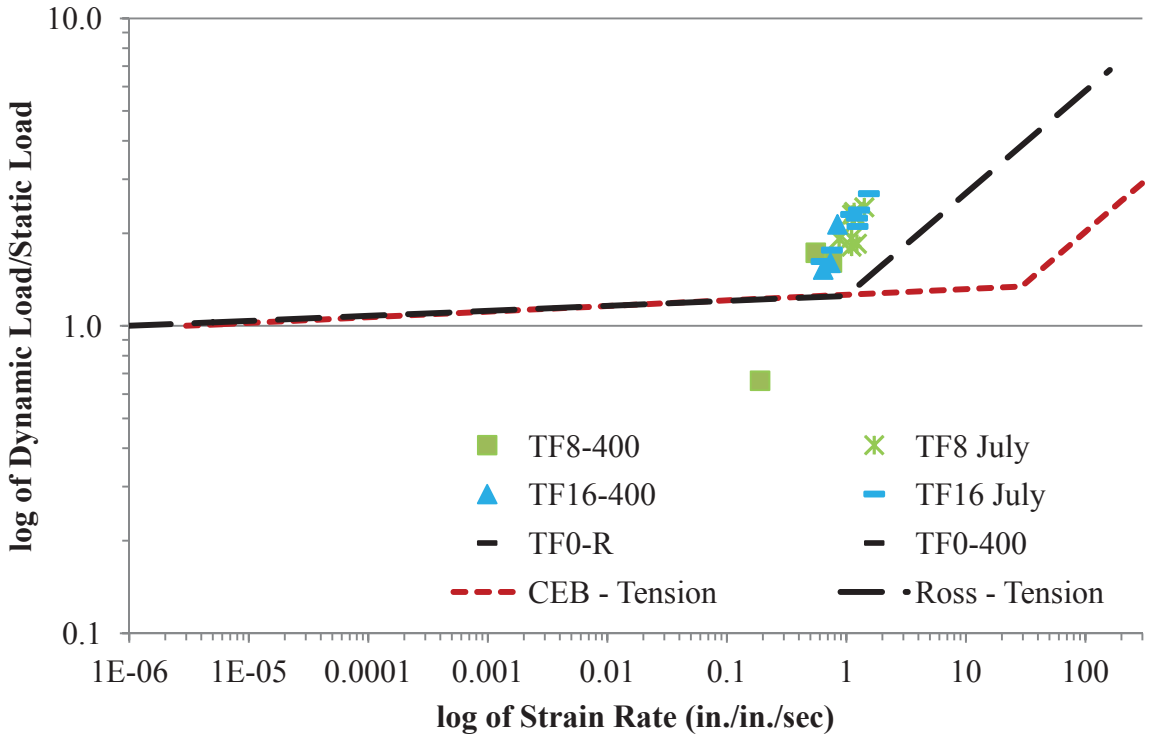

Figure F.16 – Tension – FRC at 400°F and Room Temperature

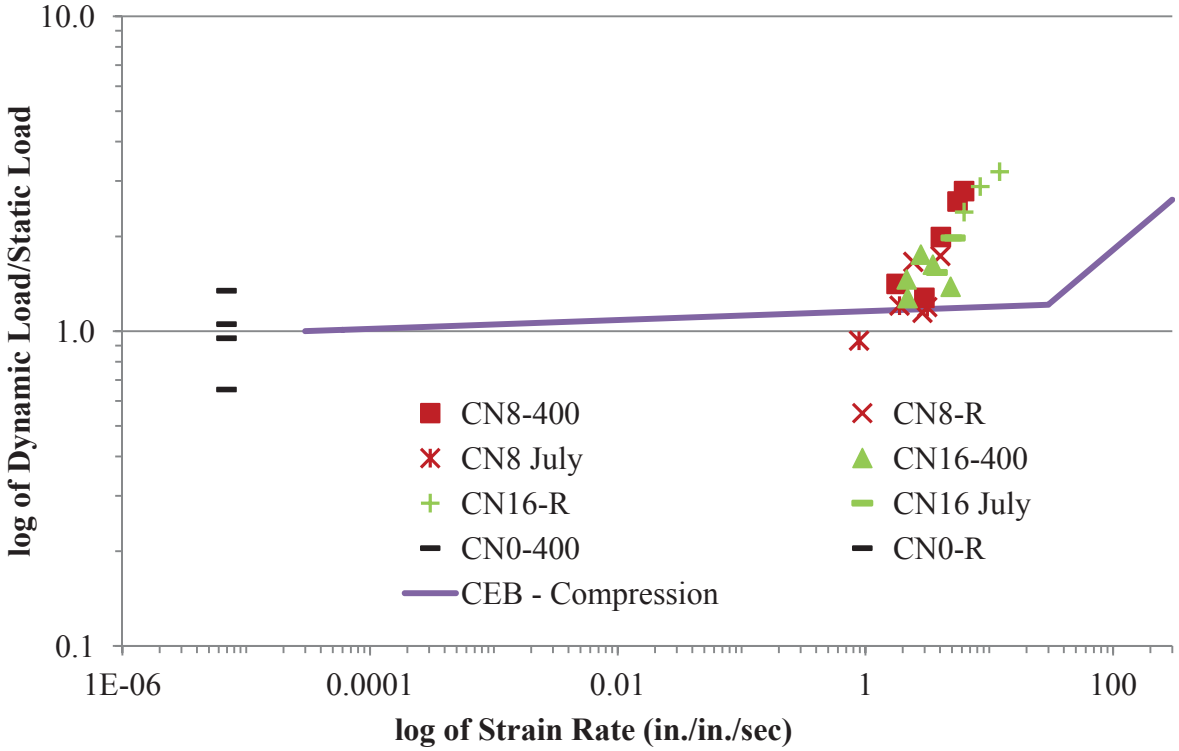

Figure F.17 – Compression – NWC at 400°F and Room Temperature

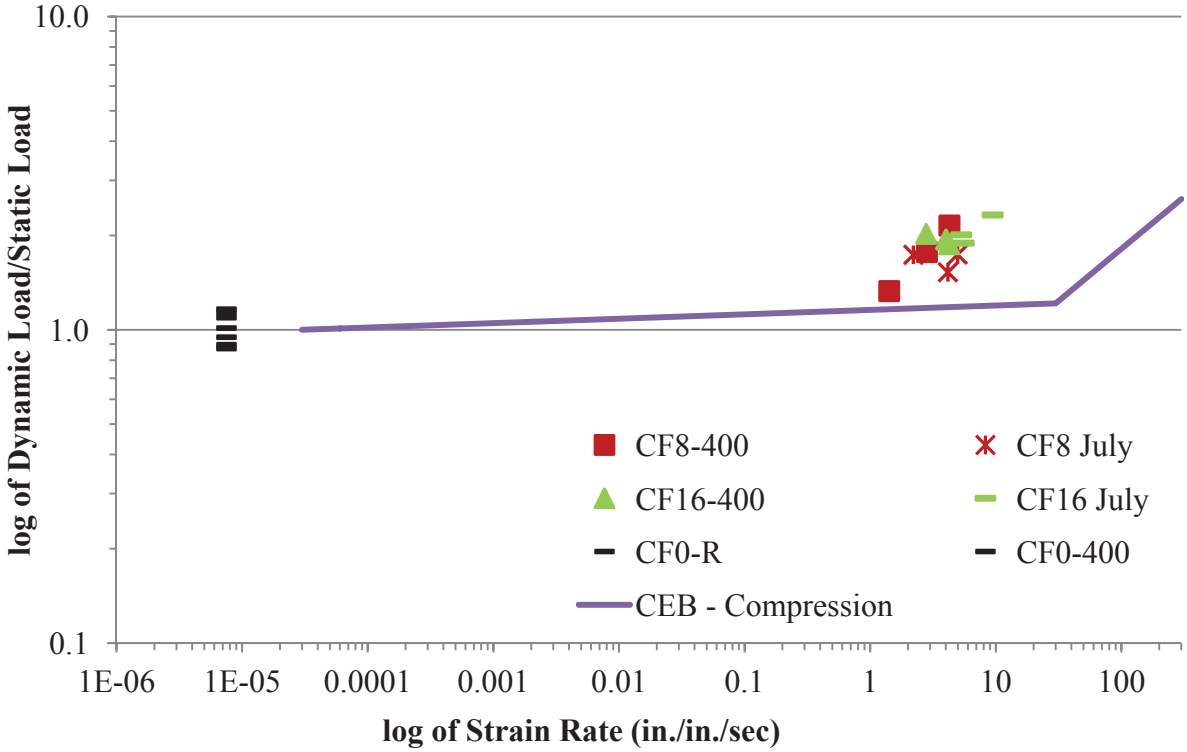

Figure F.18 – Compression – FRC at 400°F and Room Temperature